DOCTORAL THESIS

The Study of Acibenzolar-*S*-methyl-Mediated Resistance to *Potexvirus* Long-distance Movement

アシベンゾラル S-メチルに対するポテックスウイルスの
長距離移行抑制機構に関する研究

2022. 3

Department of Biological Production Science
United Graduate School of Agricultural Science
Tokyo University of Agriculture and Technology

FAWZIA NOVIANTI

学 位 論 文 要 旨

The Study of Acibenzolar-*S*-methyl-Mediated Resistance to *Potexvirus* Long-distance Movement
アシベンゾラル S-メチルに対するポテックスウイルスの長距離移行抑制機構に関する研究

生物生産科学専攻
生物制御大講座
FAWZIA NOVIANTI

Plant viruses depend on their host plant to establish their infection steps: replication, cell-to-cell, and long-distance movement. In long-distance movement, viruses translocate from the initially infected leaf to the rest of the plant through the phloem vascular tissue. Long-distance movement can be characterized by the three steps: loading into, translocation inside, and unloading from the phloem. To load into the phloem, viruses exploit the plasmodesmata, complex cytoplasmic bridges interconnecting plant cells. The permeability of plasmodesmata is highly regulated by the level of callose accumulation. Previous studies have shown that each step in long-distance movement, including loading, translocation, and unloading, can be a bottleneck during the long-distance movement of viruses.

The detailed mechanisms underlying the restriction of long-distance movement of plant viruses remain unknown; however, there is some evidence that phytohormone-mediated plant defense responses are involved. Salicylic acid (SA) is a well-studied phytohormone that induces defense responses and restricts viral cell-to-cell and long-distance movements. Acibenzolar-*S*-methyl (ASM) is a member of a group of agrochemicals called plant defense activators. It mimics the function of SA in restricting infection by plant viruses and other plant pathogens. A previous study has found that pre-treatment of *Nicotiana benthamiana* with ASM restricted infection by a potexvirus, plantago asiatica mosaic virus (PlAMV), a causal agent of devastating necrotic diseases in lilies. This treatment restricted viral replication and long-distance movement, but did not restrict cell-to-cell movement. Because the cell-to-cell movement was as efficient in ASM-treated leaves as in untreated leaves, the ASM-mediated delay in viral long-distance movement was not simply caused by the suppression of viral accumulation in the ASM-treated, inoculated leaves. Thus, it is of interest to elucidate the mechanism by which ASM delays the long-distance movement of PlAMV. In this study, *N. benthamiana* and PlAMV expressing a green fluorescent protein (PlAMV-GFP) were used as a model system to examine where and when viral movement is inhibited upon ASM treatment. I also employed fluorescence microscopy to monitor the cell-to-cell and long-distance movement of PlAMV-GFP and examine the distribution of the virus in the vasculature.

In the loading step, PlAMV-GFP entered into the vascular tissue in the inoculated leaf by around four days-post inoculations, and this step is inhibited by ASM treatment. When I observed GFP fluorescence in the vascular tissue in the inoculated leaf, PlAMV-GFP was located in the vascular tissue (i.e., xylem, adaxial/internal, and abaxial/external phloem) and the mesophyll cells in the major veins and the petiole of untreated control plants. However, in ASM-treated plants, GFP fluorescence was detected in the vascular tissues but not in the mesophyll cells. Moreover, ASM treatment drastically reduced the accumulation of PlAMV-GFP in the vascular tissues of the major veins and the petiole of the inoculated leaf.

In ASM-treated plants, translocation of PlAMV-GFP was delayed in the stem above the inoculated leaf and the basal stem compared to control plants. GFP fluorescence was located in all types of vascular tissues in the main stems of both control and ASM-treated plants. However, areas of GFP fluorescence detected in ASM-treated plants were much more limited than in the control plants. RT-qPCR-based quantification of PlAMV-RNA levels confirmed that the ASM-treated plants had lower viral accumulation in the main stem than in control plants, although there were no statistically significant differences.

A stem girdling experiment, which blocked viral movement downward into the roots through phloem tissues, demonstrated that downward movement of PlAMV-GFP from the inoculated leaf into the roots is responsible for rapid and efficient viral movement to the upper leaf. On the other hand, the movement of PlAMV-GFP to the upper leaves was restricted by ASM treatment, even though the downward movement was impaired. This result indicated that the downward movement of PlAMV-GFP in the main stem is not essential for ASM-mediated delay of systemic infection.

Viruses unload in sink organs (where the photoassimilates are imported), including the roots and the upper leaves. ASM treatment has a more restrictive effect on the unloading of PlAMV-GFP into the upper leaves than in the roots. I also found that ASM treatment allows the viral unloading and localization into the vascular tissues of uninoculated upper leaves but restricts its subsequent accumulation in mesophyll cells.

To gain insight into the function of callose in ASM-mediated inhibition of viral loading, I analyzed the levels of callose accumulation in phloem. The accumulation of callose in phloem was elevated in both control and ASM-treated plants. This result indicated that ASM-mediated restriction on loading of PlAMV is callose deposition-independent.

In conclusion, ASM treatment delays the loading of PlAMV-GFP into vascular tissues in the inoculated leaf, which leads to restricted viral translocation and unloading and reduced accumulation in sink organs. Because vascular loading is an essential and prerequisite step for viral long-distance movement of plant viruses, ASM treatment could efficiently control plant virus disease.

CONTENTS

LIST OF TABLES

CHAPTER 1

CHAPTER 4

LIST OF FIGURES

CHAPTER 1

CHAPTER 2

CHAPTER 3

CHAPTER 6

LIST OF ABBREVIATIONS

ASM	acibenzolar-*S*-methyl
AbP	abaxial phloem
AdP	adaxial phloem
AltMV	alternanthera mosaic virus
AVIII	asparagus virus 3
BaMV	bamboo mosaic virus
BS	bundle sheath
CC	companion cell
CalS	callose synthase
CP	coat protein
CVX	cactus virus X
CsCMV	cassava common mosaic virus
CymMV	cymbidium mosaic virus
CMV	cucumber mosaic virus
ClYMV	clover yellow mosaic virus
DVX	daphne virus X
dpi	days post inoculation
EP	external phloem
ER	endoplasmic reticulum
FoMV	foxtail mosaic virus
GFP	green fluorescent protein
GSL	glucan synthase-like
HEL	helicase domain
HVX	hosta virus X
HRSV	hydrangea ringspot virus
IP	internal phloem
kDa	kilodalton
LeVX	lettuce virus X
LVX	lily virus X
MS	mesophyll
MET	methyltransferase domain
NMV	narcissus mosaic virus
NTP	nucleoside triphosphates
ORF	open reading frame
PA	plant defense activators
POL	polymerase domain
PapMV	papaya mosaic virus
PepMOV	pepino mosaic virus
Pi	pith cells
PD	plasmodesmata
Phloem SEs	phloem sieve elements
PPU	plasmodesmata pore unit

PlAMV	plantago asiatica mosaic virus
PAMV	potato aucuba mosaic virus
PMTC	pre-membrane-targeting-complex
PVX	potato virus X
RdRp	RNA-dependent RNA polymerases
RNA	ribonucleic acid
RNP complex	ribonucleoprotein complex
TGB	triple gene blocks
TMV	tobacco mosaic virus
TVX	tulip virus X
SA	salicylic acid
SAR	systemic acquired resistance
SEL	size exclusion limit
ScaVX	scallion virus X
sgRNAs	subgenomic RNAs
SMYEV	strawberry mild yellow edge virus
TuMV	turnip mosaic virus
VP	vascular parenchyma
VRC	virus replication complex
X	xylem
µm	micrometer
˚C	degree celsius
M	molarity
h	hours
min	minutes
s	seconds

CHAPTER 1
GENERAL INTRODUCTION

1.1 Rationale and Significance of the Study

Plant viruses infect their host plants systemically and cause severe yield and quality losses in various crops (Agrios, 2005; Kang et al., 2005). Plant viruses depend on their host plant to establish their infection steps, which are separated into replication, cell-to-cell, and long-distance movement. In long-distance movement, viruses translocate from the initially infected leaf to the rest of the plant through the phloem vascular tissue (Leisner & Howell, 1993; Nelson & Bel, 1998; Santa Cruz, 1999). Long-distance movement can be characterized by the three steps: loading into, translocation inside, and unloading from phloem vascular tissue. Numerous studies have found that those steps have represented the points at which plant viral infection can be restricted (Ali & Roossinck, 2008; Culver et al., 2020; Hipper et al., 2013; Leisner et al., 1993).

To date, there is no antiviral compounds available to cure plants infected with virus disease. However, taking efficient control measures can significantly prevent virus disease in the field (Faoro & Gozzo, 2015; Gergerich & Dolja, 2006). Various mitigation measures have been implemented to prevent plant virus disease. For instance, infection of vector-transmitted viruses can be minimized in the field by eradicating the vectors, but it has a significant environmental impact (Mrema et al., 2013). In addition, the use of conventional breeding methods to obtain virus-resistant plants plays an important role in controlling virus disease. However, genetic resistance is not durable owing to viral genomic plasticity (Faoro & Gozzo, 2015; Hull, 2014). Therefore, we need further studies focusing on resistance mechanisms to virus disease, for the development of new control methods. The alternative methods to manage plant virus disease by employing plant innate defense response have been developed. Both local and systemic defense responses of plants can be induced to become more resistant to viral infections. Plant defense activators (PAs) are agrochemicals that have been

discovered to activate the salicylic acid-mediated defense responses in plants (Bektas & Eulgem, 2015; Matsuo et al., 2019; Oostendorp et al., 2001). The new antiviral treatment that targeted one or multiple critical infection steps of viruses may be an alternative approach in the future (Mazzon & Marsh, 2019).

Acibenzolar-*S*-methyl (ASM) is one of the best-studied PAs in the study of plant viruses. It mimics the function of salicylic acid-mediated defense responses in restricting infection by plant viruses and other plant pathogens (Ishiga et al., 2020, 2021; Noutoshi et al., 2012; Matsuo et al., 2019; Takeshita et al., 2013). Our previous study have found that pre-treatment of *Nicotiana benthamiana* with ASM restricted infection by a potexvirus, plantago asiatica mosaic virus (PlAMV). This treatment restricted viral replication and long-distance movement, but did not restrict cell-to-cell movement (Matsuo et al., 2019). Because the cell-to-cell movement was as efficient in ASM-treated leaves as in untreated leaves, the ASM-mediated delay in viral long-distance movement was not simply caused by the suppression of viral accumulation in the ASM-treated, inoculated leaves (Matsuo et al., 2019). Thus, it is of interest to elucidate the mechanism by which ASM delays the long-distance movement of PlAMV.

Unfortunately, we lack reference about the mechanisms involved in viral long-distance movement in plants where its innate defense is activated by treatment of PA. This lack of knowledge is partially due to technical difficulties in observing the phloem tissues. Therefore, in this study, we used *N. benthamiana* as a plant model, GFP-expressing PlAMV, cryohistological fluorescence imaging, and RNA analysis to examine where and when viral movement is inhibited upon ASM treatment. The main goal of the study is to provide novel insights into the mechanism of antiviral resistance in the plant, particularly delays on long-distance movement mediated by plant immune activators and new strategies to control plant virus disease.

1.2 Impact of infection of potexviruses on crop losses

Plant virus disease became a significant threat to world crop production as well as that of ornamental or medicinal plants (Agrios, 2005; Rubio et al., 2020). Plant viruses infect their host plants systemically and cause severe disease symptoms with the magnitude of resultant losses in quantity and quality of crop yields (Rao & Reddy, 2020). Furthermore, food security can be threatened when virus diseases become pandemics and epidemics in essential staple food crops (Jones, 2021). Jones (2021) also reviewed that virus disease pandemics and epidemics in global staple foods caused more than US$30 billion in economic losses annually. In addition, 47% of the pathogens that cause emerging plant disease epidemics worldwide are viruses.

Among 70 genera of plant viruses, the genus *Potexvirus* from the family *Alphaflexiviridae* includes important viruses with a broad geographic distribution and infect a wide range of plants, notably those in the family *Solanaceae* (reviewed in Table 1). The genus *Potexvirus* contains 54 definite and possible species, and it was named after its type a species, *Potato Virus X* (PVX) (van der Vlugt & Berendsen, 2002).

In general, plants infected with potexviruses show chlorotic mosaic or mottle symptoms and varying degrees of stunting (AbouHaidar & Gellatly, 1999; Loebenstein, 2001). Symptoms on systemically infected hosts range from undetectable to severe necrotic, depending on different plant-potexvirus combinations. In some cases, the necrotic patterns occur in the veins when viruses move in the infected tissues. Upon further potexviruses infection, necrotic spreads rapidly to the growing point, which is killed, and subsequently, all leaves may collapse and reduce yields (AbouHaidar & Gellatly, 1999; Hull, 2014). Yield losses due to potexviruses infection can be as high as 30% of agricultural plants (Agrios, 2005; AbouHaidar & Gellatly, 1999; Hancinsky et al.,2020).

Table 1 Review of potexviruses infection on crop losses

Potexviruses	**Species infected**	**Symptoms/ disease impact**	**Distribution**	**Citation**
AltMV	*Amaranthaceae*, *Brassicaceae*, *Cucurbitaceae*, *Fabaceae*, and *Solanaceae*. Ornamental plants: *Phlox stolonifera*	Reduced growth on seedlings	Australia, United States, Europe, Brazil, and most of Asia	Donchenko et al., 2018; Park et al., 2013
AVIII	*Asparagus officinalis*, *Chenopodiaceae*, *Solanaceae*, and *Fabaceae*	Yellowing in young leaves	Japan	Fujisawa et al., 1986; Hashimoto et al., 2008; Park et al., 2013
BaMV	*Poaceae*, *Amaranthaceae*, *Chenopodiaceae*, and *Gramineae*	Severe production losses in bamboo shoot	Australia, China, Philippines, Taiwan, India, Indonesia, United States	Abe et al., 2019; Park et al., 2013
CVX	All species of cacti plants	Systemic mottling and reduced growth	United States, Taiwan, China, Korea	Evallo et al., 2021
CsCMV	*Manihot esculenta*	Significant yield losses in cassava crops from 30%-60%	South America, China	Park et al., 2013; Zanini et al., 2021
CymMV	*Orchidaceae*	Significant losses in orchids flowering	Worldwide	Frowd & Tremaine, 1977; Hu et al., 1993
ClYMV	*Fabaceae*, *Rosaceae*, and *Chenopodiaceae*	Stunted with bushy leaves and yellowed veins	United States, Canada, Russia, Europe, and Australia	Sit et al., 1990
DVX	*Chenopodiaceae*, *Cucurbitaceae*, and *Fabaceae*	Systemic necrotic and chlorotic	New Zealand, North America	Forster & Milne, 1978

Table 1 (*cont.*) Review of potexviruses infection on crop losses

Potexviruses	**Species infected**	**Symptoms/ disease impact**	**Distribution**	**Citation**
FoMV	*Sorghum bicolor*	Systemic necrosis and yield losses in sorghum	United States	Bancroft et al., 1991; Seifers et al., 1999
HVX	*Hosta* sp.	Severe mosaic, tissue desiccation, and reduced growth of host plants	South Korea and United States	Adedire et al., 2009
HRSV	*Hydrangea macrophylla*	Chlorotic ringspots on leaves	Worldwide	Yusa et al., 2016
LeVX	*Amaranthaceae* and *Asteraceae*	Yellowing and necrosis in plant veins	Worldwide	Dizadji et al., 2008
LVX	*Lilium formosanum*	Systemic necrosis in lily plants	Worldwide	Nijo et al., 2018; Chen et al., 2004
NMV	*Narcissus* spp.	Mild mosaic disease	Europe and Japan	Brunt, 1966
PapMV	*Carica papaya* L.	Limit papaya fruits production	United States and South America	Noa-Carrazana et al., 2006
PepMOV	*Solanaceae*	Severe yield losses in tomato crops	Worldwide	Gomez et al., 2009; Jones et al., 1980
PlAMV[a]	*Liliaceae* and *Solanaceae*	Systemic necrosis and losses in lily tubers production	Almost worldwide	Tanaka et al., 2019; Komatsu et al., 2008
PAMV	*Solanaceae*	Typical chlorotic patches in infected leaf	Europe, China, and United States	Susaimuthu et al., 2007; Wu et al., 2018

Table 1 (*cont.*) Review of potexviruses infection on crop losses

Potexviruses	**Species infected**	**Symptoms/ disease impact**	**Distribution**	**Citation**
PVX	*Solanaceae*	Systemic necrosis in potato plants, yield losses of potato crops	Worldwide	Wright & Bishop, 1981
TVX	*Liliaceae*	Systemic necrosis	Netherlands, Japan, New Zealand	Sochacki & Komorowska, 2012
ScaVX	*Allium chinense*	Yield losses in scallion plants	China	Chen et al., 2001
SMYEV	*Fragaria* × *ananassa*	Yield losses in strawberry plants when it co-infected with potyviruses	Worldwide	Jelkmann et al., 1990

[a] PlAMV was used as a plant virus models in this study.

No biotic vectors of potexviruses are known to date. However, they are easily transmitted from infected to healthy plants by mechanical inoculation while workers or animals contact infected plants. High levels of accumulation of potexviruses in their host plant would encourage their distribution in the field by contact (Agrios, 2005; Hull, 2014). During postharvest storage, potexviruses are commonly transmitted by infected tubers, bulbs, and seeds (Hanssen et al., 2009; Klap et al., 2020; Tanaka et al., 2019). A recent study by Chang et al. (2017) found that the dipterans insect could transmit bamboo mosaic virus from infected to healthy seedlings in a mechanical-like manner. Finally, understanding how viruses transmit in their host is essential for developing effective disease management measures.

1.3 Plantago asiatica mosaic virus (PlAMV)

1.3.1 Natural host range of PlAMV

PlAMV was firstly isolated from *Plantago asiatica* L. (Chinese plantain) in the Russian Far East by Kostin & Volkov (1976), and for about the next 25 or more years, *P. asiatica* was the only known natural host. However, additional natural hosts began to emerge in the early 2000s. The report of PlAMV infection in lilies (*Lilium* spp. and hybrids) in Japan (Ozeki et al., 2006; Komatsu et al., 2008) was followed a few years later the emergence of PlAMV in the commercial lily trade. Further isolates were found in other plant species and countries, including *P. asiatica* in Korea (Lim et al., 2016), *Nandina domestica*, and *Viola grypoceras* in Japan (Komatsu et al., 2017), *Rehmannia glutinosa* in Korea (Kwak et al., 2018) and Japan (Uehara-Ichiki et al., 2018), and *Stellaria media*, *Primula vulgaris*, and *Urtica urens* in the Netherlands (Kock et al., 2013).

1.3.2 Symptoms of PlAMV

The natural hosts of PlAMV vary in the degree of symptom expression. *P. asiatica* has been reported to show mottling or mottled chlorosis (Lim et al., 2016), whereas other plants may show few obvious symptoms depending on the environment or nutrient status. Symptoms between different lily cultivars may vary widely, with some showing only mild mottling on the leaves while others may show necrotic spotting or streaking on both the foliage and the sepals (Lim et al., 2016; Tanaka et al., 2019).

1.3.3 Lineage of PlAMV

Domain: Virus

Realm: *Riboviria*

Kingdom: *Orthornavirae*

Phylum: *Kitrinoviricota*

Classes: *Alsuviricetes*

Order: *Tymovrales*

Family: *Alphaflexiviridae*

Genus: *Potexvirus*

Species: plantago asiatica mosaic virus

The information of lineage of PlAMV was adapted from NCBI taxonomy database (Schoch, et al., 2020).

1.3.4 Genome organization of PlAMV

PlAMV has filamentous virions ranging from 490 to 530 nm in length, about 13 nm in width, and 11 nm in diameter (Fig. 1.1A; Komatsu et al., 2008). PlAMV has a monopartite, single-stranded RNA (ss), positive-sense (+) RNA genome capped at the 5′ end, and polyadenylated at the 3′-terminus. The length of PlAMV RNA is approximately 6.1 kb. Similar to other potexviruses, the genome of PlAMV has five open reading frames (ORFs). The first ORF encodes RNA-dependent RNA polymerases (RdRp), which is essential for the replication of viral RNA. ORFs 2 (25 kDa), 3 (12 kDa), and 4 (13 kDa) are referred as triple-gene-block (TGB) proteins (TGBp1, TGBp2, and TGBp3). These proteins play a key role in the viral movement in the host plant. In addition, TGBp1 possesses RNA-silencing suppressor activity. ORF 5 (18 kDa to 27 kDa) encodes the coat protein (CP), whose N-terminal is important for cell-to-cell and long-distance movement (Fig. 1.1B; AbouHaidar & Gellatly, 1999; Minato et al., 2014; Solovyev et al., 1994).

Replicase encoded in ORF1 is translated directly from genomic RNA, as indicated by *in vitro* experiments, while other proteins are translated from three subgenomic RNAs (sgRNAs) (Yoshida et al., 2019). Only two sgRNAs are detected from plant tissues infected with PlAMV, sgRNA1 (about 1.9 kb in length) and sgRNA2 (about 0.8 kb). TGBp2 and TBGp3 are mainly translated from sgRNA1, which encodes TGBp1 in its most 5′-terminal ORF via leaky scanning. CP encoded in the most 3′-

terminal ORF5 is likely to be translated from sgRNA2 (Figure 1.1B; Komatsu et al., 2008; Solovyev et al., 1994; Minato et al., 2014).

(A)

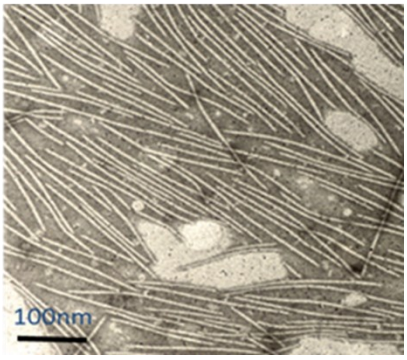

(B)

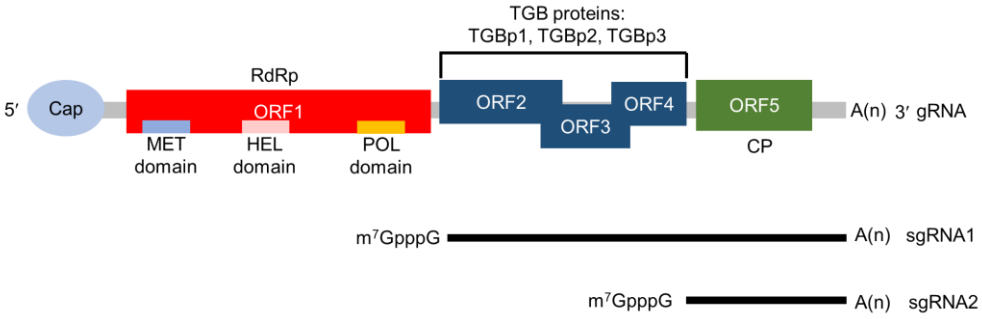

Figure 1.1 Properties of PlAMV. (A) The electron micrograph of PlAMV showing long filamentous viral particles. From Komatsu, K with permission. (B) Genome organization (gRNA) and two subgenomic RNAs (sgRNA1 and sgRNA2) of PlAMV. M^7GpppG represents the cap structure. A(n) represents the poly(A) tail. ORF1 encodes RNA-dependent RNA polymerase, which possesses a methyltransferase domain (MET), a helicase domain (HEL), and polymerase domain (POL); ORF2, ORF3, and ORF4 encode triple gene block proteins ; ORF5 encodes coat protein (CP). Figure adapted from AbouHaidar & Gellatly (1999).

1.4 Infection steps of potexviruses

The high accumulation of plant viruses throughout their host plant is critical for virus survival. A massive titer of virions may lead to systemic infection and facilitate both virus vertical and horizontal transmissions of viruses (Hull, 2014). Plant viruses must complete their infection cycle, i.e. replication, cell-to-cell, and long-distance movement (Fig. 1.2). Because plant viruses are obligate intracellular parasites, they are dependent on the host plant to complete the infection cycle. The infection cycle of viruses is a complex interplay between host cell factors and viral genomic function. (Hipper et al., 2013).

1.4.1 Replication of potexviruses

One of the significant features of viruses is their ability to replicate their genomic nucleic acid in the cells. Viruses code for the enzymes involved in the synthesis of their nucleic acids (Hull, 2014). Replication of (+)-sense RNA genomes, including PlAMV, by the virus-encoded replicase, starts with the synthesis of a complementary (-) strand using the (+) strand as a template, followed by a synthesis of new (+) strands using the (-)-strand as a template. Synthesis of new RNA is from the 3′-5′ ends of the templates (Hull, 2014; Park et al., 2013).

ORF1 of PlAMV encodes replicase, a putative RdRP, which possesses enzymatic activities involved in the replication of (+)-sense ssRNA, including a methyltransferase domain/MET (aa 1-405); an NTP-binding helicase domain/HEL (aa 540-914) and a polymerase domain/POL (aa 933-1380) (Fig. 1.1B; Komatsu et al., 2008). PlAMV replicase forms the high-molecular-weight complex, called pre-membrane-targeting complex (PMTC), in soluble fractions. Likely that this PMTC is subsequently targeted to the cellular membrane, possibly endoplasmic reticulum (ER), to form a mature virus replication complex (VRC) (Komatsu et al., 2021).

1.4.2 Cell-to-cell movement of potexviruses

Viruses move from their initially infected cell into neighboring cells to continue their infection (Benitez-Alfonso et al., 2010; Carrington et al., 1996; Tilsner, 2013). This infection step is referred to as cell-to-cell movement (Hull, 2014). For completing this step, viruses exploit the plasmodesmata (PD), plant-specific intercellular nanopores that connect the plasma membrane, cytoplasm, and ER through the cell wall (Tilsner et al., 2011). Most PD have a size exclusion limit (SEL) as large as 800-1000 Da, indicating the upper size limit of a transported molecule is 1.5 nm in diameter. Thus the SEL of PD is considerably smaller than the size of plant virus particles (Leisner & Turgeon, 1993; McLean et al., 1993). In addition, viruses encode the movement proteins (MPs) to associate with PD, increase the SEL, also interact with host cellular machinery for viral RNA/DNA trafficking between cells (Lough et al., 2000).

ORF2,3 and 4 encode TGBps required for cell-to-cell movement, as mutations in these ORFs prevent the development of systemic infection in plants but not of viral replication in protoplast (AbouHaidar & Gellatly, 1999). In addition to TGBps, CP is required for cell-to-cell movement of potexviruses (Lough et al., 2000; Ozeki et al., 2009; Park et al., 2013; Scholthof, 2005). The functions of TGBps and CP are observed well in a new model for intercellular transport of PVX viral RNA (vRNA). Microprojectile bombardment studies revealed that TGBp1 and CP are co-translocated between cells with viral RNA, known as ribonucleoprotein (RNP) complex (Lough et al., 2000). The RNP complex requires TGBp2 and TGBp3, which are ER-located proteins to move through PD. TGBp2 and TGBp3 are either involved in the intracellular transport or interact with the host's cellular machinery/docking sites at the PD (Lough et al., 2000). Tilsner et al. (2013) found that in the early infection stage of PVX, TGBp2 is concentrated in lateral walls of PD rather than in ER. This finding suggests that TGBp2 first target PD and then localize at the ER. TGBp3 also localizes at PD caps with TGBp2 (also reviewed in Park et al., 2014 and Verchot-Lubicz, et al., 2010).

1.4.3 Long-distance movement of potexviruses

After the completion of replication and cell-to-cell movement in the initially infected leaf, viruses try to translocate to the rest of the plant, to establish the systemic infection. This infection step is referred to as systemic or long-distance movement. Three stages characterize the long-distance movement of plant viruses. First, viruses are loaded into the phloem sieve elements (phloem SEs) in the veins of a source leaf, where photoassimilates are synthesized. Second, viruses translocate through the phloem SEs from the source to sink tissues. Finally, after reaching the sink tissues, viruses are unloaded from the phloem SEs to begin a new round of infection (Carrington et al., 1996; Leisner et al., 1993; Seron & Haenni, 1996). Despite the general notion that the phloem is the main route for long-distance movement, recent studies have also suggested that xylem tissues may provide an additional/alternative pathway for the long-distance movement of plant viruses, including potexviruses (Betti et al., 2012) and potyviruses (Mochizuki et al., 2016; Wan et al., 2015).

Long-distance movement involves viruses and host plant functions. Specific interactions between viral or plant cellular factors are necessary for long-distance movement, to facilitate the virus to load, translocate through, and unload from the phloem SEs (Carrington et al. 1996; Hipper et al., 2013). CP and TGB1 of potexviruses are needed to establish long-distance movement (Hipper et al., 2013; Verchot-Lubicz et al., 2010). Potexviruses have been considered to move as a form of RNP complexes or virions, which depend on the viral species. For instance, white clover mosaic virus moves as RNP complexes (Lough et al., 2001), while PVX moves as virions (Betti et al., 2012). However, the detailed information for the long-distance movement of PlAMV is unknown.

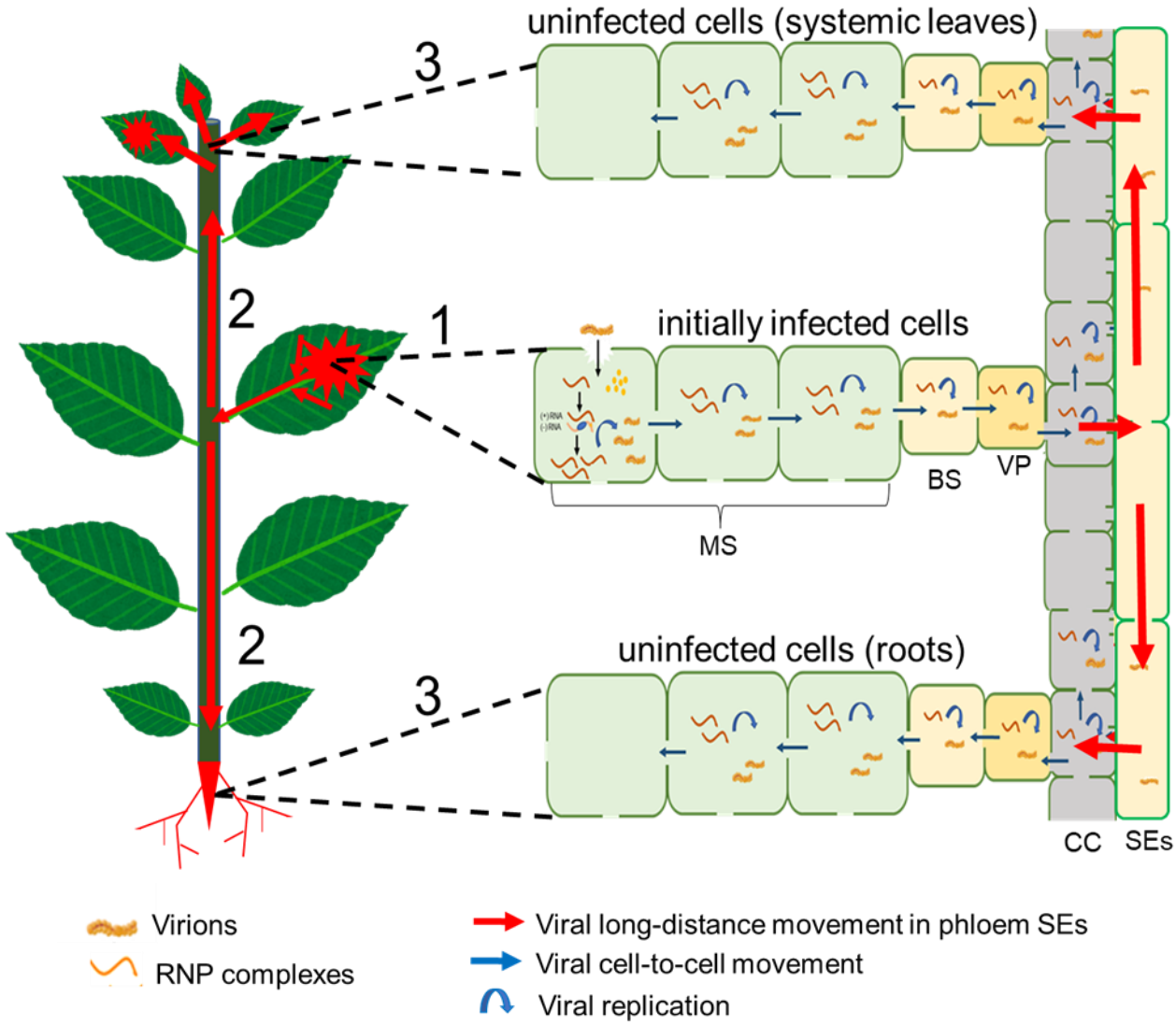

Figure 1.2 The general view of virus replication, cell-to-cell, and long-distance movement in the plant cells. In the initial infected cells, virions are disassembled for replication and translation of viral genome and move cell-to-cell between MS-BS-VP as virions or RNP complexes through plasmodesmata. Virions or RNP complexes are loaded to phloem SEs to begin the long-distance movement (1). Then, virion or RNP complexes translocate through phloem SEs to reach uninfected cells in the sink tissues (systemic/upper leaves and roots) (2). Finally, virions or RNP complexes unload from phloem SEs to set up new infection steps (3). MS, mesophyll cells; BS, bundle sheath; VP, vascular parenchyma; CC, companion cells; SEs, phloem sieve elements. Figure adapted from Hipper et al. (2013); Leisner & Howell (1993).

1.5 Host factors involved in long-distance movement of viruses

1.5.1 Vascular tissue in plant

Viruses take the same route that plants use to transport of the photoassimilates, for instance, PD and phloem vasculature to establish long-distance movement (Seron & Haenni, 1996). Viruses also follow the source-to-sink transportation of photoassimilates (Leisner & Howell, 1993). To reach phloem SEs, viruses have to move between several different types of cells, which start from mesophyll into specific phloem cells, including bundle sheath (BS), vascular parenchyma (VP) and companion cells (CC), and load to phloem SEs. In addition, some viruses translocate into xylem-associated cells from the VP. After loading to phloem SEs and/or xylem, viruses rapidly translocate in phloem SEs to systemic tissues of the plant. Finally, viruses unload from the CC/phloem SEs complex into VP-BS and mesophyll to complete the systemic infection (Figure 1.2; Dawson & Hilf, 1992; Nelson & van Bell, 1998; Hipper et al., 2013).

The leaf vein system is classified into major (classes I-III) and minor veins (classes IV-V) (Roberts et al., 1997). Several studies have revealed that the loading of viruses occurred in both minor and major veins of the inoculated leaf. In contrast, virus unloading occurs from major veins of the uninfected leaf (Andrianifahanana et al., 1997; Cheng et al., 2000; Silva et al., 2002). In addition, viruses can enter two structurally different types of phloem, the internal and external phloem, for their upward to the sink leaves and downward movement to the roots (Cheng et al., 2000; Gosalvez-Bernal et al., 2008; Ueki & Citovsky et al., 2007).

Viruses specifically interact with the host factors to move through the boundaries between the phloem cell types. In the absence of compatible interaction, viruses are unable to establish long-distance movement, indicating that these boundaries can act as natural barriers for virus movement (Ueki & Citovsky et al., 2007). Ding et al. (1996) found that systemic infection by a masked strain of tobacco mosaic virus (M-TMV) is delayed because M-TMV is unable to efficiently enter the

companion cells. In cucumber plants, systemic infection of a chimeric cucumber mosaic virus (CMV) expressing CP of the Florida strain of tomato aspermy virus (TAV) was restricted at boundaries between BS and VP (Thompson and Garcia-Arenal, 1998). At last, the efficiency of cell-to-cell movement can affect the long-distance movement of viruses, and these two interconnected processes are difficult to distinguish (Waigmann et al., 2004). In chapter III, I discussed the effect of ASM treatment on the cell-of-cell and its relation to the long-distance movement of PlAMV in phloem SEs.

1.5.2 Plant immune system

Two classes of plant immune receptors are critical for defense activation. One is pattern-triggered immunity (PTI); its signaling is initiated by microbe-associated molecular patterns (MAMPs) (Bigeard et al., 2015). Another mode of induced immunity in plants is called effector-triggered immunity (ETI) (Bektas & Eulgem, 2015). ETI signaling is initiated by disease resistance (*R*)-genes, which recognize the presence or activity of effectors from plant pathogens (Qi et al., 2011). Numerous studies have shown that ETI and PTI utilize the phytohormones salicylic acid (SA), ethylene (ET), and jasmonic acid (JA) (Glazebrook, 2005). While PTI and ETI are local responses limited to infected pathogen tissues, plants also activate long-lasting systemic immunity. Local interactions between plant and pathogen can initiate this systemic immunity, resulting in systemic acquired resistance (SAR). On the other hand, induced systemic resistance (ISR) can be triggered by the strains of non-pathogenic plant growth-promoting rhizobacteria (PGPR) (Bektas & Eugem, 2015; Pieterse et al., 1998).

SAR mediates long-lasting, broad-spectrum resistance to a wide range of pathogens in uninfected tissues and organs. SA is an essential component in the signal transduction pathway leading to SAR accompanied by pathogenesis-related (*PR*) gene expression (Ward et al., 1991; Naylor et al., 1998). Salicylic acid (SA; 2-hydroxybenzoic acid) is one of many phenolic compounds that plants were synthesized. In addition to its essential role in disease resistance, SA is a critical

hormone that plays direct or indirect roles in regulating many aspects of plant growth and development and thermogenesis (Dempsey & Klessig, 2017).

Previous studies have reported that SA-mediated defense restricts viral infection steps (Huang et al., 2019; Naylor et al., 1998; Murphy et al., 2001). The replication of PVX (Naylor et al., 1998) and TMV (Chivasa et al., 1997) was suppressed by SA treatment. Huang et al. (2020) found that SA treatment induces PD closure, thus impeding the cell-to-cell movement of the tobacco rattle virus. In addition, the loading of CMV into the vasculature at the point of inoculation was restricted by SA treatment (Naylor et al., 1998).

NONEXPRESSOR OF PATHOGENESIS-RELATED GENES1, 3, and 4 (NPR1, NPR3, and NPR4) are the receptors of SA that function as transcriptional regulators. As SA receptors, NPR1 functions as a transcriptional activator promoting SA-induced defense gene expression (Chen et al., 2021). Loss of NPR1 results in reduced *PR* gene expression and increased susceptibility to pathogens (Cao et al., 1994; Delaney et al., 1995). In addition to regulating the level of NPR1 protein, NPR3 and NPR4 serve as redundant transcriptional co-repressors that prevent activation of defense gene expression when SA levels are low (Chen et al., 2021).

1.5.3 Function of callose in plasmodesmata

It has been described in the previous chapter that successful systemic infection by plant viruses depends on symplastic viral movement between the PD of the cells (subchapter 1.3.6; Folimonova & Tilsner, 2018). The permeability of PD is regulated by the accumulation of callose (β-1,3-glucan), which significantly impacts the cell-to-cell diffusion of molecules in plant tissues (Wu et al., 2018; Zavaliev & Epel, 2015). Callose is a linear amorphous wall polysaccharide formed by a β-1,3-linked homopolymer of glucose that contains β-1,6-branches. Callose is specifically enriched in the extracellular space between the cell wall and the PD, where it spans the entire length of the PD channel or is concentrated on PD neck regions (Sager & Lee, 2018).

Functionally, callose accumulation reduces the permeability of PD and eventually leads to PD closure by narrowing the cytoplasmic sleeve at the PD orifice. In contrast, callose degradation increases the permeability of PD (Sager & Lee, 2014; 2018). Two antagonistic enzymes highly regulate the level of callose: callose synthase (CalS) or glucan synthase-like (GSL) is callose synthase enzyme, while β-1-3-glucanases (GLU/in some papers are abbreviate in BG) are the hydrolytic enzymes which degrade callose (Koziel et al., 2021; Nedukha, 2015; Wu et al., 2018; Zavaliev et al., 2011).

Callose plays an essential role in controlling the transportation of molecules and water, pollen development, cell growth and differentiation, and responses to biotic and abiotic stresses (Barratt et al., 2009; Chen et al., 2009; Cui et al., 2016; Wang et al., 2021; Wu et al., 2018). Callose deposits at cell plates during differentiation of cells, but it degrades from the new cell wall after the completion of cell division except in the portions of cell walls adjacent to PD (reviewed in Sager & Lee, 2018). A high abundance of callose finds in new sieve pores, which plays a significant role in regulating the transportation through symplast. Callose is engaged in forming pores in sieve plates and their closing as well. Thus, callose plays an important role in intracellular communications of plant organs and tissues (Nedukha, 2015).

Apart from these functions in the development of cells, callose is also highly deposited in PD as a response to various abiotic (wounding, temperature, chemical treatment, and metal toxicity) and biotic stresses (pathogen and insect invasion) (Cui et al., 2016; Ellinger & Voigt, 2014; Lucas et al., 1993; reviewed in Levy & Epel 2009; Wang et al., 2021). As reviewed in Zavaliev et al. (2011), callose deposition appears to be nonspecific defense response to infection by many pathogens, but there have been several reports suggesting that it is presumably aimed at restricting pathogen invasion and/or spread. For instance, in response to fungal and bacterial infections, callose-rich papillae are formed at pathogen penetration sites between the plasma membrane and the cell wall. Indeed, several

previous studies suggested that callose accumulation also plays a key role in resistance response against viruses. For instance, a high accumulation of callose was detected in leaf tissues around necrotic lesions formed by *N*-gene-mediated resistance against TMV in tobacco plants (Beffa et al., 1996). In accordance with this finding, cell-to-cell movement of TMV and long-distance movement of PVX were restricted in the *GLU I* -deficient mutant, which shows an elevated deposition of callose (Iglesias & Meins Jr., 2000). Callose also accumulates as a systemic response to viral infection in a resistant host, which is correlated with the development of SAR to TMV infection (reviewed in Zavaliev et al., 2011). These findings prompt us to investigate the mechanism of callose deposition in the long-distance movement of PlAMV.

1.6 Control of plant virus disease

As reviewed in Table 1, viruses cause considerable yield losses, and taking efficient control measures can significantly prevent virus disease from occurring in the field (Gergerich & Dolja, 2006). Several practices have been introduced in the field to control the virus disease. For instance, eradication of the virus-infected crop and weeds by burning and burying (Sosnowski et al., 2009), crop rotation (Curl, 1963), improving worker hygiene (Hull, 2014), and changing planting dates (Hull, 2014). However, these measures offer no effective and permanent solution to control virus disease in the field (Hull, 2014). Maury et al. (1998) also proposed using virus-free seeds to control viral transmission between host plants. It is feasible to monitor the manifestation of viruses in seeds and to certificate the virus-free seeds by serological techniques. However, the production of antisera for this technique is lengthy, unpredictable, and costly (Rubio et al., 2020).

To date, there is no available compound to cure plants infected with viruses (Faoro & Gozzo, 2015). However, chemical pesticides are commonly used to control viral vectors. Hull (2014) divided

vectors into air-borne and soil-borne. Insecticides can be used to control air-borne vectors, for example, insects in Family *Aphididae*, while to control the soil-borne virus, fungicide is used for the fungal-transmitted virus, and nematicide for the nematode-transmitted virus. Therefore, to approach the effective management of insect vectors in the transmission of viruses, it is crucial to identify the vectors, which is sometimes difficult (Hull, 2014). Another issue appeared when Castle et al. (2009) found *Bemisia tabaci* and *Myzus persiscae* as vectors of cucurbit yellow stunting disorder virus that are likely to develop resistance to the insecticide. Moreover, improper and long-term use of pesticides is the main issue for human and environmental health (Mrema et al., 2013).

Using plant-resistant variety to manage viral infection is the favored control strategy because it is highly effective and has a minimum deleterious effect on the environment (Kang et al., 2005). A resistant cultivar can be achieved by Mendelian inheritance, finding natural resistance genes, and genetic engineering. However, the durability of resistant cultivars is not permanent because of the ability of viruses to mutate and thus counters the resistance (Garcia-Arenal et al., 2003). For instance, for many decades, potato resistance cultivar USDA 4195 had been considered immune to PVX, although the mutated virus was discovered to be able to infect this plant.

1.6.1 Acibenzolar-S-methyl (ASM) treatment to suppress viral infection

Synthetic chemicals called plant activators (PA) are proposed as crop protection practices due to their function to induce plant defense responses. S-methyl benzo[1,2,3]thiadiazole-7-carbothiate or acibenzolar-*S*-methyl (ASM) is the first commercial product of PA that is marketed under the trade names BION®, ACTIGARD®, and BOOST®. ASM mimics the function of SA in restricting infection by plant viruses (Vlot et al., 2009; Oostendorp et al., 2001; Pieterse et al., 2012; Murphy et al., 2020; Matsuo et al., 2019; Ishiga et al., 2020, 2021; Noutoshi et al., 2012; Takeshita et al., 2013). Matsuo et al. (2019) found that ASM-mediated defense requires the *NPR1* gene to suppress the infection of PlAMV.

In the field trial, ASM treatment with doses 12-37 g/ha successfully reduced the disease symptoms of TMV, CMV, and potato virus Y up to 60% in tobacco plants (reviewed in Oostendorp, 2000). Meanwhile, in the lab trial, ASM treatment reduced symptoms severity and delayed disease progression of the insect-borne virus, for instance, CMV and cucurbit yellow stunting disorder virus in melon plants (Kenney et al., 2020). In a previous study, we found that pre-treatment of *N. benthamiana* with ASM restricted infection by three viral species, PlAMV and PVX from the genus *Potexvirus*, and turnip mosaic virus (TuMV) from the genus *Potyvirus* in the inoculated cells. ASM delayed PlAMV replication and long-distance movement, but did not restrict cell-to-cell movement. Furthermore, the delayed long-distance movement of PlAMV by ASM was not due to the suppression of viral accumulation in the inoculated leaves, indicating that ASM restricts PlAMV infection in at least two independent steps (Matsuo et al., 2019). The detailed mechanism of ASM-mediated delay on long-distance movement will be explained in the following chapters.

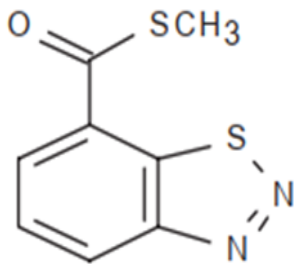

Figure 1.3 A molecular structure of acibenzolar-*S*-methyl (ASM). Figure adapted from Oostendorp et al. (2000).

1.7 Research objectives

Concerning our previous findings, ASM treatment restricted viral replication and long-distance movement but did not restrict cell-to-cell movement. Thus, it is of interest to elucidate the mechanism by which ASM delays the long-distance movement of PlAMV. In order to elucidate when and where ASM delays the long-distance movement of PlAMV, I carried out the experiment by using fluorescence microscopy to monitor the cell-to-cell and long-distance movement of PlAMV-GFP and investigate the accumulation and localization of PlAMV-GFP in the vascular tissues. This study was conducted with the following objectives: to evaluate the effect of ASM on loading (1), translocation (2), and unloading (3), and analyze the function of callose deposition in ASM-mediated restriction of long-distance movement of PlAMV-GFP (4). I divided the results into five chapters:

1. ASM treatment delays loading of PlAMV in an inoculated leaf
2. ASM treatment reduces viral accumulation in vascular tissues of the main stem.
3. Downward movement of PlAMV-GFP in the main stem is not essential for ASM-mediated delay of systemic infection.
4. ASM treatment affects the eventual viral localization and reduces its accumulation in sink organs.
5. ASM-mediated restriction on the loading of PlAMV is callose deposition-independent.

CHAPTER 2
MATERIALS AND METHODS

2.1. Plant materials and ASM treatment

Nicotiana benthamiana plants were grown in a growth chamber under a 16/8 light/dark cycle at 25˚C. ASM (50% by weight active ingredient; Actigard®, Syngenta, Tokyo, Japan) was dissolved in water containing 0.004% by volume Silwet L-77 (Nippon Unicar, Kanagawa, Japan) to a final concentration of 1 mM. Water containing Silwet L-77 was used as a control. One-fully and expanded upper leaf of *N. benthamiana* (thirty-day-old) was sprayed with ASM and control by foliar spraying about three times and incubated in the same condition with the growth condition (Matsuo et al., 2019).

2.2 Agroinfiltration and Purification of PlAMV-GFP

In this study, we used GFP-expressing plantago asiatica mosaic virus (PlAMV-GFP), whose GFP is expressed as a fusion protein with its coat protein. The fusion protein is cleaved after translation via the foot-and-mouth disease virus (FMDV) 2A peptide (Minato et al., 2014; Fig. 2.1).

Agrobacterium tumefaciens harboring a binary plasmid of PlAMV-GFP (preserved in 50% sterile glycerol) was cultured in 4 ml of 2 x YT liquid medium (16 g tryptone, 10 g yeast extract, 5 g NaCl/1000 ml) containing 100 mg/L kanamycin in the shaker incubator at 180 rpm, 28˚C, for 24 h. *A. tumefaciens* cells were harvested by centrifugation (5000 rpm) for 15 min at 28˚C and resuspended in agroinfiltration buffer (10 mM MES, 10 mM $MgCl_2$, 200 μM acetosyringone, pH5.6) to an optical density at 600 nm=1.0. The resuspended culture was incubated for three hours at room temperature in the dark and infiltrated to mature *N. benthamiana* leaves. Inoculated plants were incubated in the same condition as a growing condition for ten days. The upper leaves that showed the massive accumulation of GFP fluorescence were harvested for virion purification (Matsuo et al., 2019).

Purification of PlAMV-GFP was performed as described previously (AbouHaidar et al., 1998) with slight modifications. PlAMV-GFP-infected upper leaves were ground into a fine powder by liquid N_2 and suspended in the extraction buffer (0.067 M phosphate buffer, pH 7.0, containing 10 mM EDTA and 0.2% β-mercaptoethanol) of about 3 ml/g of leaves. Then, the homogenized mixture was filtrated through two layers of Miracloth (Merck Millipore, Darmstadt, Germany). *n*-butanol was added to this solution to a final concentration of 6% and mixed by stirring for 45 min on ice. Next, the supernatant was collected by centrifugation (9,500 rpm) for 15 min at 4˚C. Virions were precipitated from the supernatant by adding polyethylene glycol (PEG) #6000 (Nacalai Tesque, Inc., Kyoto, Japan) to a final concentration of 8% in the presence of 2% NaCl and 2% of Triton X-100, and the mixture were homogenized by stirring for 60 min on ice. Then, pellets were collected by centrifugation (9,000 rpm) for 15 min at 4˚C and resuspended in 0.2 M of PBS containing 0.002 % (w/v) $MgCl_2$ without vortexing. Virus solutions were incubated for about five days by rotating at 4˚C.

After incubating, the solutions were centrifugated at 8,000 rpm for 15 min at 4˚C to collect the supernatant. The supernatant was overlaid onto sucrose cushion solution (30 % (w/v) sucrose in 0.067 M PBS pH 7.0). Virions of PlAMV-GFP were pelleted by ultracentrifugation at 50,000 rpm for 3 h at 4˚C. The pellets were precipitated with 30 µl/g of leaves of PRI water (1 ml of RNase-free water (Funakoshi, Tokyo, Japan) containing 4 µl/ml (v/v) of recombinant RNase Inhibitor (Takara Bio, Shiga, Japan). The concentration of virions of PlAMV-GFP was measured by NanoDrop 1000 spectrophotometer (Thermo Fisher Scientific, Massachusetts, USA). The standard of viral purity (A260/A280 ratio) is 1.2 for potexviruses and viral concentration (µg/µl) was obtained by dividing absorbance 260 nm by three. The purified virions were stored at -80˚C until use.

2.3 *Virus inoculation and visual observation of GFP fluorescence*

Three days after spraying with ASM or water, the purified virions of PlAMV-GFP were mechanically inoculated to the ASM or water-treated leaves using carborundum as an abrasive (Matsuo et al., 2019). The virions were used to inoculate ASM-treated or water-treated leaves with virus titers, that can produce about 20–30 GFP lesions per leaf. The inoculated plants were incubated in a chamber under the same conditions as described above. Infectivity of *N. benthamiana* was evaluated by observing GFP fluorescence (Fig. 2.2). Fluorescent images of inoculated leaves, stems, and upper leaves of the plant inoculated with PlAMV-GFP were acquired using a handheld UVGL-58 UV lamp (Funakoshi, Tokyo, Japan) and EOS 90D camera (Canon, Tokyo, Japan), with an exposure time of 8 sec. The numbers of fluorescent spots in each image were counted manually.

2.4 *Evaluation of systemic infection by detachment of inoculated leaves*

An inoculated leaf with petiole was detached from *N. benthamiana* plant using a sterile razor blade, each day between 3 and 9 days post-inoculation (dpi). Systemic infection by PlAMV-GFP in the upper leaves and the main stem was evaluated at 15 dpi based on visual observations of GFP fluorescence under a UV lamp. This experiment was repeated twice with three plants per detaching day.

Figure 2.1 The genome structure of PlAMV expressing green fluorescent protein (PlAMV-GFP). A diagonally hatched boxes represent FMDV 2A peptide. ORF1 encodes RNA dependent RNA polymerase; ORF2, ORF3, ORF4 encode triple gene block proteins; ORF5 encodes coat protein (CP). Figure was adapted from Minato et al. (2014).

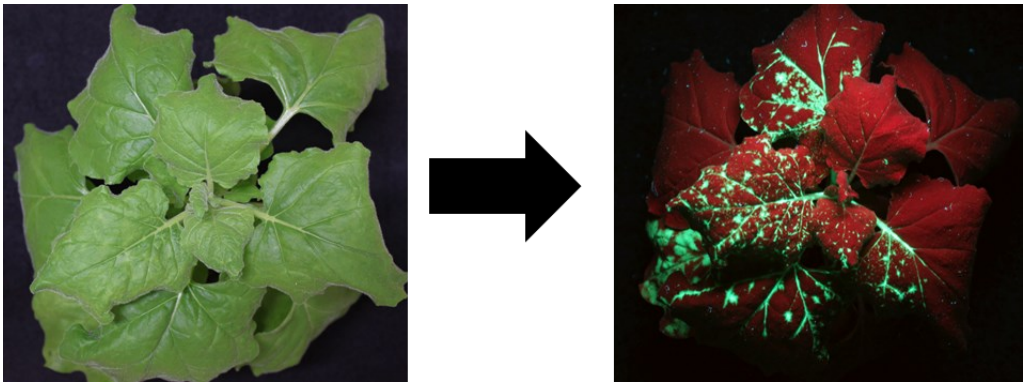

Figure 2.2 Infection with PlAMV-GFP does not cause severe symptoms in *Nicotiana benthamiana* (left panel), but its infectivity can be evaluated by observing GFP fluorescence (right panel, GFP is shown as green color). The photograph in systemic leaves were taken under UV light at 15 dpi.

2.5 RNA extraction

Total RNA was extracted from various parts of ASM-treated and control plants at 3, 4, 6, and 9 dpi using ISOGEN reagent (Wako, Osaka, Japan) following the manufacturer's instruction with slight modification. Plant parts included the petiole of the inoculated and upper leaves (leaf base) (Fig. 2.3), one internode of stem above and below the inoculated leaf, the basal stem (located below the hypocotyl leaves), and the primary root were cut about 10 mm to extract their total RNAs (Fig. 2.4). The samples were ground into a fine powder by liquid N_2 and added with 1 ml of ISOGEN reagent. Then, this mixture was centrifugated at 15,000 rpm for 8 min or 10 min for stems and roots at 4˚C. Chloroform (200 µl/sample) was added into the resultant supernatant with vortexing for about 15 s and centrifugated at 15,000 rpm for 10 min at 4˚C. Total RNAs from the supernatant were

precipitated with 500 µl 2-propanol (for 500 µl supernatant) and incubated for 20 min at room temperature. Pellets containing total RNAs were collected by centrifuge at 15,000 rpm for 20 min or 30 min for stems and roots at 4˚C. Pellet was rinsed with 1 ml of 70% ethanol followed by centrifugation at 15,000 rpm for 5 min at 4˚C. Afterward, the supernatant was discarded, and the pellet was air-dried at room temperature for about 5 minutes. The pellets were redissolved in 30 µl PRI water, and total RNAs concentration (ng/µl) was evaluated using NanoDrop 1000 spectrophotometer.

2.6 Detection of RNAs by RT-PCR and quantitative RT-PCR

About 500 ng of total RNA was reverse transcribed into cDNA using PrimeScript™ Reverse Transcriptase (Takara Bio) according to the manufacturer's instruction. Reverse-transcription PCR (RT-PCR) was performed using KOD FX Neo (Toyobo, Osaka, Japan) with the following conditions: 2 min at 94˚C followed by 35 cycles 98˚C for 10 s, 55˚C for 30 s, and 68˚C for 1 min, ending with 68˚C for 7 min. The primer pair PlAMV uni-F4 (5′-CTCTCRGGVCTCATHYTWYTACT-3′) and PlAMV uni-R4 (5′-TAAGTTTGRCRATRCGTGGA-3′) was used to amplify the overlapping region corresponding to the triple gene block (TGB) proteins 2 and 3 into 3′ untranslated regions of the PlAMV-GFP genomic RNA. Resultant PCR products were electrophoresed in 1% agarose gel at 135 volt for 25 min. 1 kb DNA ladder (#N3232S, New England BioLabs, Massachusetts, USA) was used to identify the approximate size of DNA. After the gel electrophoresis, DNA was stained with ethidium bromide for 20 min and DNA was visualized with UV transilluminator at time of exposure is 1 min. The image of gel was photographed with the polaroid camera.

For quantitative RT-PCR (RT-qPCR), about 2,000 ng of total RNAs of each sample were treated with RQ1 RNase-free DNase (Promega, Wisconsin, USA) and about 1,000 ng of DNase-treated total RNA were reverse transcribed using SuperScript® IV Reverse Transcriptase (Thermo

Fisher Scientific, Lithuania) following manufacturer protocols. For monitoring PlAMV RNA accumulation, synthesized cDNA was used for RT-qPCR by using the Thermal cycler dice real-time system II MRX [TP960] (Takara Bio) with GoTaq qPCR master mix (Promega) with the following condition: enzyme activation at 95 ˚C for 2 min, followed by 40 cycles at 95˚C for 5 sec and 60 ˚C for 30 sec. The dissociation protocol is added after the final PCR cycle. *18S rRNA* was used as the internal standard. The primer sets used for RT-qPCR were: PlAMV-3877F (5′-CCTCATTCTCCCTGCTGAAG-3′) and PlAMV-4010R (5′-CTTGAGGGGGTCTTTGATGA-3′) (Tanaka et al., 2019). Nb18S-193F (5'-ATA CGT GCA ACA AAC CCC GAC-3') and Nb18S-280R (5'-TGA ATCATCGCAGCAACG G-3') for *18S rRNA* (Hashimoto et al., 2012). The standard curve for PlAMV is y= -3.333ln(x)+23,8 and for *18S rRNA* is y= -3.527ln(x)+12.94 (Matsuo et al., 2019). Thermal Cycler Dice® Real Time System (Takara) was used for analyzing the result. This experiment was repeated twice with three plants each, with and without ASM treatment.

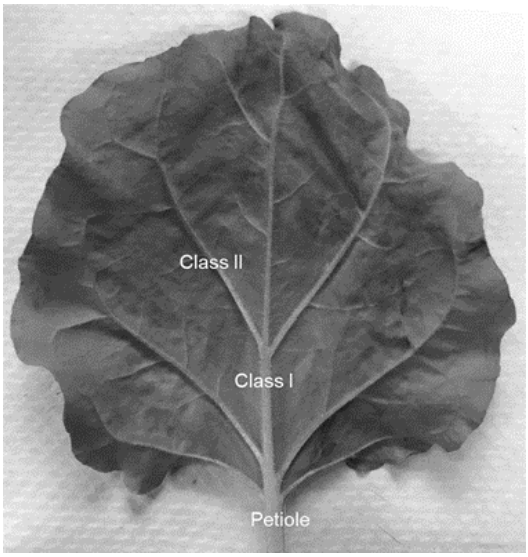

Figure 2.3 Illustration of a position of sampling in *N. benthamiana* leaf: major veins of class I and class II and leaf base (petiole) of the inoculated leaf.

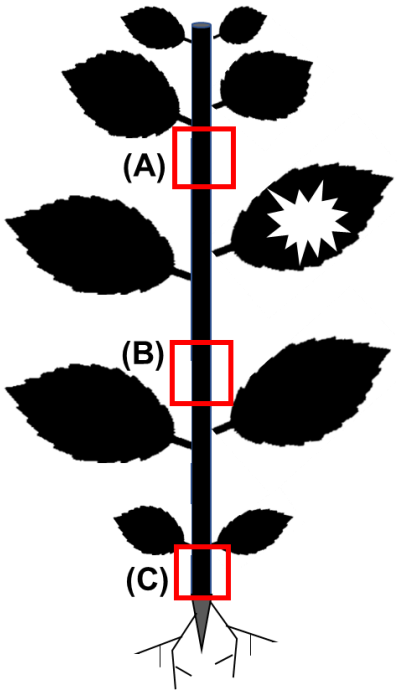

Figure 2.4 Illustration of the positions of the stem segments of *N. benthamiana* of one internode of stem above (A), stem below (B) the inoculated leaf, and the basal stem (located below the hypocotyl leaves) (C) (indicated by red boxes). The inoculated leaf indicated by a white star.

2.7 Cryohistological Protocols and Confocal Laser Scanning Microscopy (CLSM)

Cryohistological preparation was performed as described previously (Kawamoto & Kawamoto, 2014; Knapp et al., 2012) with slight modifications. Plant tissues, including major veins of class I and II, petiole (leaf base) of the inoculated and upper leaves (Fig. 2.3), and stems were vacuum-infiltrated with 4% paraformaldehyde fixation solution (Knapp et al. 2012) for 3 h at room temperature then moved to 4˚C for overnight incubation. The fixation solution was replaced with phosphate-buffered saline (PBS, pH 7.0) and the samples were incubated for 15 min. PBS was then replaced with 20% sucrose and the samples were left at 4˚C overnight. The samples were embedded

in super cryoembedding medium (SCEM; SECTION-LAB, Hiroshima, Japan) as described by Kawamoto and Kawamoto (2014). The SCEM-frozen blocks with the samples were sectioned using a cryostat CM3050S (Leica Microsystem GmbH, Wetzlar, Germany) with the blade angle at 5˚. The sectioned samples (10 μm thickness) were adhered to 2.5-cm wide cryofilm type 2C(9) (SECTION-LAB, Hiroshima, Japan) and incubated inside a cryostat for two hours. The cryofilm was then placed on Platinum Pro adhesive glass slides (Matsunami Glass, Osaka, Japan) and washed with PBS for 45 min. After PBS was dried at room temperature, the samples were mounted in ProLong™ Diamond Antifade Mountant (Thermo Fisher Scientific) according to the manufacturer's instructions, and covered with micro slide covers with 0.12–0.17 mm thickness (Matsunami Glass). The sectioned samples were imaged using a confocal laser scanning microscope LSM-710-NLO (Carl Zeiss, Jena, Germany) with a Plan-Apochromat 40 x/0.95 Korr M27 objective lens. Argon lasers with 405 nm and 488 nm excitation beams were used for detection of Fluorescent brightener 28 and GFP, respectively. ZEN 2012 software was used for image processing. This experiment was repeated twice with three plants each, with and without ASM treatment. Microscopy observations were conducted with 6 sections in each repetition.

2.8 Steaming treatments

Six-week-old *N. benthamiana* plants were used for steaming treatments. One internode of the main stem below an ASM-treated or untreated leaf was treated with a jet of steam generated by boiling water for about 15 s (Mochizuki et al., 2016; Wan et al., 2015) with boiling stone (Nacalai Tesque, Kyoto, Japan) was used to keep the temperature. The ASM-treated or untreated leaf was inoculated with virions of PlAMV-GFP at 6 hours after the steaming treatment. Systemic infection of PlAMV-GFP in the upper leaves and the main stem was evaluated at 14 dpi. The destroyed cells in the stem

were observed using cryohistological protocols as described above. This experiment was repeated independently three times with three plants each time.

2.9 Callose staining in a phloem sieve plate

Callose staining was conducted as described previously (Barrat et al., 2010; Zavaliev & Epel, 2015). 0.01% (w/v) aniline blue (Sigma Aldrich) solution in 0.1 M sodium phosphate buffer (pH 11) was incubated for about 48 h at room temperature before use to decolorize the solution followed by filtering through a Millipore filter (Merck Millipore 0.45 μm, Carrigtwohill, Ireland) to storage for about one week. One entire inoculated leaf with petiole of infected *N. benthamiana* at 9 dpi was gently submerged in 96% ethanol overnight at room temperature in the dark. The petiole (leaf base) and major vein of class I were trimmed for about 1 cm using a sterile razor blade and incubated in sterilized water containing 0.01% Tween-20 for 1 h. Afterward, the samples were gently dried by wipes and embedded in 5% agar (Nacalai Tesque, Kyoto, Japan). Microslicer DSK-1000 (Dosaka EM CO., LTD, Kyoto, Japan) was used for sectioning the samples (80-100 μm), and the sectioned samples were incubated in decolorized 0.01 % aniline blue solution described above for about 15 min. The sectioned samples were then washed with PBS three times and placed on micro slide glass with thickness of 0.8-1.0 mm (Matsunami Glass). PBS and micro slide covers with 0.12–0.17 mm thickness were used for mounting and covering the sectioned samples, respectively. The sectioned samples were imaged using the epifluorescence microscope Olympus BX-50 (Olympus, Tokyo, Japan) with filter for CFP XF 88-2 (Olympus), and Plan-Apochromat 20 x was used as the objective lens.

2.10 Statistics

The RT-qPCR results were analyzed in a one-way analysis of variance (ANOVA) using R version 3.6.0 (R Core Team, 2019) and the post-hoc Student's *t* test at the confidence level of 95%, to evaluate statistically significant differences between the data.

CHAPTER 3
ASM TREATMENT DELAYS LOADING OF PLAMV IN AN INOCULATED LEAF

3.1 *Introduction*

To start the long-distance movement, plant viruses load into phloem vascular tissues in the initially infected plant parts. The first step in this process involves cell-to-cell movement through nonvascular tissue via small apertures of the plasmodesmata (PD) in the mesophyll, bundle sheath (BS), and vascular parenchyma (VP) cells. Finally, viruses cross the specialized branched PD connections known as plasmodesmal pore units (PPUs) to load into the phloem sieve elements (phloem SEs) and move systemically. Once viruses are translocated in enucleated phloem SEs, viruses follow the source-sink transportation of photoassimilates (Hipper et al., 2013; Leisner et al., 1993).

The phloem SEs not only provide the allocation of photoassimilates, but also enables the rapid and systemic distribution of host components, for instance, amino acids, secondary compounds, RNAs (mRNA and tRNA), micro-RNAs, and small molecules involved in plant responses, including defense-related response, development, flowering, also gene regulation by RNA silencing (Kehr & Buhtz, 2007; Turgeon & Wolf, 2009). Due to the critical function of phloem SEs, PPUs exhibit an increased size exclusion limit (SEL), which allows host components to diffuse into phloem SEs without any specific interaction. In contrast, this increased SEL does not enable the movement of viral particles (virions or infectious ribonucleoprotein (RNP) complexes) into phloem SEs, because viral particles are much larger than the SEL of PPUs (Carrington et al., 1996; Leisner & Turgeon, 1993; Kappagantu et al., 2020).

The most well-studied barrier to the long-distance movement of plant viruses resides in the loading step, in particular, viral entry into the phloem SEs from the companion cells (CC) (Folimonova & Tilsner, 2018; Lucas & Gilbertson, 1996; Mekuria et al., 2008; Vuorinen et al., 2011). Restricting viral loading can confer the host plants resistance to the viruses (Hipper et al., 2013; Leisner & Howell, 1993; Navarro et al., 2019; Zhang et al., 2019).

Indeed, Revers et al. (2003) and Decroocq et al. (2006) found that the resistance of *Arabidopsis thaliana* accession Cvi-1 to potyviruses (i.e., lettuce mosaic virus and plum pox virus) was due to the restrictions in phloem loading, which prevented accumulation of the viruses in uninoculated leaves. Similarly, the restriction of systemic infection by cowpea chlorotic mottle virus (CCMV-S) in soybean accession PI 346304 was caused by blocks in viral loading into and/or viral unloading out from the vascular tissues (Goodrick et al., 1991). Furthermore, the confinement of virus to the inoculated leaves underlies the resistance of *A. thaliana* ecotype En-2 to cauliflower mosaic virus and the resistance of cucumber to tomato aspermy virus (1-TAV strain) (reviewed in Lucas & Gilbertson, 1996). However, the detailed mechanisms underlying the restriction of viral long-distance movement remain unknown.

Our previous study found that pre-treatment of plant defense activators, acibenzolar-*S*-methyl (ASM) restricted infection by potexvirus, plantago asiatica mosaic virus (PlAMV) in *Nicotiana benthamiana*. This treatment restricted viral replication and long-distance movement, but did not restrict cell-to-cell movement (Matsuo et al., 2019). Because the cell-to-cell movement was as efficient in ASM-treated leaves as in untreated leaves, the ASM-mediated delay in viral long-distance movement was not caused simply by the suppression of viral accumulation in the ASM-treated, inoculated leaves (Matsuo et al., 2019). ASM-mediated delay of the long-distance movement of PlAMV may occur either in the three steps involved in viral long-distance movement (loading into,

translocation inside, and unloading from phloem SEs). Therefore, in this chapter, we evaluated the effect of ASM treatment on the viral loading in the inoculated leaves.

3.2 Result

3.2.1 ASM treatment delays loading of PlAMV in an inoculated leaf

Our previous study has shown that pre-treatment of a leaf of *N. benthamiana* with ASM significantly delayed the long-distance movement of PlAMV-GFP (Matsuo et al., 2019). To analyze how this treatment restricted viral movement, I first examined the timeline between ASM treatment and the delay in long-distance movement. I treated young leaves (the third leaf from the top of each plant) of *N. benthamiana* plants with 1 mM ASM or water as a control. Then the leaves were inoculated with PlAMV-GFP at 3 days after treatment. The titer of PlAMV-GFP used to inoculate control leaves was adjusted to be lower than that used to inoculate the ASM-treated leaves, to produce similar number of fluorescent spots in each leaf (Matsuo et al., 2019; Fig. 3.1). Observation of the development of fluorescent spots throughout each inoculated leaf revealed that ASM treatment has no or negligible effects on the cell-to-cell movement of PlAMV-GFP, as reported previously (Matsuo et al., 2019; Fig. 3.1).

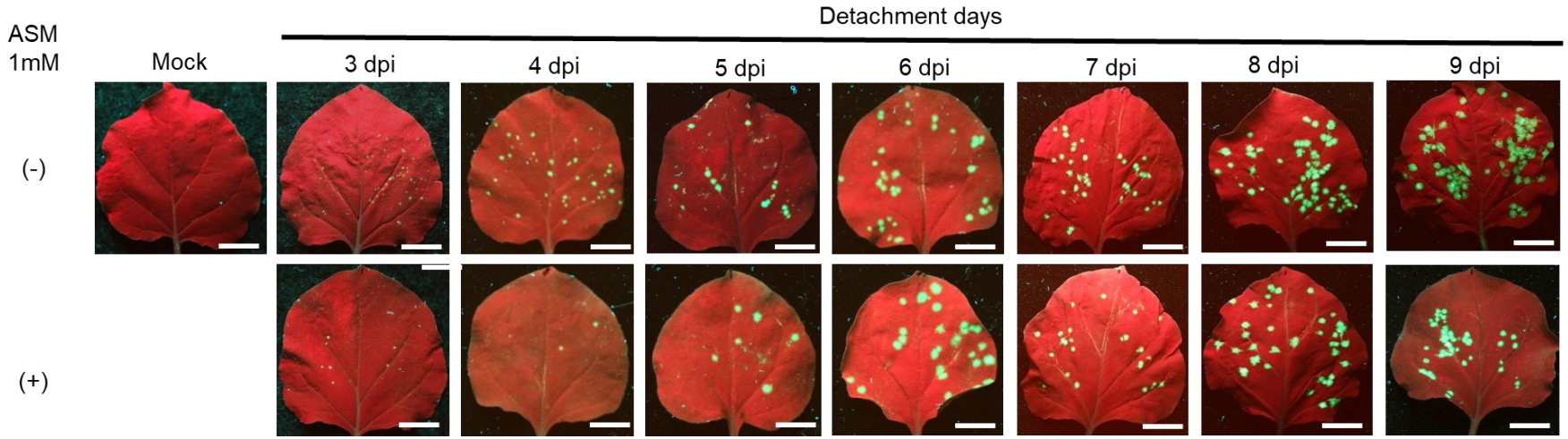

Figure 3.1 ASM-treated (+) or untreated control (-) leaves of *N. benthamiana* inoculated with PlAMV-GFP. Photographs were taken under a UV light at 3 up to 9 dpi prior detaching. Bars, 1 cm. The experiment was repeated twice with three plants for each treatment.

I used groups of treated and control *N. benthamiana* plants, and from 3 to 9 days post-inoculation (dpi), I detached the entire inoculated leaf, including the petiole, from six plants in each group. I then investigated the viral systemic infection at 15 dpi, which was visualized by GFP fluorescence in the upper uninoculated leaves. I expected that viral systemic infection would not occur when the inoculated leaf was cut off before the virus reached the vasculature, and it would occur when the inoculated leaf was cut off after virus successfully entered the vasculature.

As shown in Figure 3.2, viral systemic infection was not detected at 15 dpi in any control or ASM-treated plants when the inoculated leaf was detached at 3 dpi. Viral systemic infection was observed in five control plants when their inoculated leaves were detached at 4 dpi, and in all six control plants when the leaves were detached at 5 dpi or later (Fig. 3.2). These results indicated that without ASM treatment, PlAMV might enter the vasculature in the inoculated leaf between 3 and 4 dpi. In contrast, no sign of viral systemic infection was detected in any ASM-treated plants whose inoculated leaves were detached at 4 to 6 dpi. However, limited infection was observed in the upper leaves of four or all six ASM-treated plants when leaf detachment was done at 7 to 9 dpi. This result suggested that ASM treatment drastically delayed the entry of PlAMV into the vascular system in the inoculated leaves.

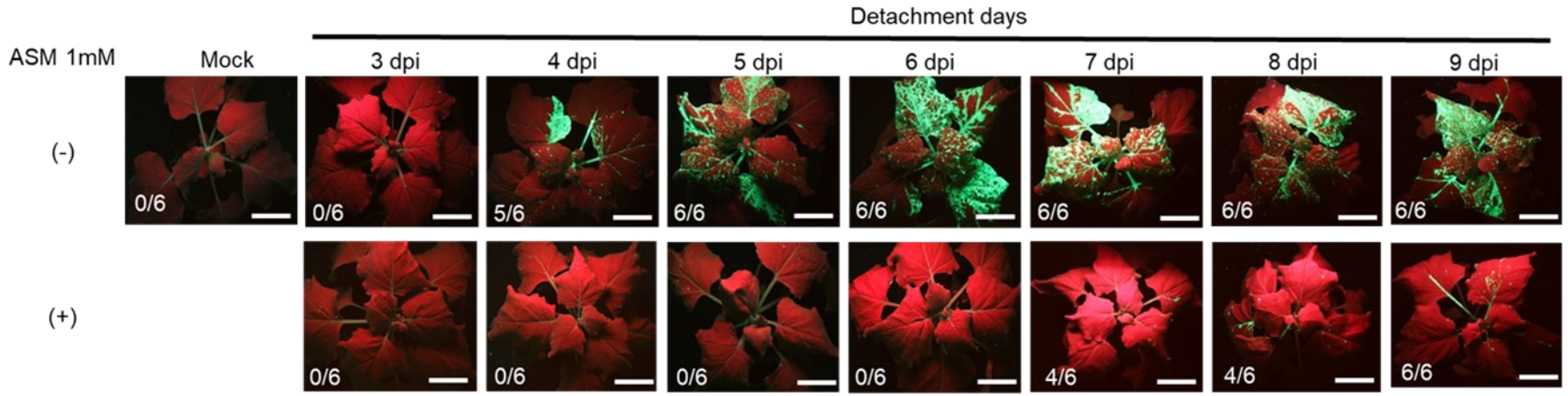

Figure 3.2 Observations of systemic infection of *N. benthamiana* plants by PlAMV-GFP following detachment of the inoculated leaves. The PlAMV-GFP-inoculated leaves were removed at 3 to 9 dpi, from either untreated plants (-; upper panels) or ASM-treated plants (+; lower panels). Uninoculated plants (Mock) were used as negative controls. Representative photographs were taken under a UV lamp at 15 dpi. The numbers within each photograph indicate the number of plants that showed systemic infection per total tested plants. Bars, 5 cm. The experiment was repeated twice with three biological replicates each.

To validate the conclusions from the detachment assay, I used RT-PCR to analyze the effect of ASM treatment on the long-distance movement of PlAMV-GFP. In this experiment, the inoculated leaves were not detached after virus inoculation. To clarify when PlAMV had reached the vasculature, I used RT-PCR to analyze the petioles of inoculated leaves at 3 and 4 dpi. No PlAMV RNA was detected in any samples of control or ASM-treated plants at 3 dpi (Fig. 3.3A). At 4 dpi, the presence of PlAMV RNA was confirmed in three of six control samples but not in any ASM-treated samples (Fig. 3.3B). These results confirmed that PlAMV could be loaded into the vascular system by around 4 dpi, and that this prerequisite step for long-distance movement is somehow inhibited by ASM treatment.

To further confirm the result from RT-PCR, I visually observed the viral accumulation in the vasculature. I prepared cryo-histological cross-sections of petiole from inoculated leaves at 3 and 4 dpi. Throughout this study, I evaluated cells with similarly high levels of GFP fluorescence intensity as virus-infected cells, and excluded from my evaluation those with faint and weak levels of GFP fluorescence intensity, which might be caused by autofluorescence or passive diffusion of free GFP.

As the result, GFP expression was not observed in the vascular tissues of petioles (i.e., the xylem and the adaxial/internal and abaxial/external phloem) in any control or ASM-treated plants at 3 dpi (Fig. 3.4A). Meanwhile, at 4 dpi, GFP expression was observed in the vascular tissues of petioles of control leaves but not of ASM-treated leaves (Fig. 3.4B). These observations are consistent with the RT-PCR results, which showed that by 4 dpi the virus could move into the petioles of untreated leaves (Fig. 3.3).

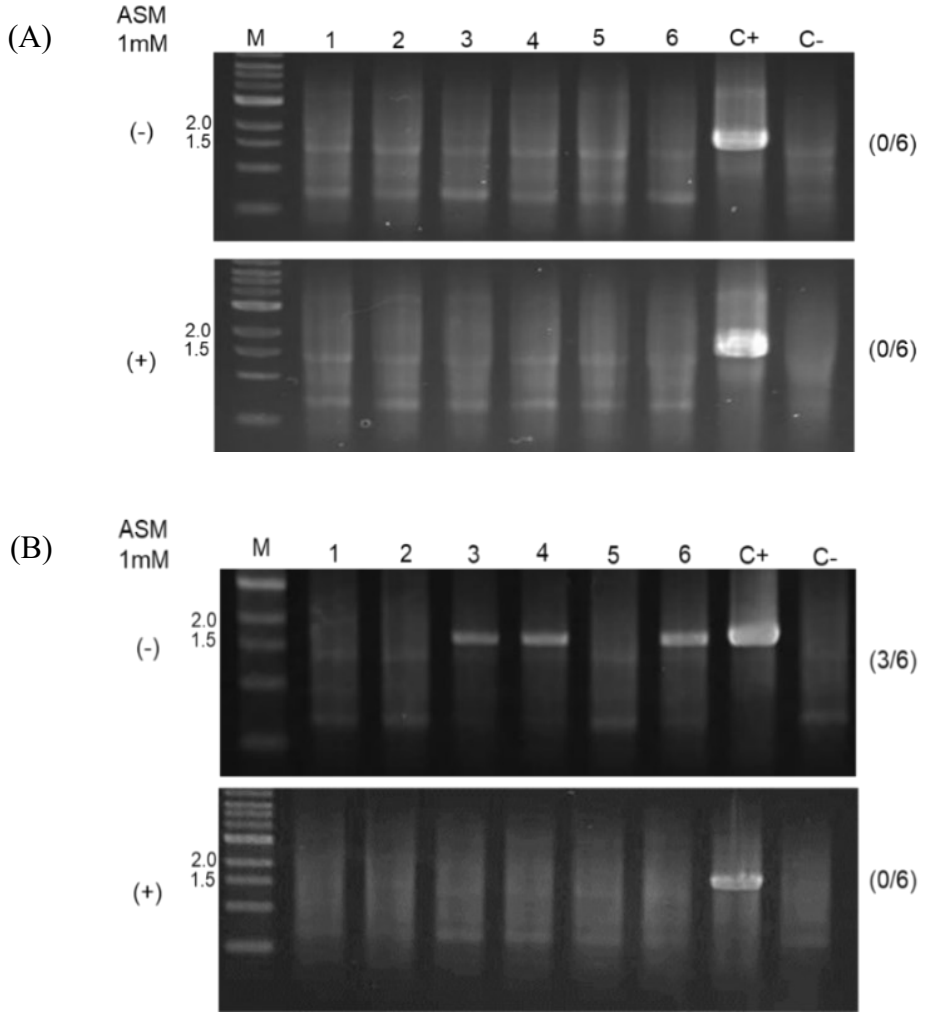

Figure 3.3 Result of RT-PCR to detect PlAMV-GFP RNAs in the petioles of inoculated leaves at 3 dpi (A) and 4 dpi (B). Lane M: 1 kb DNA ladder (#N3232S, New England BioLabs). Total RNA from PlAMV-GFP-inoculated leaves at 15 dpi and mock-inoculated leaves were used as positive (C+) and negative (C-) controls, respectively. The expected size of PCR products is 1.5 kb (approximately). Numbers at the right indicate the numbers of infected plants per total number of plants tested. The experiment was repeated twice with three biological replicates each.

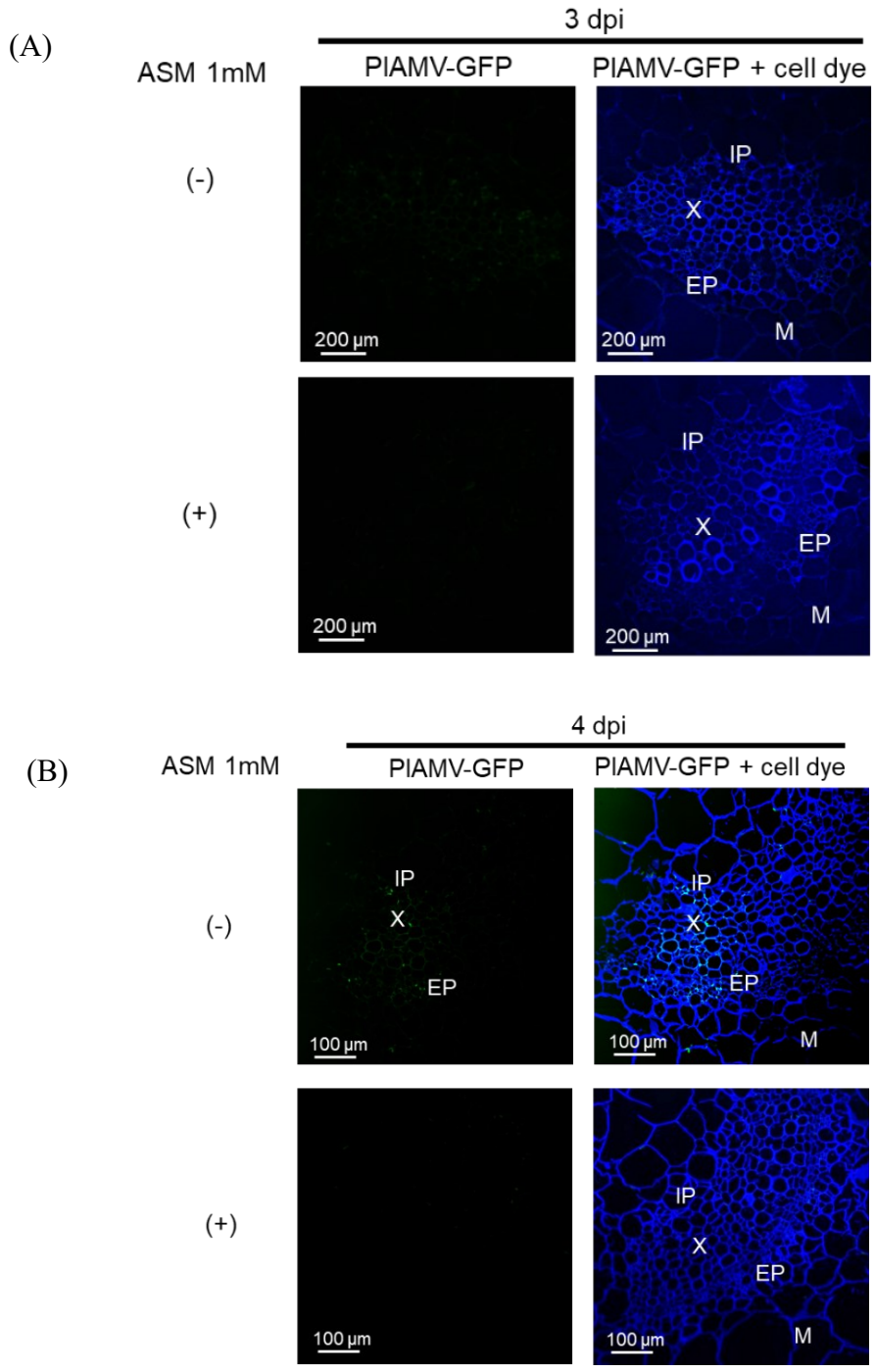

Figure 3.4 Viral accumulation in the vascular tissue in the petiole of the inoculated leaf at 3 dpi (A) and 4 dpi (B) from untreated plant (-) or ASM-treated plants (+). PlAMV accumulation is shown in green and Fluorescent Brightener 28–labeled plant cell walls is shown in blue. IP, internal phloem; EP, external phloem; X, xylem; M, mesophyll cells. Pictures are representatives of the two independents with three plants for each treatment.

3.2.2 ASM treatment reduces viral accumulation in the vascular tissues of inoculated leaf

The results shown above prompted me to analyze the differences in more detail the viral localization patterns in vascular tissues between ASM-treated and untreated control plants. To clarify this, I observed the major veins (classes I and II) in addition to the petiole (Fig. 2.3) of inoculated leaves at 9 dpi, when systemic infection of PlAMV-GFP was established both with and without ASM-treatment (Fig. 3.2).

Although faint autofluorescence was detected in the vascular tissues of mock-inoculated plants (Fig. 3.5), GFP-specific fluorescence was clearly distinguishable from the autofluorescence in the virus-infected leaves (Fig. 3.6). In the control plants, GFP fluorescence was observed widely in the vascular tissues (i.e., the xylem and the adaxial/internal and abaxial/external phloem) and/or in the mesophyll cells in the major veins and the petiole. GFP fluorescence in class II veins was largely limited to the adaxial and abaxial phloem cells (Fig. 3.6). GFP fluorescence in class I veins seemed to be distributed in the abaxial phloem and the mesophyll cells (indicated by the red arrow in panel II). The petiole showed another localization pattern, with GFP fluorescence in the internal and external phloem and in the mesophyll cells (indicated by red arrows in panels I and II in Fig. 3.6). On the other hand, the intensity of GFP fluorescence in the vascular tissues of the ASM-treated inoculated leaves was generally much weaker than in the untreated leaves (Fig. 3.7 compared to Fig. 3.6). In the class II veins, weak GFP fluorescence was observed in the abaxial phloem, the xylem, and mesophyll cells, but not in the adaxial phloem (Fig. 3.7, upper row). In the class I veins, GFP fluorescence was detected in all types of vascular tissues but not in the mesophyll cells (Fig. 3.7, middle row). In contrast with the class I veins, the weak GFP fluorescence in the petiole was detected in both the vascular tissues and the mesophyll cells (Fig. 3.7, bottom row). These results indicated that ASM treatment drastically reduced the viral accumulation in the vascular tissues of the main veins and the petioles of inoculated leaves, even though the virus did reach the vascular system.

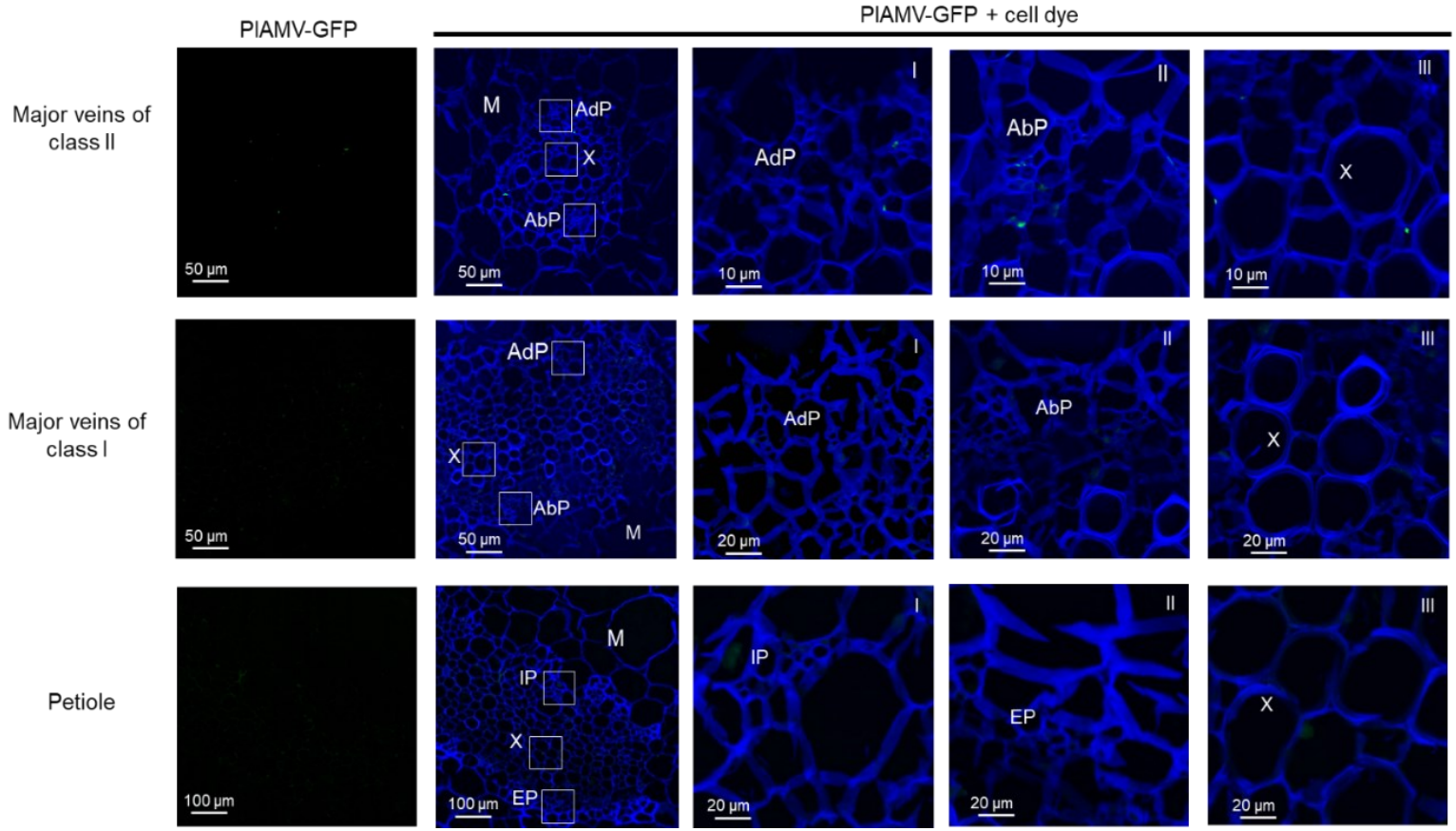

Figure 3.5 Cross sections of the major veins of class II, major veins of class I, and the petiole of the inoculated leaf of an ASM-untreated and mock-inoculated plants. The unspecific green fluorescence is shown in blurred green and Fluorescent Brightener 28–labeled plant cell walls are shown in blue. Panels with numbers I, II, III are enlarged images of vascular tissues for AdP/IP, AbP/EP, and X, respectively, in white boxes of panels of the left. PlAMV accumulation is shown in green and Fluorescent Brightener 28–labeled plant cell walls is shown in blue. AdP, adaxial phloem; AbP, abaxial phloem; IP, internal phloem; EP, external phloem; X, xylem; M, mesophyll cells. Pictures are representatives of the two independents with three plants for each treatment.

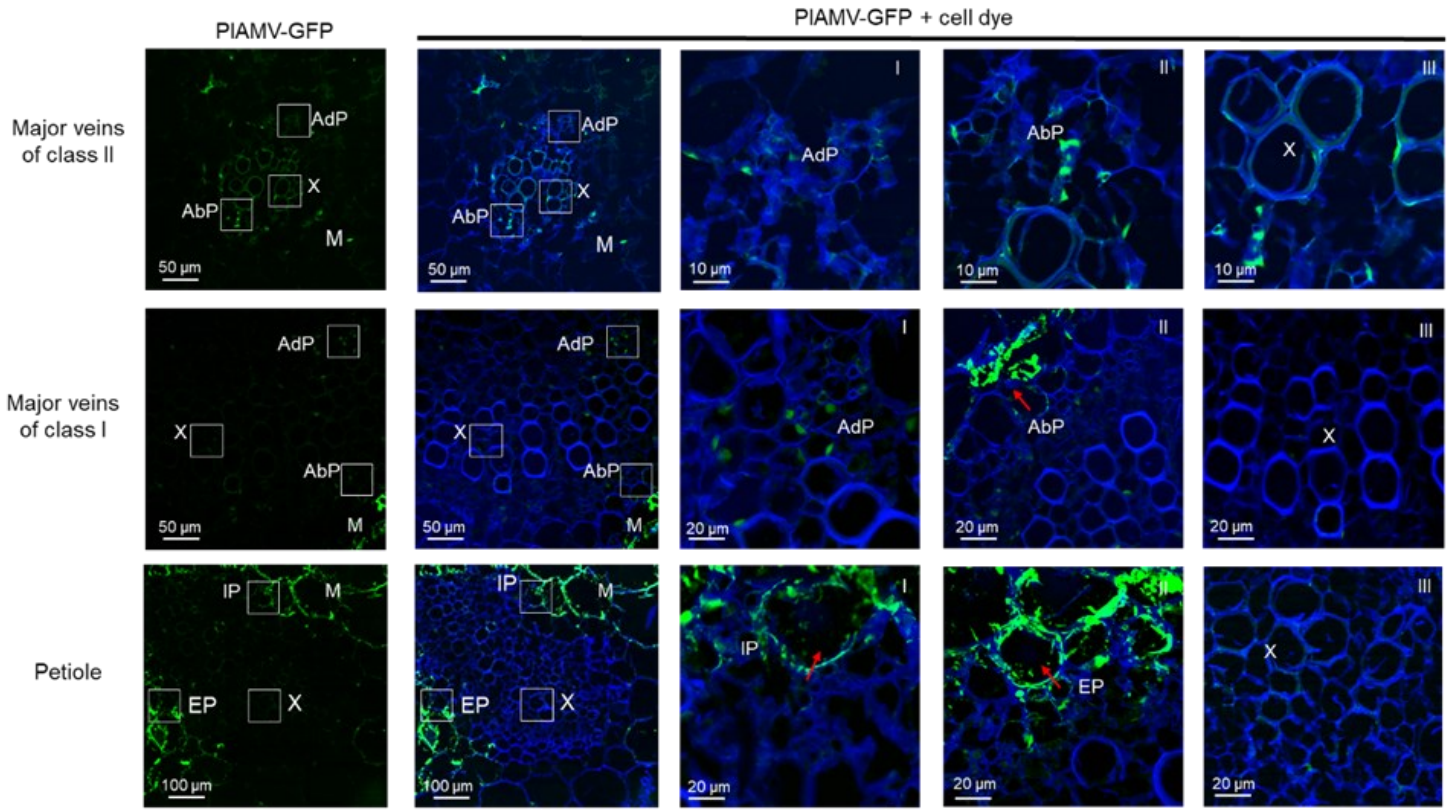

Figure 3.6 Effect of 1 mM ASM treatment on the viral localization in the vascular tissues of inoculated leaves at 9 dpi. Images of vascular tissues in untreated control plants. Upper panels, cross sections of major class II veins; middle panels, cross sections of major class I veins; lower panels, cross sections of petioles. Panels with numbers I, II, and III are enlarged images of the AdP/IP, AbP/EP, and X tissues, respectively, shown in white boxes in the panels on the left. PlAMV-GFP appears as green, and the Fluorescent Brightener 28-labeled plant cell walls are blue. AdP, adaxial phloem; AbP, abaxial phloem; IP, internal phloem; EP, external phloem; X, xylem; M, mesophyll cells. Red arrows indicate PlAMV-GFP in mesophyll cells. Pictures are representative of two independent experiments with three plants in each treatment.

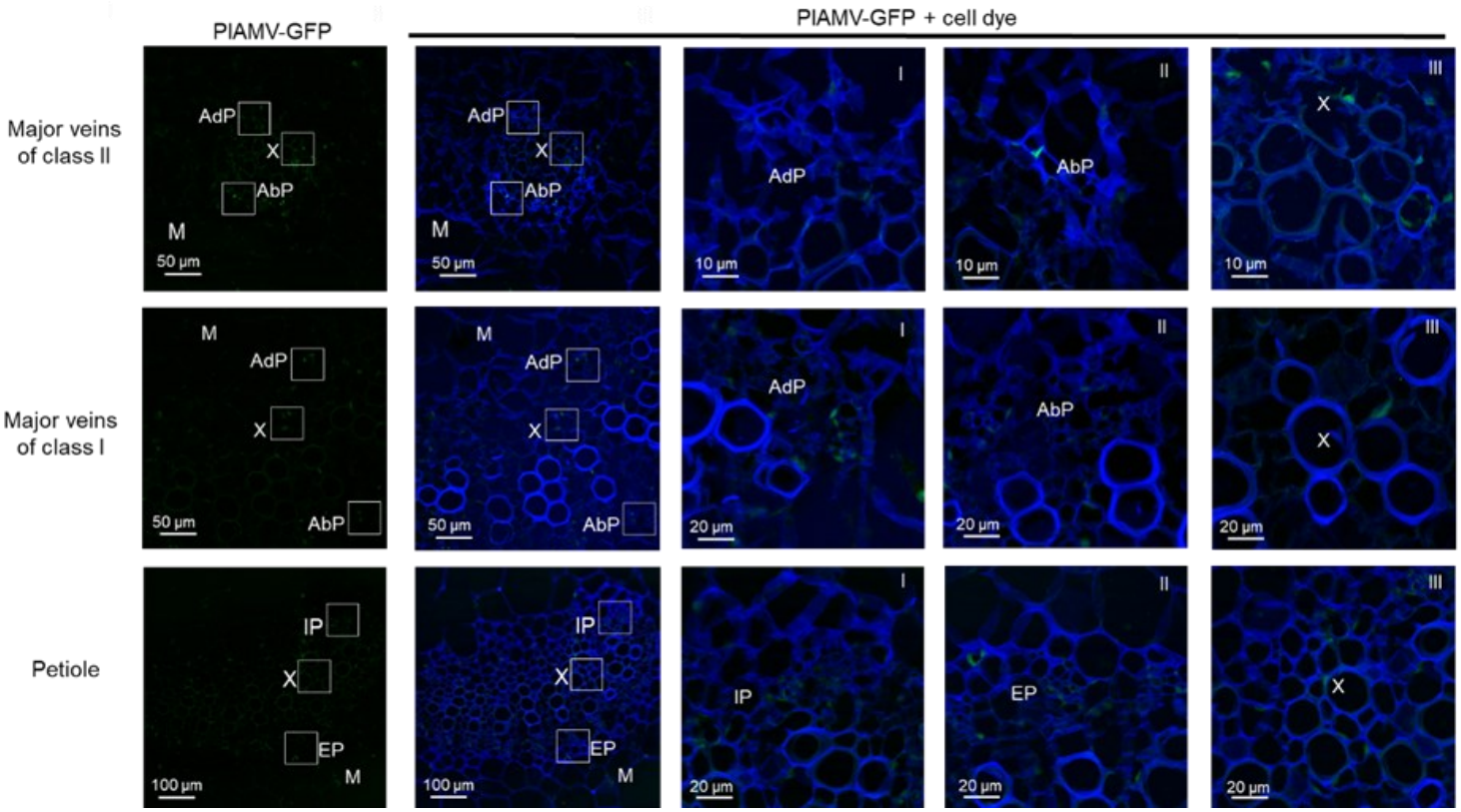

Figure 3.7 Effect of 1 mM ASM treatment on the viral localization in the vascular tissues of inoculated leaves at 9 dpi. Images of vascular tissues in ASM-treated plants. Upper panels, cross sections of major class II veins; middle panels, cross sections of major class I veins; lower panels, cross sections of petioles. Panels with numbers I, II, and III are enlarged images of the AdP/IP, AbP/EP, and X tissues, respectively, shown in white boxes in the panels on the left. PlAMV-GFP appears as green, and the Fluorescent Brightener 28-labeled plant cell walls are blue. AdP, adaxial phloem; AbP, abaxial phloem; IP, internal phloem; EP, external phloem; X, xylem; M, mesophyll cells. Red arrows indicate PlAMV-GFP in mesophyll cells. Pictures are representative of two independent experiments with three plants in each treatment.

CHAPTER 4
ASM TREATMENT REDUCES VIRAL ACCUMULATION IN VASCULAR TISSUES OF THE MAIN STEM

4.1 Introduction

After loading into phloem SEs, viruses translocate through phloem SEs from the inoculated leaf into distal uninfected tissues. For their translocation, viruses take the same route that the plant used to transport its photoassimilates (Leisner et al., 1993). Both viruses and photoassimilates are transported from the source (where photoassimilates are exported) to sink organs (where photoassimilates are imported) (Leisner et al., 1993). Plant family with specialization of phloem (bicollateral phloem) for example *Solanacearum*, photoassimilates are exported through external phloem into roots (downward movement), while imported through internal phloem into upper leaves (upward movement) (Turgeon, 1989). But some studies revealed that this bidirectional of assimilates can occur in the same type of phloem (Reviewed in Trip & Gorham 1967).

Some viruses, for instance, TMV (Cheng et al., 2000), cowpea mosaic virus (Silva et al., 2002), pepper mottle potyvirus (PepMoV) (Andrianifahanana, et al., 1997), and melon necrotic spot virus (MNSV) (Gosalvez-Bernal et al., 2008) are exported from the inoculated leaf toward roots by the external phloem, whereas they are exported the upward spread into developing young leaves by the internal phloem. In addition, Andrianifahanana et al. (1997) and Cheng et al. (2000) found that the viral upward movement occurs significantly faster than downward. Therefore, young leaves represent the major and preferential target for systemic movement (Ueki & Citovsky, 2007).

Several previous studies have found different patterns in the translocation of viruses between susceptible and resistant cultivars. For instance, in a susceptible pepper cultivar *Capsicum annuum* cv. Early Calwonder Florida, isolates PepMoV (PepMoV-FL) translocated in both external and

internal phloem (Andrianifahanana et al., 1997). On the other hand, in resistant pepper cultivar *C. annuum* cv. Avelar, PepMoV-FL only translocated in external phloem, but not in internal phloem, resulting in the young stem tissues free from viral systemic accumulation (Guerini et al. 1999). Interestingly, TMV (Cheng et al., 2000) and MNSV (Gosalvez-Bernal et al., 2008) failed to translocate in the internal phloem of shoot apical meristem in a susceptible host. Although the reason remains unclear, recent studies indicated that RNA silencing mechanisms might involve this exclusion (reviewed in Gosalvez-Bernal et al., 2008; Tournier et al., 2006).

In chapter 3, I found that ASM treatment delays the loading of PlAMV-GFP in the inoculated leaf and reduces its accumulation in the vascular tissues. In regard to this result, I assumed that the translocation of viruses from the inoculated leaf into the sink organs is also affected by ASM-mediated delays of loading of PlAMV-GFP. Therefore, in this chapter, I evaluated the effect of ASM treatment on the translocation of PlAMV-GFP in the stem of *N. benthamiana*. The direction of translocation of PlAMV-GFP in the vascular tissue in the stem was also discussed in this chapter.

4.2 Result

4.2.1 ASM treatment delays translocation of PlAMV-GFP in the stem

In chapter 3, I detached the inoculated leaf at the determined days-post inoculation and observed the systemic infection of PlAMV-GFP in the upper leaves. In addition to this observation, I also observed the systemic infection of PlAMV-GFP in the main stem at 15 dpi following detachment of the inoculated leaf. Although faint autofluorescence was detected in the main stem of mock-inoculated plants, GFP-specific fluorescence was clearly distinguishable from the autofluorescence in the virus-infected main stem (Figure 4.1). As shown in Figure 4.1, systemic infection of PlAMV-GFP was not detected at 15 dpi in any control or ASM-treated plants when the inoculated leaf was detached at 3 dpi. Systemic infection of PlAMV-GFP was observed in the main

stem of control plants when the inoculated leaves were detached at 4 to 9 dpi. In contrast, no systemic infection of PlAMV-GFP was detected in ASM-treated plants when the inoculated leaf was detached at 4 to 5 dpi. Meanwhile, systemic infection of PlAMV-GFP was firstly observed in the main stem of ASM-treated plants when inoculated leaf detachment was performed at 6 dpi. At this time point, systemic infection of PlAMV-GFP was not observed in the upper leaves of the ASM-treated plants (Fig. 3.2). Systemic infection of PlAMV-GFP was also detected in the ASM-treated plants when the inoculated leaves detached at 7-9 dpi. However, the accumulation of GFP fluorescence in the main stem of ASM-treated plants was generally weaker than in control plants. These results indicated that ASM treatment might delay the translocation of PlAMV-GFP.

This observation led me to examine whether ASM treatment inhibits the viral translocation of PlAMV-GFP in the main stem. For this experiment, I used plants at 6 dpi and prepared total RNA from three parts of the main stem: one internode above the inoculated leaf, one internode below the inoculated leaf, and the basal stem (Fig. 2.4). I used RT-PCR to analyze the RNA samples and found PlAMV RNA in the stems above the inoculated leaves in two of six control plants and in zero of six ASM-treated plants (Fig. 4.2A). In contrast, we found PlAMV RNA in the stems below the inoculated leaves in all six control plants and (at relatively weak levels) in five of six ASM-treated plants (Fig. 4.2 B). The presence of the virus was confirmed in the basal stem of all control plants but in none of the ASM-treated plants (Fig. 4.2C).

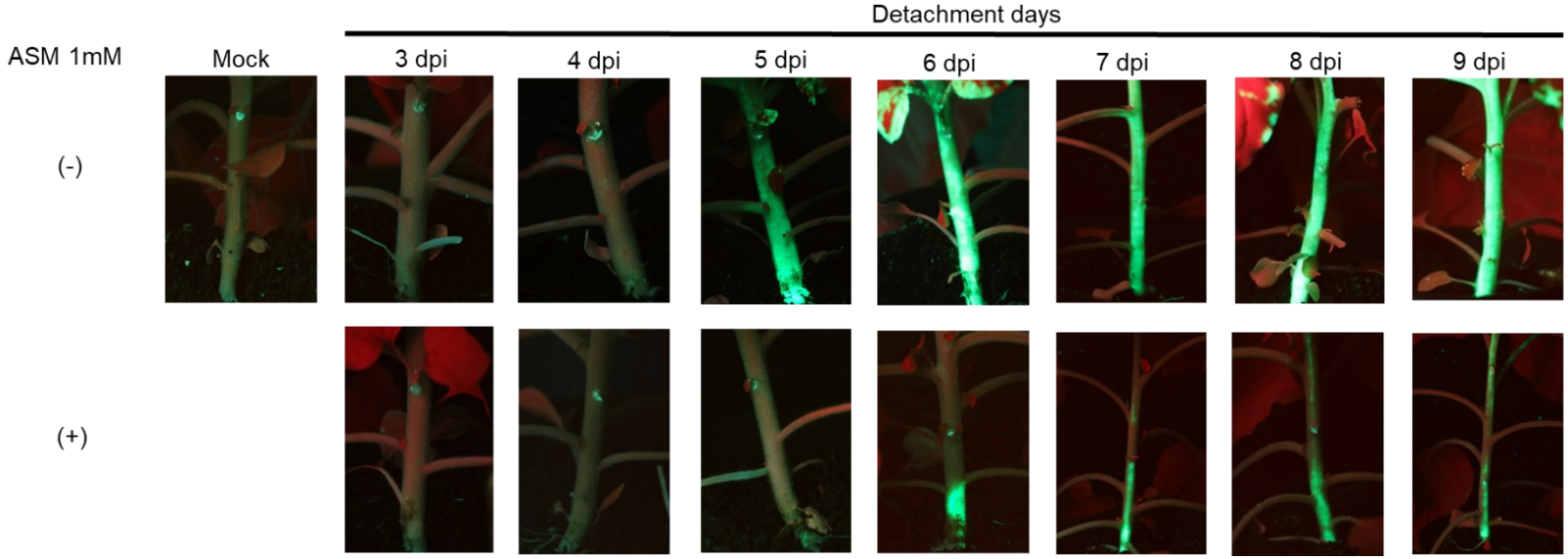

Figure 4.1 GFP expression in the main stem after detachment of the inoculated leaf. PlAMV-GFP-inoculated leaf was cut at 3-9 dpi, from either untreated plant (upper panels, shown as "(-)") or ASM-treated plants (lower panels, shown as "(+)"). Uninoculated plants (shown as Mock) were used as a negative control. Representative photographs were taken under a UV lamp at 15 dpi. The experiment was repeated twice with three plants for each treatment.

This observation led me to examine whether ASM treatment inhibits the viral translocation of PlAMV-GFP in the main stem. For this experiment, I used plants at 6 dpi and prepared total RNA from three parts of the main stem: one internode above the inoculated leaf, one internode below the inoculated leaf, and the basal stem (Fig. 2.4). I used RT-PCR to analyze the RNA samples, and found PlAMV RNA in the stems above the inoculated leaves in two of six control plants and in zero of six ASM-treated plants (Fig. 4.2A). In contrast, we found PlAMV RNA in the stems below the inoculated leaves in all six control plants and (at relatively weak levels) in five of six ASM-treated plants (Fig. 4.2 B). The presence of the virus was confirmed in the basal stem of all control plants but in none of the ASM-treated plants (Fig. 4.2C).

4.2.2 ASM treatment reduces viral accumulation in vascular tissues of the main stem

To confirm this result, I next examined the viral localization in the vascular tissues of the main stem by confocal microscopy at 9 dpi, when GFP fluorescence was constantly observed above and below the stem in ASM-treated plants. Faint non-specific autofluorescence was observed in the vascular tissues of the main stem in mock-inoculated plants (Fig. 4.3). GFP-specific fluorescence in vascular tissues, including the xylem and the external and internal phloem, was observed in the three parts of the main stems of both control and ASM-treated plants (Fig. 4.4 and 4.5). However, the areas of GFP fluorescence detected in the three stem parts were much more limited in the ASM-treated plants than in the control plants. In addition, RT-qPCR-based quantification of PlAMV RNA levels at 9 dpi confirmed that the ASM-treated plants had lower viral levels in all three parts of the main stem than the control plants did, although there were no statistically significant differences (Table 2). These results corroborated my conclusion that ASM treatment reduces the viral accumulation in the vascular tissues of the main stem as well as an in the inoculated leaf.

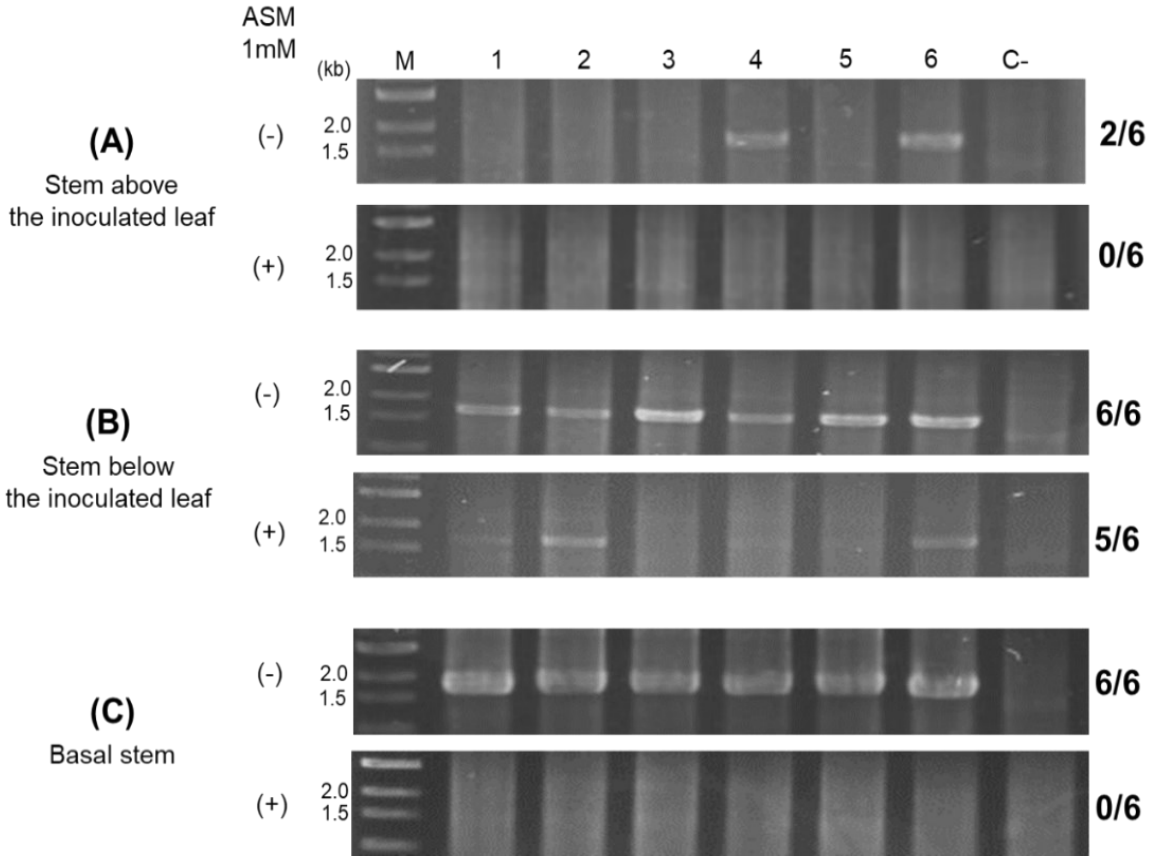

Figure 4.2 Detection of PlAMV-GFP within the main stem by RT-PCR at 6 dpi. Total RNA was extracted from the internode above the inoculated leaf (A), the internode below the inoculated leaf (B), or the basal stem (C) of untreated control (-) or ASM-treated (+) plants. Lane M: 1 kb DNA ladder. Total RNA from mock-inoculated leaves was used as a negative control (C-). Numbers at the right represent the numbers of infected plants per total number of plants tested. The expected size of PCR products is 1.5 kb (approximately). The experiment was repeated twice with three biological replicates each.

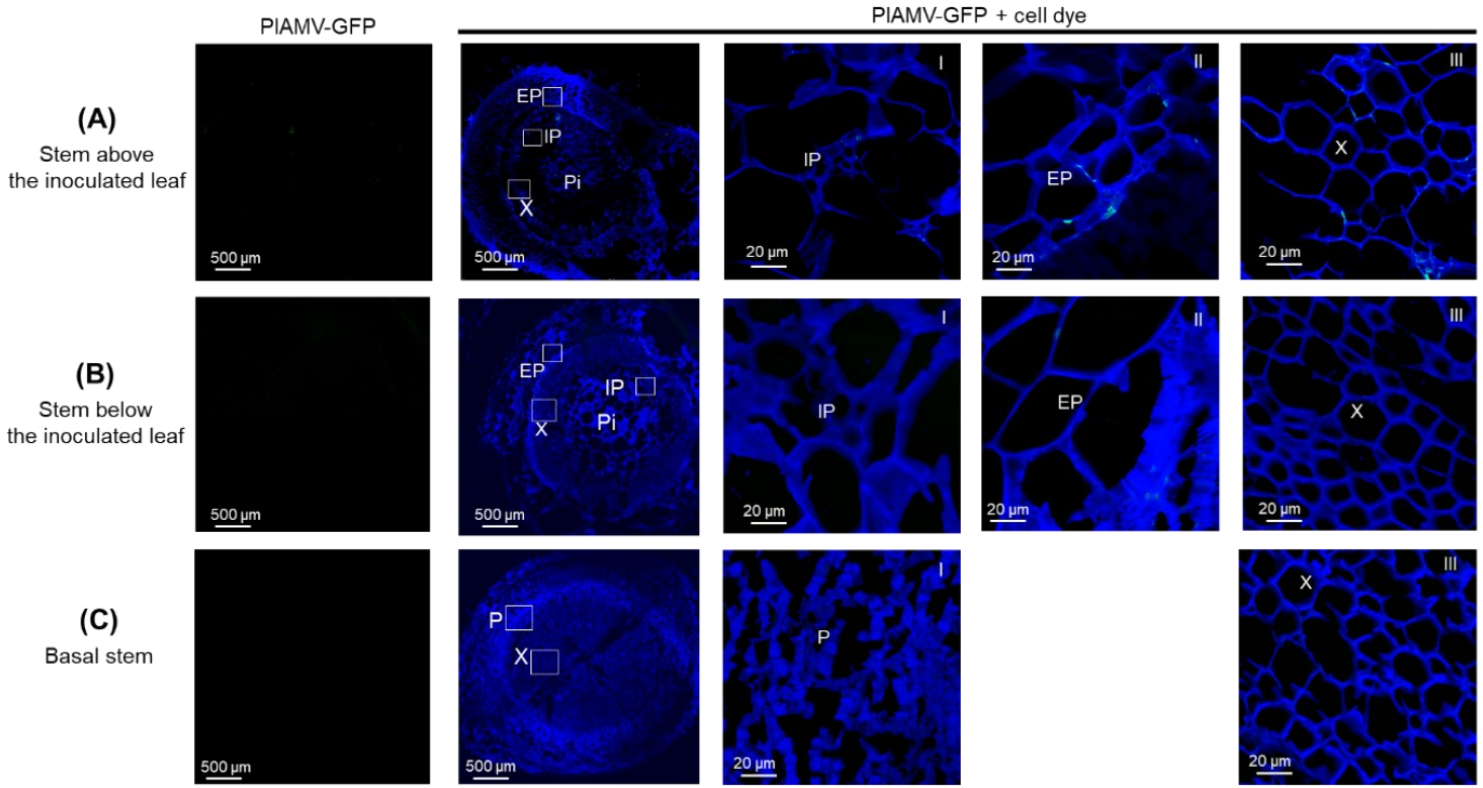

Figure 4.3 The cross section of (A) one internode of the stem above the inoculated leaf, (B) one internode of the stem below the inoculated leaf, and (C) the basal stem of untreated and mock-inoculated plants. The unspecific green fluorescence is shown in blurred green and Fluorescent Brightener 28–labeled plant cell walls is shown in blue. Panels with numbers I, II, III are enlarged images of vascular tissues for AdP/IP (or P in the basal stem), AbP/EP, and X, respectively, in white boxes of panels of the left. PlAMV accumulation is shown in green and Fluorescent Brightener 28–labeled plant cell walls is shown in blue. AdP, adaxial phloem; AbP, abaxial phloem; IP, internal phloem; EP, external phloem; P, phloem; X, xylem; M, mesophyll cells; Pi, pith tissue. Pictures are representatives of the two independents with three plants for each treatment.

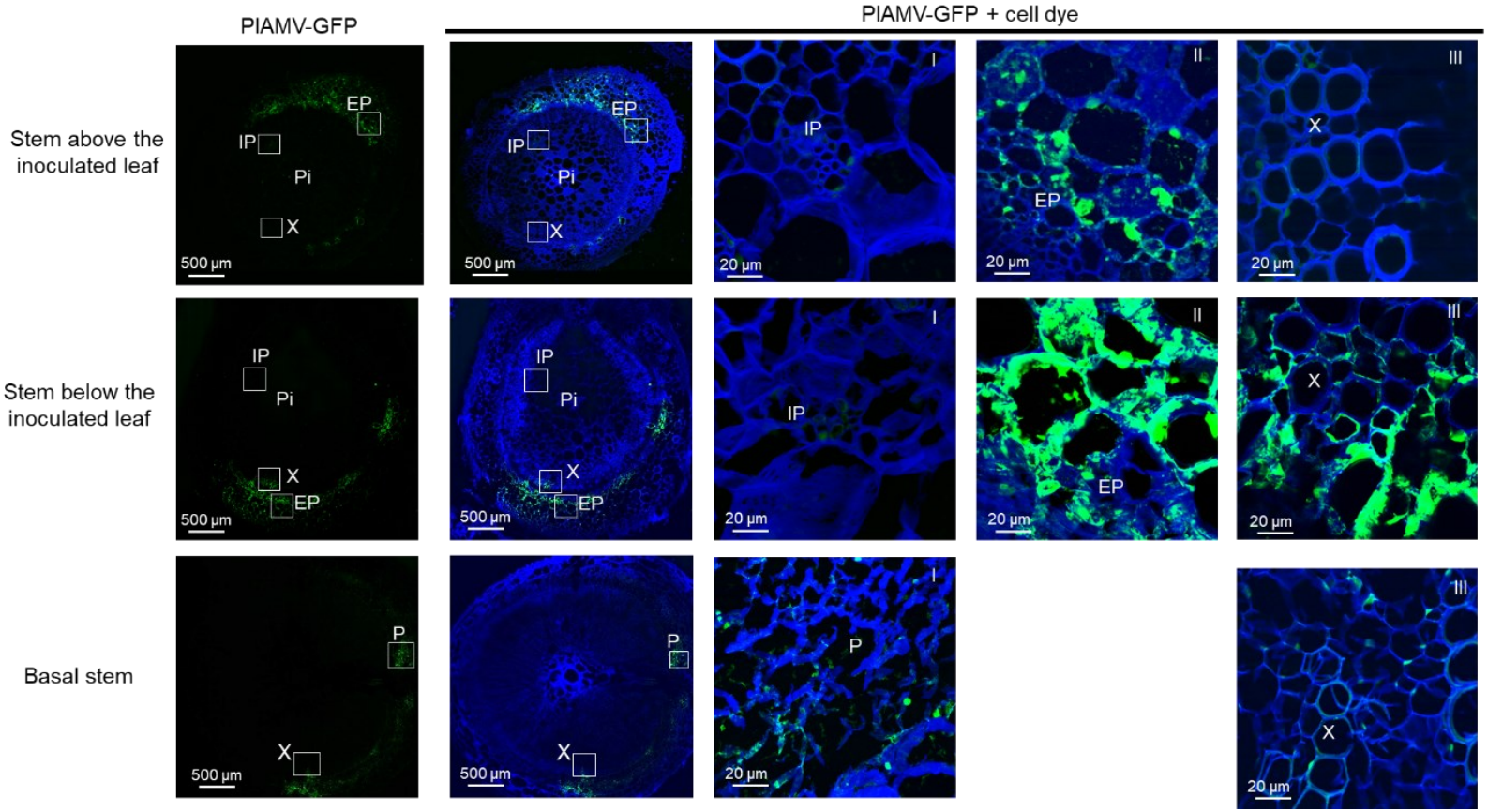

Figure 4.4 Effect of 1 mM ASM treatment on the viral localization in vascular tissues of the main stem at 9 dpi. Images of vascular tissues in untreated control plants. Upper panels, cross sections of the internode above the inoculated leaf; middle panels, cross sections of the internode below the inoculated leaf; lower panels, cross sections of the basal stem. Panels with numbers I, II, and III are enlarged images of the IP (or P in the basal stem), EP, and X, respectively, shown by white boxes in the panels on the left. PlAMV-GFP is green, and the Fluorescent Brightener 28-labeled plant cell walls are blue. IP, internal phloem; EP, external phloem; X, xylem; P, phloem; Pi, pith tissue. Pictures are representatives of two independent experiments with three plants in each treatment.

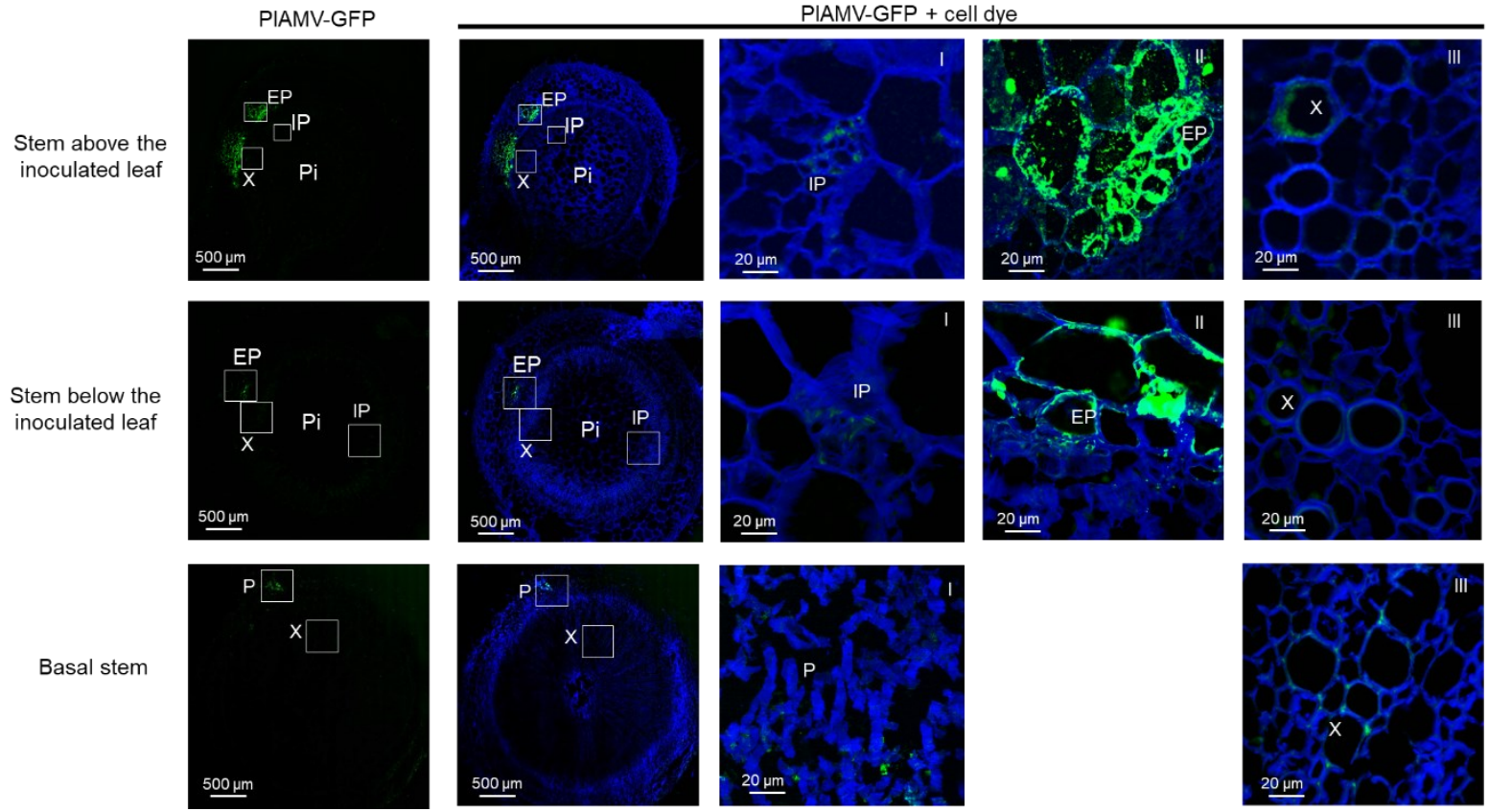

Figure 4.5 Effect of 1 mM ASM treatment on the viral localization in vascular tissues of the main stem at 9 dpi. Images of vascular tissues in ASM-treated plants. Upper panels, cross sections of the internode above the inoculated leaf; middle panels, cross sections of the internode below the inoculated leaf; lower panels, cross sections of the basal stem. Panels with numbers I, II, and III are enlarged images of the IP (or P in the basal stem), EP, and X, respectively, shown by white boxes in the panels on the left. PlAMV-GFP is green, and the Fluorescent Brightener 28-labeled plant cell walls are blue. IP, internal phloem; EP, external phloem; X, xylem; P, phloem; Pi, pith tissue. Pictures are representatives of two independent experiments with three plants in each treatment.

Table 2 Accumulation of PlAMV-GFP RNA at 9 dpi in the main stem, analyzed by RT-qPCR.

µg PlAMV-GFP RNA/g total RNA (Mean ± SE) [a]			
Samples	Control	ASM 1mM	P-value [b]
Stem above inoculated leaf	1.135 ± 0.480	0.597 ± 0.571	0.5108
Stem below inoculated leaf	1.502 ± 0.399	0.636 ± 0.621	0.3065
Basal stem	1.772 ± 1.063	0.631 ± 0.599	0.4031

[a] The experiment was conducted once with three plants for each treatment.

[b] $P < 0.05$, Student's *t* test

CHAPTER 5
DOWNWARD MOVEMENT OF PLAMV-GFP IN THE MAIN STEM IS NOT ESSENTIAL FOR ASM-MEDIATED DELAY OF SYSTEMIC INFECTION

5.1 Introduction

Several papers have appeared dealing with different conclusions of the translocation of viruses through the vasculature of their host plant. Holmes (1930) and Samuel (1934) revealed the direction of TMV translocation in a tomato plant. These authors determined that in the vegetative stage of tomato plants, TMV travels first to the roots of the plant from the inoculated leaf, and about a day later, it travels at the same rate with downward movement to the top of the plants (Fig. 5.1) (reviewed in Samuel 1934; Hull, 2014). Using PVX, Capoor (1949) found that in the tomato plants, PVX firstly translocates from the inoculated leaf into the roots, but in some experimental plants, both upward and downward movement occurred simultaneously, while others upward movement occurred first. This finding suggested that the translocation route of plant viruses can differ, depending on the virus species, the condition or developmental stage of an experimental plant, techniques to collect the data, and temperatures (Capoor, 1949). Schneider & Worley (1959) revealed that southern bean mosaic virus was entered xylem vessels and/or phloem as a pathway to translocate in plants. Similar to these findings, some viruses also found in the xylem vessels, for instance, PVX (Betti et al., (2012), TMV (Cheng et al., 2000), TuMV (Wang et al., 2007), zucchini yellow mosaic virus (Mochizuki et al., 2016), and MNSV (Gosalvez-Bernal et al., 2008).

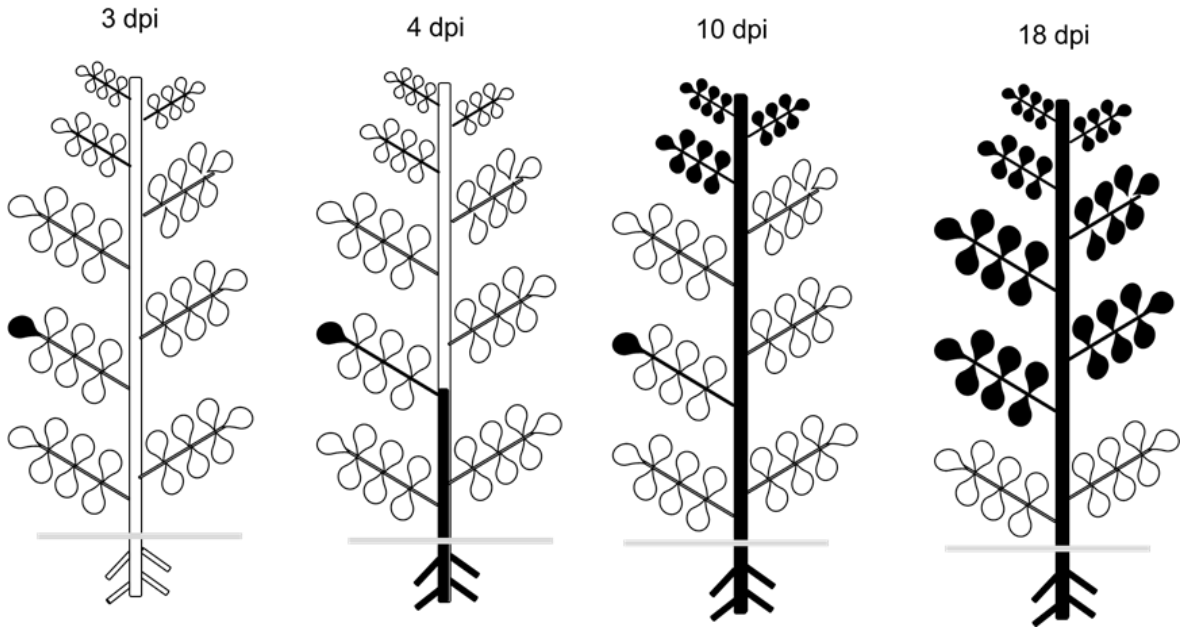

Figure 5.1 Diagram to show the progress of the spread of mosaic by TMV (represent in black) through a medium young tomato plant. dpi, days post inoculation. TMV was inoculated into one leaf in one tomato leaflet. Figure adapted from Samuel (1934).

Recent studies revealed that viruses utilize a different type of phloem to translocate from source to sink organs; viruses use external phloem to the roots, whereas they exclusively use internal phloem to the upper leaves (Andrianifahanana et al., 1997; Cheng et al., 2000; Sudharsana 1997). In some cultivar or lines resistant to infection, the accumulation of virus is limited to the specific phloem, either internal or external, compared with susceptible plants, which is translocated in both types of phloem (Derrick & Barker, 1997; Guerini & Murphy, 1999; Goodrick, 1991). These findings indicate that viruses infect the vascular tissue in the stem with a specific pattern and that access to the particular host cells in this tissue is highly regulated (Cheng et al., 2000; Kappagantu et al., 2020).

In this study, I found that in the early stages of systemic infection after loading into the vascular system (at 6 dpi), PlAMV-GFP was mainly present in the basal stem and the stem below the

inoculated leaf in untreated control plants. Meanwhile, in ASM-treated plants, PlAMV-GFP was not found in the basal stem and the stem above the inoculated leaf (Chapter 4, Fig. 4.2). According to these results, the relative accumulation of PlAMV RNA was lower in ASM-treated plants than the control plant in the later stages of systemic infection (9 dpi) (Chapter 4, Table 2). These results prompted me to further examine whether the delays of translocation of PlAMV-GFP into the basal stem are necessary for ASM-mediated delays of systemic infection of PlAMV-GFP in the upper leaves. The correlation between the downward and upward movement of PlAMV in stem, also the rate of PlAMV-GFP movement were discussed in this chapter.

5.2 Result

5.2.1 Downward movement of PlAMV-GFP in the main stem is not essential for ASM-mediated delay of systemic infection

To clarify whether the downward movement is necessary for systemic infection by PlAMV-GFP, I used steam treatment to destroy the phloem tissues of the main stem below the inoculated leaf to block the downward movement of PlAMV-GFP. We steamed the internodes below the ASM-treated or untreated leaves six hours before inoculation with PlAMV-GFP or water. Necrosis was observed in the internode stem exposed to heated steam (indicated by white circles in bottom panels of Fig. 5.2A), and microscopic observations confirmed that all cells except the xylem tissues were collapsed (Fig. 5.2B).

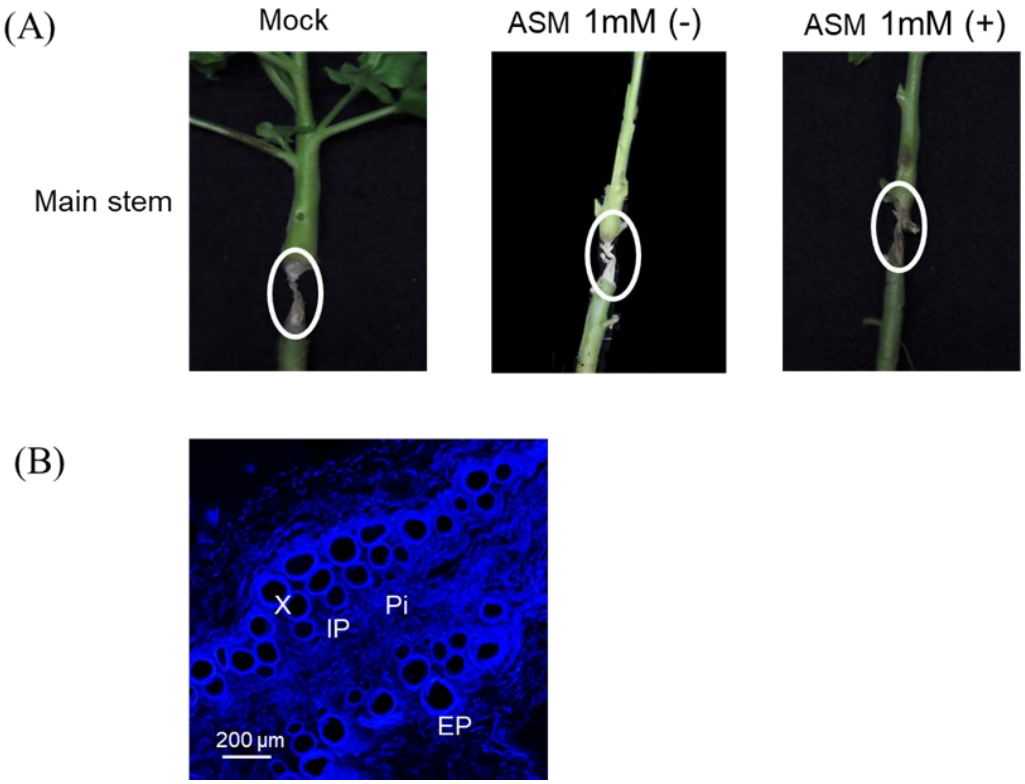

Figure 5.2 The effect of steam treatment to the main stem of *Nicotiana benthamiana* plants. (A) Representative images of the main stem of mock-inoculated (Mock), untreated control (-) and ASM-treated (+) plants at 6 hours after exposure to hot steam treatment. The steamed points are indicated with white circles. Bars, 5 cm. The experiment was repeated third with three biological replicates in each experiment. (B) A cross section of the stem following steaming treatment, which showed that phloem tissues were disrupted. Fluorescent Brightener 28–labeled plant cell walls is shown in blue. IP, internal phloem; EP, external phloem; X, xylem; Pi, pith tissue.

Visual observations of these steam-treated plants at 14 dpi under a UV lamp showed nonspecific autofluorescence at the steamed point and no GFP fluorescence below the steamed point, as expected (Fig. 5.3B). In accordance with this result, we did not detect PlAMV RNA in any stem samples taken from below the steamed point, in either ASM-treated or untreated plants (Fig. 5.4B). Without steam treatment, PlAMV RNA was detected in all samples from the main stem below the steamed point of the control and ASM-treated plants (Figure 5.5). This result indicated that the downward movement of PlAMV needs the phloem tissue. In contrast, GFP fluorescence was observed in the stems above the steam-treated parts of the control and ASM-treated plants, although the intensity of GFP fluorescence in the ASM-treated plants was weaker than in the control plants (indicated by white arrows in the middle panels of Fig. 5.3B). In line with this result, PlAMV RNA was detected in upper stem samples from five of six ASM-treated plants, with weaker bands than those observed in all six samples from the control plants (Fig. 5.4A). In the upper uninoculated leaves, GFP fluorescence was observed in six of nine plants in both the ASM-treated and control groups (Fig. 5.3A). However, the intensity of GFP fluorescence in the ASM-treated plants appeared to be lower than that in the control plants (Fig. 5.3A). These results demonstrated that the downward movement of PlAMV, which requires the phloem tissue, is unnecessary for systemic infection to the upper leaves. Thus, it is likely that ASM treatment delayed systemic infection by PlAMV-GFP regardless of downward movement or viral accumulation in the main stem below the inoculated leaf.

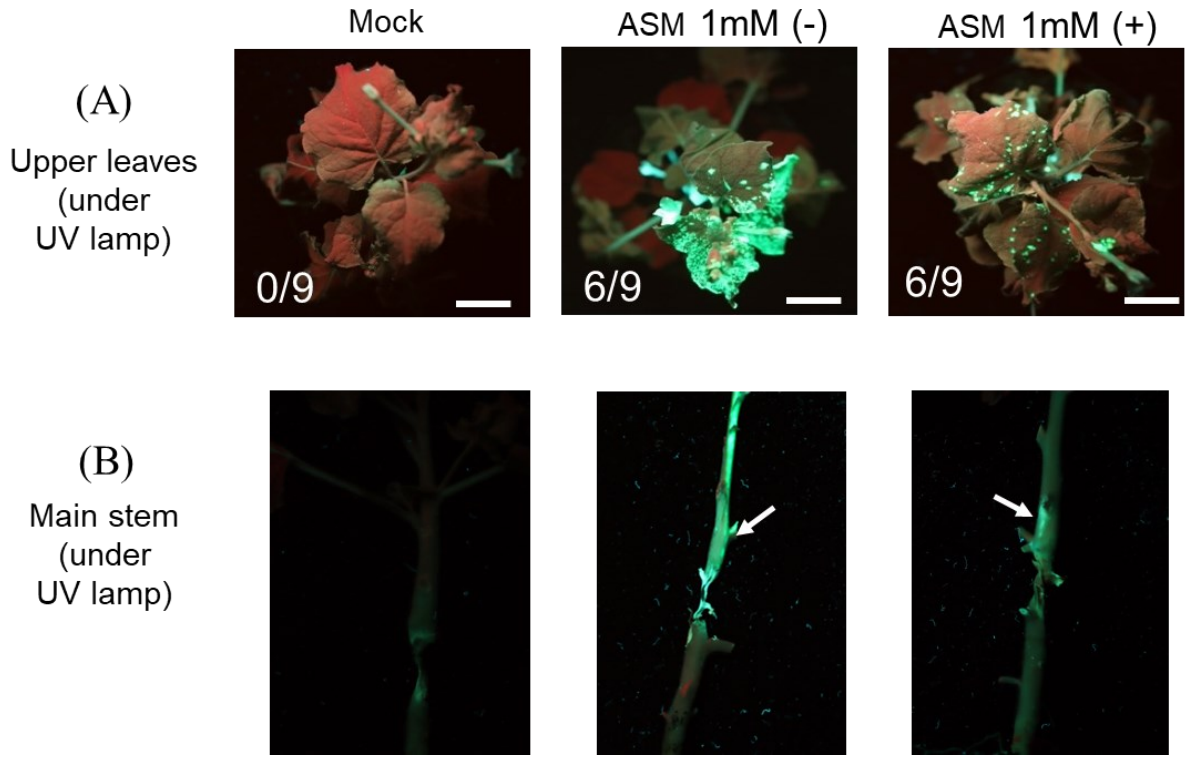

Figure 5.3 A role of phloem tissue in the downward movement of PlAMV-GFP. (A) Representative images of PlAMV-GFP infection in upper leaves of mock-inoculated (Mock), untreated control (-) and ASM-treated (+) plants following steaming treatment to destroy phloem tissues below the inoculated leaf. The numbers within each photograph indicate the number of plants that showed systemic infection per total of plants tested. (B) Images of PlAMV-GFP infection in the main stem. The photographs in the upper and lower panels were taken under UV light at 14 dpi. White arrows indicate GFP fluorescence. Bars, 5 cm. The experiment was repeated third with three biological replicates in each experiment.

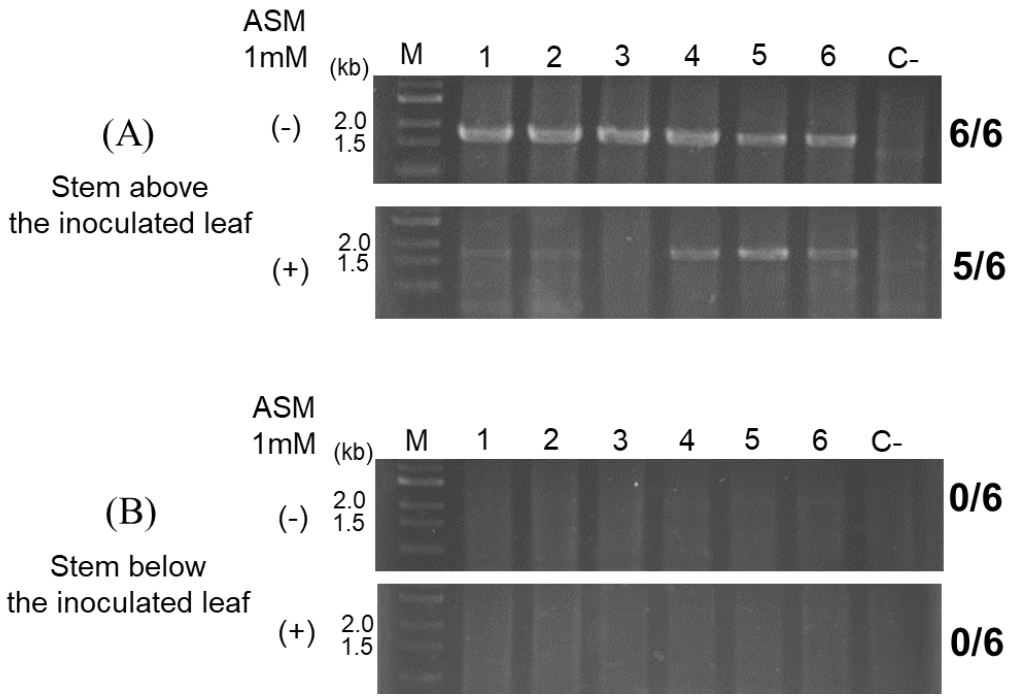

Figure 5.4 A role of phloem tissue in the downward movement of PlAMV-GFP. RT-PCR-mediated detection of PlAMV-GFP at 14 dpi in the stem above the inoculated leaf (A) or the stem below the inoculated leaf (B) in mock-inoculated (Mock), untreated control (-) and ASM-treated (+) plants following steaming treatment to destroy phloem tissues below the inoculated leaf. Lane M: 1 kb DNA ladder. Total RNA from mock-inoculated leaves was used as a negative control (C-). Numbers at the right represent the numbers of infected plants per total number of plants tested. The expected size of PCR products is 1.5 kb (approximately). The experiment was repeated twice with three biological replicates in each experiment.

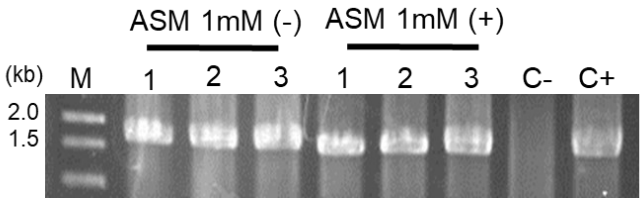

Figure 5.5 Detection of PlAMV-GFP within the main stem by RT-PCR at 14 dpi in untreated plants (-) and ASM-treated plants (+) without steam treatment. Lane M: 1 kb, DNA ladder (#N3232S, New England BioLabs). Total RNA from PlAMV-GFP-inoculated leaf at 15 dpi and mock-inoculated leaf were used as positive (C+) and negative (C-) controls, respectively. The expected size of PCR products is 1.5 kb (approximately). The experiment was done once with three each biological replicates.

5.2.2 Downward movement is essential for the efficient systemic infection of PlAMV-GFP

The result in Figure 5.3A showed that the percentage of systemic infection of PlAMV-GFP in steam-treated control plants is about 60%, which is similar to the steam-treated ASM plants. This result indicated that the downward movement of PlAMV-GFP might support its efficient systemic infection to the upper leaves. To clarify this, I compared the rate of systemic infection of PlAMV-GFP between steam-treated and non-steamed control plants by evaluating GFP fluorescence in the upper leaves. As shown in Figure 5.6, systemic infection of PlAMV was detected in one of ten non-steamed control plants at 5 dpi, and in seven of ten plants at 7 dpi. The systemic infection of PlAMV-GFP was detected from all non-steamed control plants at 9 to 11 dpi (Fig. 5.6). In steam-treated control plants, no systemic infection of PlAMV-GFP was detected at 5 dpi. Systemic infection of PlAMV was firstly detected from four of six steam-treated control plants at 7 dpi, followed by six of ten plants at 9 dpi, and eight of ten plants at 11 dpi (Fig. 5.6). These results confirmed that the downward movement of PlAMV-GFP is responsible for the rapid and efficient viral movement to the upper leaves. On the other hand, impaired downward movement by ASM treatment is not responsible for the ASM-mediated delay of viral movement to the upper leaves (Fig. 5.3).

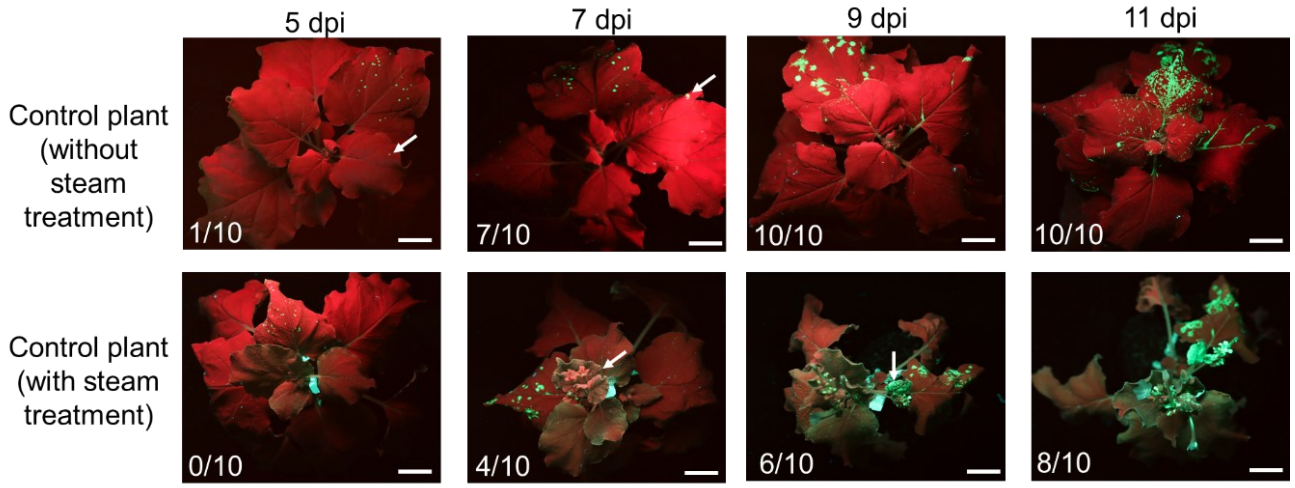

Figure 5.6 Representative images of PlAMV-GFP infection in upper leaves of untreated control plant without steaming treatment (upper panels) and following steam treatment (lower panels). The numbers within each photograph indicate the number of plants that showed systemic infection per total of plants tested. The photographs in the upper and lower panels were taken under UV light at 5, 7, 9, 11 dpi. White arrows indicate GFP fluorescence. Bars, 5 cm. The experiment was repeated twice with five biological replicates in each experiment.

CHAPTER 6
ASM TREATMENT AFFECTS THE EVENTUAL VIRAL LOCALIZATION AND REDUCES ITS ACCUMULATION IN SINK ORGANS

6.1 Introduction

In the last step of long-distance movement, viruses unload from the phloem SEs into the surrounding nonvascular tissues in the sink organs (Santa Cruz, 1999; Seron & Haenni, 1996; Ueki & Citovsky, 2007; Waigmann et al., 2007). Sink organs are plant organs that act as receivers of assimilates, including upper leaves, roots, fruits, flowers, and seeds (Ho, 1988). During the unloading process, viruses carried by photoassimilates exit from the phloem SEs to companion cells and are transported through a diverse range of cells, including vascular parenchyma, bundle sheath, and mesophyll cells (Hipper et al., 2013; Leisner & Howell, 1993).

Roberts et al. (1997) compared the unloading of PVX expressing GFP and fluorescent solute carboxyfluorescein (CF) in *N. benthamiana*. Although the systemic movement of PVX is slower than CF transportation, both PVX and CF are predominantly unloaded from the major veins (class III and larger) in the upper leaf. After unloading from phloem SEs in major veins (class III), viruses distribute to the minor veins by cell-to-cell movement through mesophyll cells (Roberts et al., 1997). Similar to this finding, TMV (Cheng et al., 2000) and cowpea mosaic virus (Silva et al., 2002) are also associated with major veins (class I-III) for the unloading but not from the minor veins. In contrast, potato virus A from the genus *Potyvirus* unload from major and minor veins in the upper leaves of wild potato species, *Solanum commersonii* (Rajamaki & Valkonen, 2002).

As reviewed in Chapters IV and V, TMV (Cheng et al., 2000), PepMoV (Andrianifahanana et al., 1997), and MNSV (Gosalvez-Bernal et al., 2008) translocate into the upper leaves through the internal phloem; therefore, these viruses apparently use the internal phloem exclusively for their route

in unloading step. Meanwhile, a study with PVX revealed that this virus utilizes the external phloem to unload from phloem SEs (Santa Cruz et al., 1999). However, the detailed information for the unloading of PlAMV in the vasculature is unknown.

Some resistant cultivar impairs the systemic movement of viruses. For instance, the restriction of systemic infection by cowpea chlorotic mottle virus (CCMV-S) in soybean accession PI 346304 was caused by blocks in viral loading into and/or viral unloading out from the vascular tissues (Goodrick et al., 1991). The resistance against systemic virus also can be obtained by the treatment of plant activators. Takeshita et al. (2013) revealed that ASM treatment reduced the accumulation of cucurbit chlorotic yellow virus (CCYV) RNAs in the uninoculated upper leaves. Pre-treatment of Benzo-(1,2,3)-thiadiazole-7-carbothioic acid *S*-methyl ester (BTH) was inhibited the accumulation of CMV RNAs in the upper leaves of tomato plants (Anfoka, 2000). Our previous study showed that ASM treatment delays the long-distance movement of PlAMV-GFP to the upper leaves but eventually allows the virus to infect not only the upper leaves (Matsuo et al., 2019) but also the main stem below the inoculated leaf (Chapter 4, Fig. 4.2B and Table 2). This result prompted me to examine whether ASM treatment influences the unloading of PlAMV-GFP in the sink organs.

6.2 Result

6.2.1 ASM treatment delays the unloading of PlAMV-GFP in an upper inoculated leaf, but not in roots

To examine whether ASM treatment influences the unloading of PlAMV-GFP in sink organs, at 9 dpi I extracted total RNA from the petiole of an upper leaf that was the 3rd leaf from the top and from the primary root, using both ASM-treated and control plants, and performed RT-PCR. PlAMV RNA was detected in all six upper petiole samples from control plants and in three of six upper petiole samples from the ASM-treated plants (Fig. 6.1A). On the other hand, the viral RNA was detected in

the primary roots of all control and ASM-treated plants (Fig. 6.1B). I also found that the DNA bands for the ASM-treated plants were generally weaker than those observed for the control plants. This result suggests that ASM treatment has a more restrictive effect on the unloading of PlAMV-GFP into the upper leaves than in the roots.

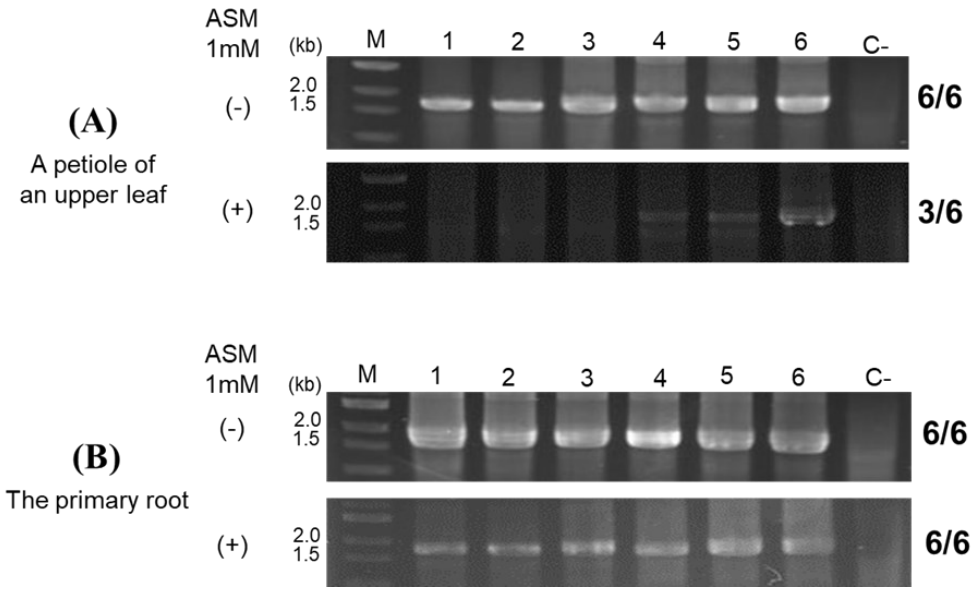

Figure 6.1 Detection of PlAMV-GFP within sink organs by RT-PCR at 9 dpi. Total RNA was extracted from upper leaves (A) or primary roots (B) of untreated control (-) or ASM-treated (+) plants . Lane M: 1 kb DNA ladder. Total RNA from mock-inoculated leaves was used as a negative control (C-). Numbers at the right represent the numbers of infected plants per total number of plants tested. The expected size of PCR products is 1.5 kb (approximately). The experiment was repeated twice with three biological replicates each.

6.2.2 *ASM treatment reduces viral accumulation in vascular tissues of the upper leaves*

To further observe the restrictive effect of ASM treatment on unloading of PlAMV-GFP, I observed cross-sections prepared from class I and II major veins and from the petioles of upper leaves at 12 dpi. The vascular tissues in mock-inoculated plants exhibited nonspecific autofluorescence (Fig. 6.2), which was distinguishable from the much brighter GFP fluorescence in inoculated plants (Fig. 6.3 and 6.4). In both the control and ASM-treated plants inoculated with PlAMV-GFP, GFP fluorescence could be observed in the vascular tissues of class I and II veins and the petioles of the upper leaves (Fig. 6.3 and 6.4). However, the intensity of GFP fluorescence appeared to be lower in the ASM-treated plants than in the control plants. I also found that in the control plants, GFP fluorescence was distributed from the abaxial or external phloem into the mesophyll cells in all of the three parts examined (indicated with red arrows in Fig. 6.3). In contrast, in the ASM-treated plants, the GFP fluorescence was observed in mesophyll cells of the class I veins and the petioles, but not in the class II veins (Fig. 6.4, indicated with red arrows). Taken together, the results in Fig. 6.3 and Fig.6.4 indicated that ASM treatment allows the viral unloading and localization into the vascular tissues of uninoculated upper leaves, but restricts its subsequent accumulation in mesophyll cells.

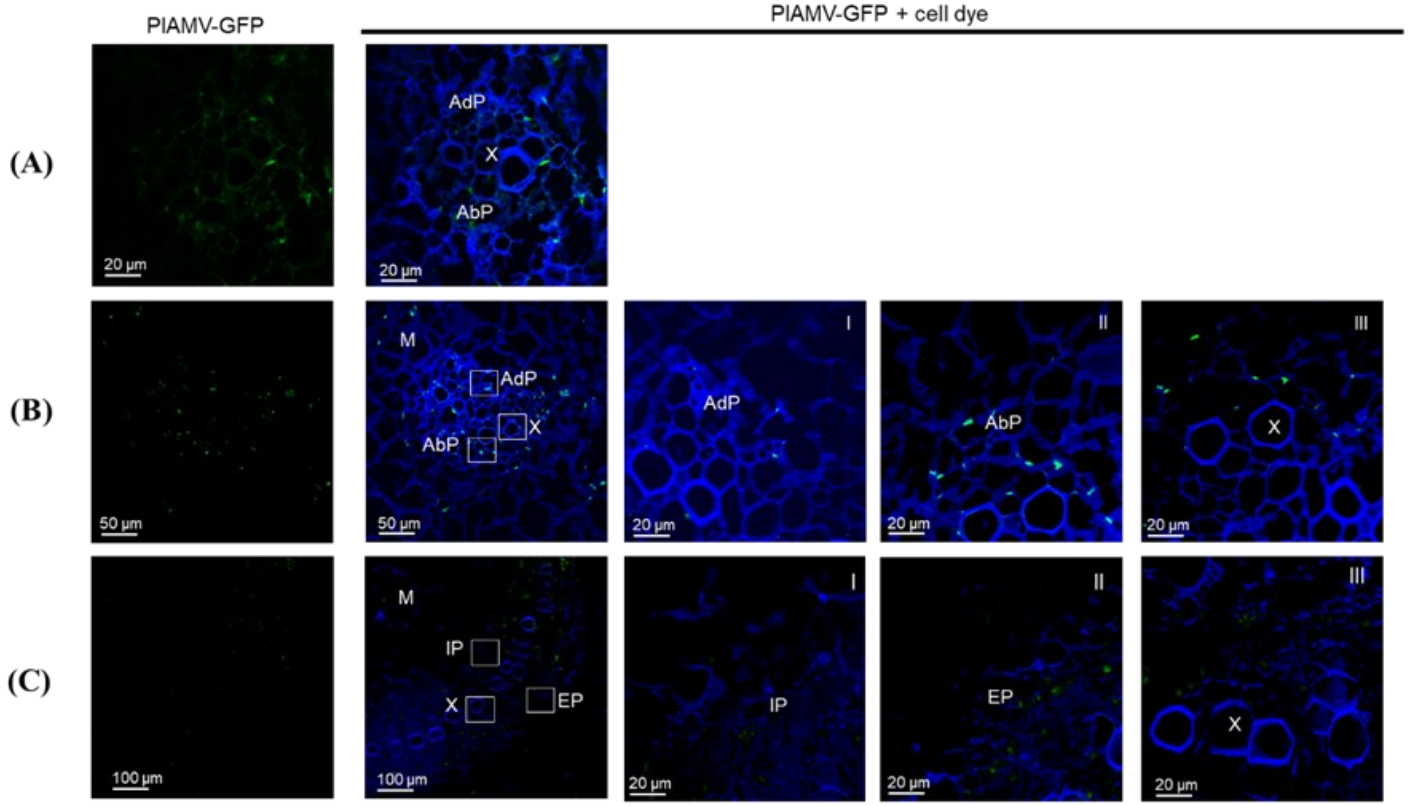

Figure 6.2 The cross section of the ASM-untreated mock-inoculated plant of (A) major veins of class II, (B) major veins of class I, and (C) the petiole of the viral-uninoculated upper leaf. The unspecific green fluorescence is shown in blurred green and Fluorescent Brightener 28–labeled plant cell walls is shown in blue. Panels with numbers I, II, III are enlarged images of vascular tissues for AdP/IP, AbP/EP, and X, respectively, in white boxes of panels of the left. PlAMV accumulation is shown in green and Fluorescent Brightener 28–labeled plant cell walls is shown in blue. AdP, adaxial phloem; AbP, abaxial phloem; IP, internal phloem; EP, external phloem; X, xylem; M, mesophyll cells. Pictures are representatives of the two independents with three plants for each treatment.

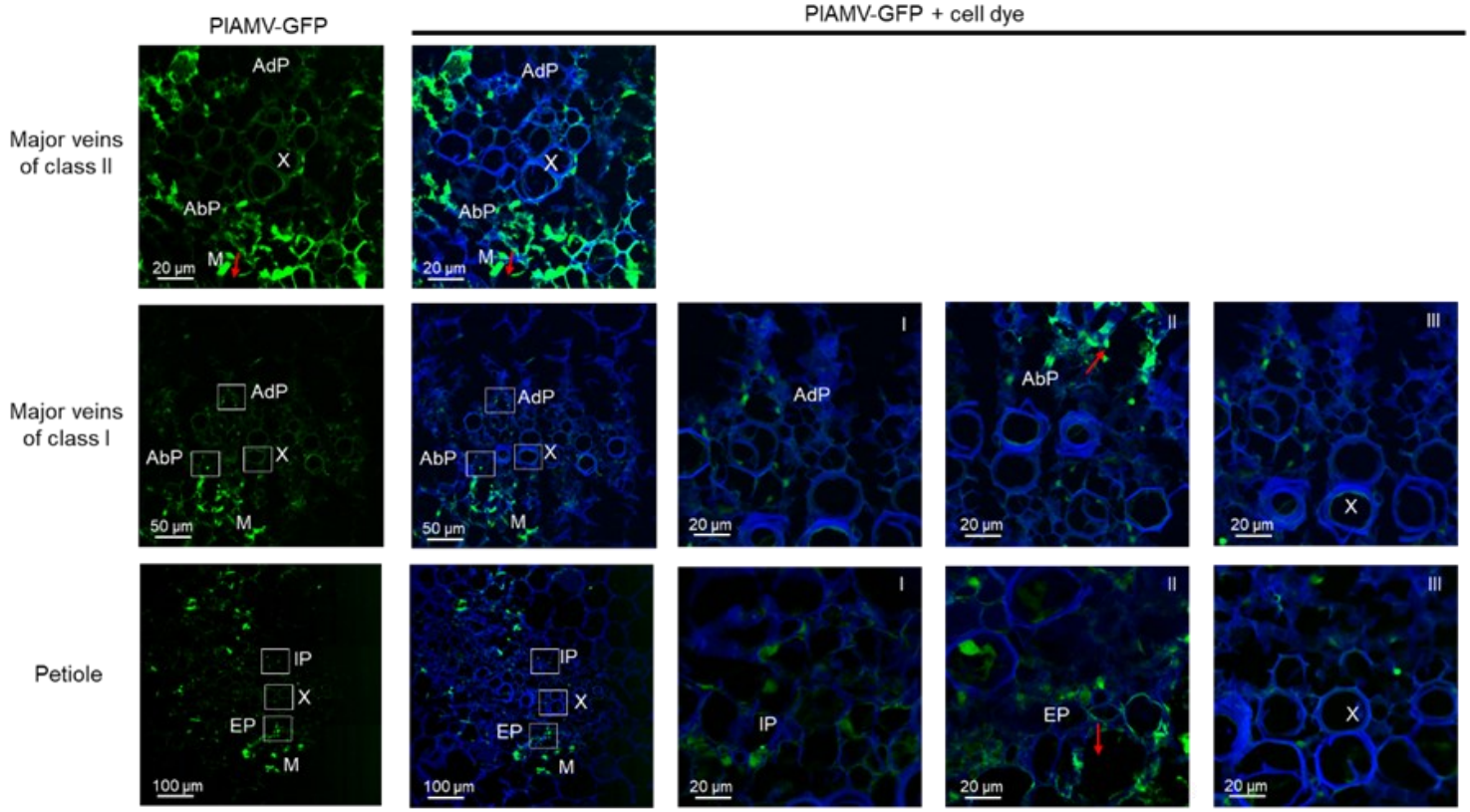

Figure 6.3 Effect of 1 mM ASM treatment on the viral localization in vascular tissues in uninoculated upper leaves at 12 dpi. Images of vascular tissues in untreated control plants. Upper panels, cross sections of major class II veins; middle panels, cross sections of major class I veins; lower panels, cross sections of petioles. Panels with numbers I, II, and III are enlarged images of the AdP/IP, AbP/EP, and X tissues, respectively, shown in white boxes in the panels on the left. PlAMV-GFP appears as green, and the Fluorescent Brightener 28-labeled plant cell walls are blue. AdP, adaxial phloem; AbP, abaxial phloem; IP, internal phloem; EP, external phloem; X, xylem; M, mesophyll cells. Red arrows indicate PlAMV-GFP distribution in the mesophyll cells. Pictures are representatives of two independent experiments with three plants for each treatment.

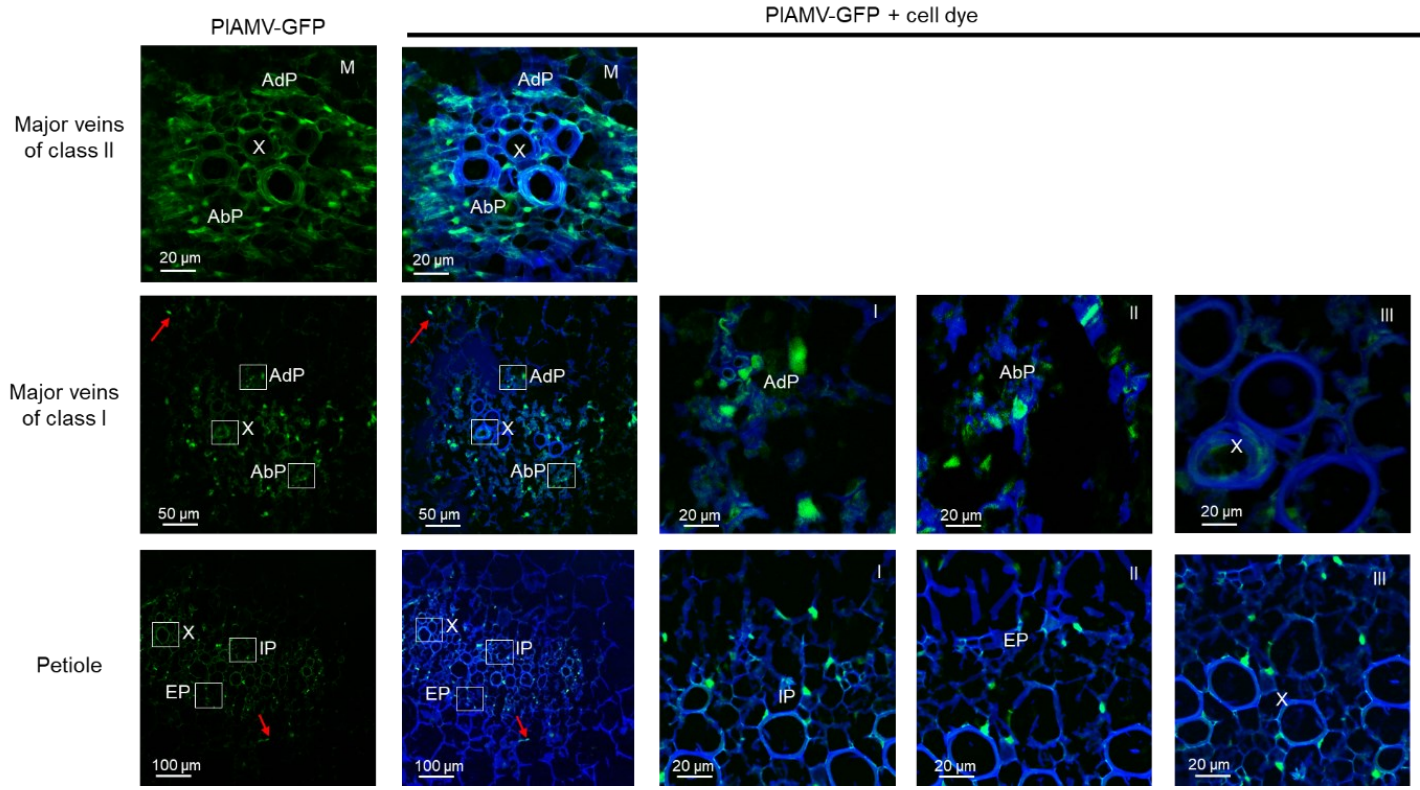

Figure 6.4 Effect of 1 mM ASM treatment on the viral localization in vascular tissues in uninoculated upper leaves at 12 dpi. Images of vascular tissues in ASM treated plants. Upper panels, cross sections of major class II veins; middle panels, cross sections of major class I veins; lower panels, cross sections of petioles. Panels with numbers I, II, and III are enlarged images of the AdP/IP, AbP/EP, and X tissues, respectively, shown in white boxes in the panels on the left. PlAMV-GFP appears as green, and the Fluorescent Brightener 28-labeled plant cell walls are blue. AdP, adaxial phloem; AbP, abaxial phloem; IP, internal phloem; EP, external phloem; X, xylem; M, mesophyll cells. Red arrows indicate PlAMV-GFP distribution in the mesophyll cells. Pictures are representatives of two independent experiments with three plants for each treatment.

CHAPTER 7
ASM-MEDIATED RESTRICTION ON LOADING OF PLAMV IS CALLOSE DEPOSITION-INDEPENDENT

7.1 Introduction

Plasmodesmata serve as intercellular bridges that allow plant cells to communicate with virtually all adjacent cells and distantly located cells, forming a symplastic network in the plant (Sager & Lee,2014). Plasmodesmata conjunction allows phloem to transport the molecules, including sugars, lipids, amino acids, nucleic acids, protein, and phytohormone (Lucas et al., 2013). During infection of the pathogen, the plant modulates the size of exclusion limit (SEL) of plasmodesmata to suppress the spread of the pathogen (Lee & Lu, 2011). The level of callose at PD plays an important role in regulating the SEL (Wu et al., 2018). Accumulation of callose at PD restricts the channel to inhibit the cell-to-cell transport of macromolecules and symplastic pathogen, whereas down-regulation of callose accumulation relaxes it to allow the macromolecular and pathogen trafficking (Zavaliev et al., 2011). Previous studies found that the infection of viruses leads to callose deposition at PD as plant defense responses (Wu et al., 2018). For instance, cell-to-cell movement of TMV and long-distance movement of PVX were restricted in the *GLU I* -deficient mutant, which shows an elevated deposition of callose (Iglesias & Meins F, 2000). Wolf et al. (1991) found that TMV inoculation induced callose deposition, thus restricting the cell-to-cell movement of TMV.

Several phytohormones, such as indole-3-acetic acid (IAA), abscisic acid (ABA), and SA, have been involved in PD callose regulation. Over-accumulation of IAA26 protein inhibits the loading of TMV. In addition, transcriptome analysis of IAA26-over-accumulation line shows significant changes in genes associated with callose regulation (Collum et al., 2016). Plasmodesmata-located protein 5 (PDLP5) mediates crosstalk between PD regulation and salicylic acid-dependent

defense responses. PDLP5 localizes at the PD, acting as an inhibitor to PD trafficking, through its capacity to modulate callose deposition at PD. PDLP5, as a regulator of PD, is also essential to enhance plant defense response against cell-to-cell movement of bacterial pathogens, *Pseudomonas syringae* in a salicylic acid-dependent manner.

Callose accumulation is also up-regulated by the treatment of chemicals. For example, liquid bioassimilable sulfur (LBS) is one type of PAs induced immune response mechanism of tomato plants by elevating the callose deposition to suppress the causal agent of powdery mildew, *Oidium neolycopersici* (Llorens et al., 2017). Ueki (2005; 2007) found that the treatment of cadmium upregulated cell-wall-associated protein, cadmium (Cd) ion-induced glycine-rich protein (cdiGRP), which increases the level of callose to inhibit long-distance movement of turnip vein-clearing virus (TVCV) (Ueki & Citovsky, 2005). In addition, the cdiGRP is expressed in vascular tissues, resulting in the inhibition of unloading of TVCV in uninoculated non-vascular tissues (Citovsky et al., 1998).

Clearly, callose deposition can be regulated by phytohormone and chemical treatment to suppress cell-to-cell movement of viruses. Thus, callose deposition can be considered as a result of plant defense responses to limit the loading or unloading of viruses (Wu et al., 2018; Leisner & Turgeon, 1993). Chapter 1 showed that ASM treatment restricted the loading of PlAMV-GFP into the vascular tissue in the inoculated leaf, but the mechanisms underlying this restriction is unknown. In this chapter, I clarified the role of callose deposition on ASM-mediated restriction of loading of PlAMV-GFP.

7.2 Result

7.2.1 Callose deposition elevated in major class I veins of ASM-treated and untreated plants

To observe the callose depositions in the phloem, using decolorized aniline blue solution, I stained the cross-section of major class I veins at 9 dpi, when PlAMV-GFP restricted in the vascular

tissues in ASM-treated plants compared to control plants (Fig. 3.6 & 3.7; Chapter 3). As shown in Figure 7.1, aniline blue-specific callose deposition was detected in the phloem of major class I veins in both the ASM-treated and control plants (indicated by the red arrow). The cell wall of the xylem referred to the autofluorescence. In healthy plants, callose deposition was not detected in adaxial or abaxial phloem (Fig. 7.1). In contrast, in the ASM-treated and control plants, callose deposition was observed in both adaxial and abaxial phloem. I also found that in ASM-treated and control plants, callose deposition was dominantly observed in the abaxial phloem than in the adaxial phloem (Fig. 7.1). This result suggests that ASM-mediated resistance does not depend on callose deposition to restrict viral loading to major class I veins.

7.2.2 Callose deposition elevated in major class I veins of ASM-treated and untreated plants

The result shown in Fig. 7.1 prompted me to analyze in more detail the differences in the callose deposition in the phloem of the petiole of the inoculated leaf between ASM-treated and control plants. In healthy plants, callose deposition was not detected in adaxial or abaxial phloem (Fig. 7.2). On the other hand, in the ASM-treated and control plants, callose deposition was detected in both internal and external phloem (Fig. 7.2, indicated by the red arrow). Similar to the major class I veins, in the petiole of the inoculated leaf, callose deposition was dominantly observed in the external phloem than in the internal phloem of ASM-treated and control plants (Fig. 7.2). This result also suggests that ASM-mediated resistance does not depend on callose deposition to restrict viral loading to the petiole of the inoculated leaf.

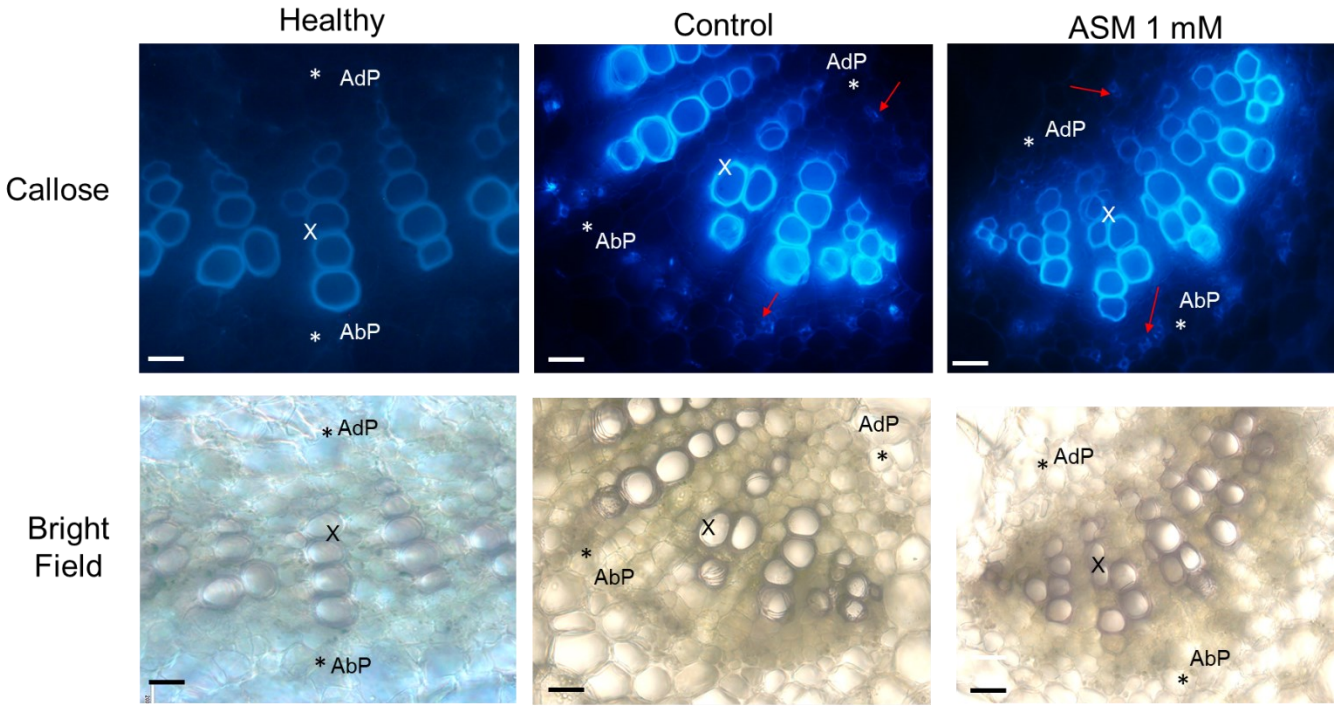

Figure 7.1 A role of callose accumulation in the ASM-mediated inhibition of viral loading. Images of cross-sections of major veins class I from healthy (left panels), untreated control plants (middle panels), and ASM-treated plants (right panels) at 9 dpi. Callose deposition in phloem was viewed by filter CFP XF 88-2 (upper panels) and bright-field images of phloem (lower panels). Callose deposition is shown in blue and emphasized with red arrows. The cell walls of the xylem are autofluorescence. Asterisks indicate the position of phloem. Bars = 200 µm. AdP, adaxial phloem; EP, abaxial phloem; X, xylem. Pictures are representatives of the three independents with three plants for each treatment.

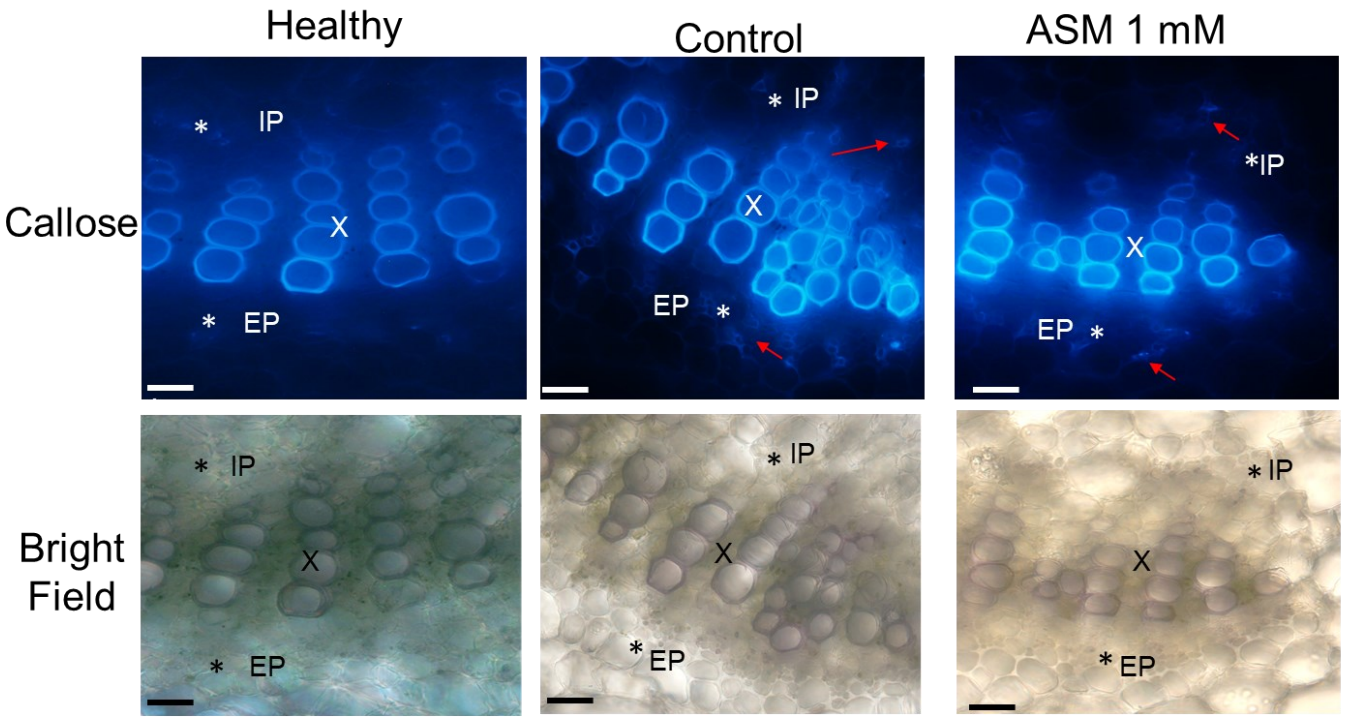

Figure 7.2 A role of callose accumulation in the ASM-mediated inhibition of viral loading. Images of cross-sections of petiole of the inoculated leaf from healthy (left panels), untreated control plants (middle panels), and ASM-treated plants (right panels) at 9 dpi. Callose deposition in phloem was viewed by filter CFP XF 88-2 (upper panels) and bright-field images of phloem (lower panels). Callose deposition is shown in blue and emphasized with red arrows. The cell walls of the xylem are autofluorescence. Asterisks indicate the position of phloem. Bars = 200 µm. IP, internal phloem; EP, external phloem; X, xylem. Pictures are representatives of the three independents with three plants for each treatment.

CHAPTER 8

DISCUSSION

Previous study found that the ASM-mediated delay of the long-distance movement of PlAMV is not simply due to the suppression of viral accumulation in inoculated leaves, because the virus is able to move from cell to cell efficiently with or without ASM treatment (Matsuo et al., 2019). However, it is unknown exactly when, where, and how the viral long-distance movement is inhibited upon ASM treatment. In this study, I employed RT-PCR and fluorescence microscopy, and carried out time-course experiments to investigate the accumulation and localization of PlAMV-GFP in the vascular tissues of ASM-treated and control plants.

The detachment experiments confirmed that systemic infection by PlAMV-GFP is delayed in the ASM-treated plants when compared with untreated control plants (Fig. 3.2 and Fig 4.1). In addition, as reported previously (Matsuo et al., 2019), ASM treatment has little or no effect on the cell-to-cell movement of the virus in inoculated leaves (Fig. 3.1). Similarly, the vascular loading of CCMV-S was restricted in inoculated leaves of the resistant soybean cultivar PI 346304, while its cell-to-cell movement in the inoculated leaves was not affected (Goodrick et al., 1991). Naylor et al. (1998) also found that the vascular loading of CMV was delayed in inoculated leaves treated with SA, an ASM analog, although they did not discuss the effect of SA on the cell-to-cell movement of CMV. From these data, I propose that the ASM-mediated delay of viral systemic infection is not simply caused by reduced cell-to-cell movement through the mesophyll to the vasculature, but rather involves restricted vascular loading in the inoculated leaves.

My observations of virus localization in the major veins and the petiole indicate that ASM treatment may restrict viral movement between the phloem and mesophyll cells, because much fewer mesophyll cells were infected with PlAMV-GFP in the ASM-treated plants than in the control plants

(Fig. 3.7 and Fig. 6.4). Indeed, it is known that phloem tissue functions as a gatekeeper to viral long-distance movement. One of the most critical barriers resides in the companion cells of the phloem. Previous studies have revealed that viral systemic infection is often impeded due to failed or reduced movement into companion cells. Nelson et al. (1993) and Ding et al. (1996) found that systemic infection by a masked strain of tobacco mosaic virus (M-TMV) is delayed because M-TMV is unable to efficiently enter the companion cells. It will be important to determine which cell types in the phloem tissues of *N. benthamiana* plants are involved in regulating the loading of viruses, especially when treated with ASM. Using PlAMV encoding an immobilized GFP reporter with a nuclear localization signal or an endoplasmic reticulum retention signal will determine in more detail the effect of ASM treatment on viral cell-to-cell movement within the phloem tissue or between phloem and mesophyll cells.

I found that the viral accumulation in vascular tissues was reduced in ASM-treated plants, most notably in the petiole of the inoculated leaf (Fig. 3.4, 3.6, and 3.7). There are a couple of possible explanations for this finding. First, the ASM-mediated restriction of vascular loading of PlAMV-GFP may simply lead to reduced viral accumulation in the rest of the plant. It is also possible that other mechanisms associated with systemic acquired resistance (SAR) play a role in the reduced accumulation of virus in systemic tissues. It is well known that ASM activates SAR by mimicking the role of SA (Oostendorp et al., 2001; Vallad & Goodman, 2004; Vlot et al., 2009). SAR is typically triggered by a cell-death associated resistance called the hypersensitive reaction, and it gives long-lasting protection against pathogens by reducing their accumulation in systemic tissues (Tripathi et al., 2010). It is essential to find out in a future study whether SAR, induced by ASM treatment, plays a role in the reduced viral accumulation in the vascular tissues.

Present study also provides a novel pattern of translocation of plant viruses from the inoculated leaf to other plant organs. Tobamoviruses (Cheng et al., 2000) and potyviruses

(Andrianifahanana et al., 1997) employ the external phloem to move downward into the roots and the internal phloem to move upward to upper leaves. This bi-directional pattern of vascular translocation is also seen in the movement of photoassimilates (Slewinski et al., 2013). Unlike this translocation pattern, I found that PlAMV-GFP was localized in both the internal and external phloem in the petiole of the inoculated leaf (Fig. 3.6 & 3.7) and the main stem (Fig. 4.4 & 4.5). These results suggest that potexviruses like PlAMV mainly utilize all of the internal and external phloem as a pathway for long-distance movement. In addition, PlAMV-GFP was often detected in the xylem as well (Fig. 3.6; 3.7; 4.4; 4.5, 6.3; 6.4; Fig. 3.4), which is similar to a previous observation of potato virus X (Betti et al., 2012). However, since no PlAMV-GFP was detected in the main stem below the steamed point (Fig. 5.4), I assume that PlAMV may not use the xylem as the pathway for long-distance movement.

We showed that systemic infection by PlAMV-GFP in the upper leaves successfully occurred even when we blocked downward viral movement from the inoculated leaf (Fig. 5.3 & 5.4). Then, what is the biological relevance of the downward movement of PlAMV into the basal stem and roots? Some potexviruses that are economically damaging to vegetatively propagated crops, including potatoes and ornamental flowers, can be transmitted between host plants through tubers and rootstock (Hull, 2014; Agrios, 2005). It should be noted that systemic upward movement of PlAMV-GFP occurred in all untreated plants with viable phloem tissues at 15 dpi, but it failed in some plants whose phloem tissue stem below the inoculated leaves was destroyed by steam treatment (Matsuo et al., 2019 and Fig. 5.3). Thus, it is possible that the downward movement of PlAMV-GFP makes some contribution to its efficient upward movement. This enhancement of systemic movement by the preceding downward movement may increase the effectiveness of horizontal transmission of PlAMV-GFP. Taken together, I propose that impaired downward movement of PlAMV-GFP by ASM treatment might result in its less efficient upward movement. It will be necessary to further determine whether a similar result is found in other potexviruses.

My present study provides an insight to the role of callose deposition to ASM-mediated restriction of loading of plant viruses into phloem vasculature. Salicylic acid (SA) increase the deposition of callose, resulting in limitation of bacterial pathogen infection (Lee, et al., 2011). Llorens et al., (2017) found that the treatment of liquid bioassimilable sulphur induces callose deposition to suppress fungal pathogen infection. Unlike this resistance mechanism, I found that ASM-mediated restriction on loading of PlAMV is callose deposition-independent (Fig 7.1 & 7.2). Although the level of callose deposition increased in ASM-untreated plants, PlAMV-GFP successfully loaded into phloem. To confirm this result, it will be necessary to evaluate whether the systemic infection of PlAMV-GFP is also inhibited by ASM treatment in callose synthase-deficient Arabidopsis plants.

A previous study found that viruses reprogrammed the host's factor to load the virus to the phloem successfully. For instance, TMV infection reprograms specific auxin/indole acetic acid transcriptional regulators to enhance phloem loading in mature tissues, and also induces plasmodesmata dilation by regulating callose deposition (Collum et al., 2016; Culver et al., 2020; Padmanabhan et al., 2006). It is possible that ASM treatment reprograms the phloem SEs in the treated leaves by regulating auxin levels to restrict the loading of PlAMV-GFP. However, whether ASM treatment regulates auxin levels in treated leaves remains unclear.

CHAPTER 9
CONCLUSION

9.1 Conclusions

ASM treatment restricted the loading of PlAMV-GFP into vascular tissues in the inoculated leaves. This led to delays in viral translocation to the petiole and the main stem, and to untreated upper leaves. ASM treatment affected the viral localization and reduced its accumulation in the phloem, xylem, and mesophyll tissues. A stem girdling experiment, which blocked viral movement downward through phloem tissues, demonstrated that ASM treatment could inhibit viral systemic infection to upper leaves, which occurred even with viral downward movement restriction. The putative mechanism of the restriction of viral loading by ASM is in callose deposition-independent manner. Taken together, our results showed that ASM treatment affects the loading of PlAMV-GFP into the vascular system in the inoculated leaf, and that this plays a key role in the ASM-mediated delay of viral long-distance movement.

9.2 Prospect for Future Research

ASM treatment delays the loading of PlAMV-GFP into vascular tissues in the inoculated leaf, and this leads to restrict the systemic infection of viruses throughout the plant. Because vascular loading is an essential and prerequisite step for viral long-distance movement, ASM treatment could be an efficient method for controlling plant virus disease.

ACKNOWLEDGEMENTS

I would like to thank my advisor, Dr. Ken Komatsu, who has been a great mentor. I am thankful for his support and guidance though out my research. He was always available when I needed him, and I thank him for his investment in my professional growth. I would like to express my gratitude to Dr. Nobumitsu Sasaki for all his support for this project and encouragement, especially when I am using microscopes and microtomes, and he provided me with ideas for experiments and constructive criticisms, which allowed me to improve both my research and scientific communication skills. I would like to thank to Dr. Tsutomu Arie for all his valuable comprehensive advice and encouragement. I am also thankful to Dr. Hiromitsu Moriyama, Dr. Hisashi Nishigawa, and Dr. Masami Nakajima for their timely suggestions and contribution to the quality of my dissertation.

Sincere appreciation is expressed to Epson International Foundation and The Foundation for Dietary Scientific Research for the financial support of my study.

I would like to thank the past and present lab members of Plant Pathology Lab for all their help and support throughout my time in the lab. Thank you to Yuki Matsuo for her endless help and all Indonesian student in TUAT, especially my dear friend Lela Susilawati.

Special thanks to my family. My dear mother, Pudji Rahayu, and my late father, Fauzi Sahlan, have always supported and encouraged me in all that I did. Thank you to my husband, Dzulfahmi, who has been with me through all the ups and downs of graduate student life.

REFERENCES

Abe, S., Neriya, Y., Noguchi, K., Hartono, S., Sulandari, S., Somowiyarjo, S., Ali, A., Nishigawa, H., Natsuaki, T. 2019. First report of the complete genomic sequences from Indonesian isolates of bamboo mosaic virus and detection of genomic recombination events. Journal of General Plant Pathology, 85(2), 158-161.

AbouHaidar, M. G., Gellatly, D. 1999. Potexviruses. In: Granoff A, Webster RG (Eds). Encyclopedia of virology, second edition. Academic Press, San Diego, USA, 1364-1368.

Adedire O. L., Wen R. H., Windham A., Windham M., Hajimorad M. R. 2009. Hosta virus X in *Hosta* identified in Tennessee, USA. Plant Pathology, 58: 405.

Agrios, G. N. 2005. Plant Pathology, fifth edition. Elsevier-Academic Press. San Diego, California.

Ali, A., Roossinck, M. J. 2008. Genetic bottlenecks. In Roossinck, M. J. (Eds.). Plant Virus Evolution. Springer, Berlin, 124-129.

Andrianifahanana, M., Lovins, K., Dute, R., Sikora, E., Murphy, J. F., 1997. Pathway for phloem-dependent movement of pepper mottle potyvirus in the stem of *Capsicum annuum*. Phytopathology, 87(9): 892-898.

Anfoka, G. H. 2000. Benzo-(1,2,3)-thiadiazole-7-carbothioic acid S-methyl ester induces systemic resistance in tomato (*Lycopersicon esculentum*. Mill cv. Vollendung) to cucumber mosaic virus. Crop Protection, 19: 401-405.

Bancroft, J. B., Rouleau, M., Johnston, R., Prins, L., Mackie, G. A. 1991. The entire nucleotide sequence of foxtail mosaic virus RNA. Journal of General Virology, 72: 2173-2181.

Barratt, D. H., Kolling, K., Graf, A., Pike, M., Calder, G., Findlay, K., Zeeman, S. C., Smith, A. M. 2011. Callose synthase GSL7 is necessary for normal phloem transport and inflorescence growth in Arabidopsis. Plant Physiology, 155: 328-341.

Beffa, R. S., Hofer, R. M., Thomas, M., Meins, F., Jr. 1996. Decreased susceptibility to viral disease of β-1,3-glucanase-deficient plants generated by antisense transformation. Plant Cell, 8: 1001-1011.

Bektas, Y., Eulgem, T. 2014. Synthetic plant defense elicitors. Frontiers in Plant Science, 5(January): 804.

Benitez-Alfonso, Y., Faulkner, C., Ritzenthaler, C., Maule, A. J. 2010. Plasmodesmata: gateways to local and systemic virus infection. Molecular Plant-Microbe Interaction. 23: 1403-1412.

Betti, C., Lico, C., Maffi, D., D'Angeli, S., Altamura, M. M., Benvenuto, E., Faoro, F., Baschieri, S. 2012. Potato virus X movement in *Nicotiana benthamiana*: new details revealed by chimeric coat protein variants. Molecular Plant Pathology, 13(2): 198-203.

Brunt, A. A. 1966. Narcissus mosaic virus. Annals of Applied Biology, 58:13-2.

Cao, H., Bowling, S. A., Gordon, A. S., and Dong, X. 1994. Characterization of an Arabidopsis mutant that is nonresponsive to inducers of systemic acquired resistance. Plant Cell, 6: 1583-1592.

Capoor, S. P. 1949. The movement of tobacco mosaic virus and potato virus X through tomato plants. Annals of Applied Biology, 36 (3): 307-319.

Carrington, J. C., Kasschau, K. D., Mahajan, S. K., Schaad, M. C. 1996. Cell-to-cell and long-distance transport of viruses in plants. Plant Cell, 8(10): 1669-1681.

Chen, X. Y., Liu, L., Lee, E., Han, X., Rim, Y., Chu, H., Kim, S. W., Sack, F., Kim, J.Y. 2009. The Arabidopsis callose synthase gene GSL8 is required for cytokinesis and cell patterning. Plant Physiology, 150: 105-113.

Chen, J., Zhang, J., Kong, M., Freeman, A., Chen, H., Liu, F. 2021. More stories to tell: NONEXPRESSOR OF PATHOGENESIS-RELATED GENES1, a salicylic acid receptor. Plant Cell and Environment, 44(6): 1716-1727.

Chen, J., Zheng, H. Y., Chen, J. P., Adams, M. J. 2002. Characterisation of a potyvirus and a potexvirus from Chinese scallion. Archives of Virology, 147: 683-693.

Chen J., Shi Y. H., Adams M. J., Chen J. P. 2005. The complete sequenceof the genomic RNA of an isolate of lily virus X (genus *Potexvirus*). Archives of Virology, 150:825-832.

Cheng, N. H., Su, C. L., Carter, S. A., Nelson, R. S., 2000. Vascular invasion routes and systemic accumulation patterns of tobacco mosaic virus in *Nicotiana benthamiana*. Plant Journal, 23(3): 349-362.

Chivasa, S., Murphy, A. M., Naylor, M., Carr, J. P. 1997. Salicylic acid interferes with Tobacco mosaic virus replication via a novel salicylhydroxamic acid-sensitive mechanism. Plant Cell, 9: 547-557.

Citovsky, V., Ghoshroy, S., Tsui, F., Klessig, D. 1998. Nontoxic concentrations of cadmium inhibit systemic movement of turnip vein clearing virus by a salicylic acid-independent mechanism. Plant Journal, 16: 13-20.

Collum, T. D., Padmanabhan, M. S., Hsieh, Y. C., Culver, J. N. 2016. Tobacco mosaic virus-directed reprogramming of auxin/indole acetic acid protein transcriptional responses enhances virus phloem loading. Proceedings of the National Academy of Sciences of the United States of America, 113(19): E2740-E2749.

Cui, W., Lee, J. Y. 2016. Arabidopsis callose synthases CalS1/8 regulate plasmodesmal permeability during stress. Nature Plants, 2: 16034.

Curl, E. A. 1963. Control of plant disease by crop rotation. Botanical Review, 29:413-479.

Dawson, W. O., Hilf, M. E. 1992. Host-range determinants of plant viruses. Annual Review of Plant Physiology and Plant Molecular Biology, 43: 527-555.

Decroocq, V., Sicard, O., Alamillo, J. M., Lansac, M., Eyquard, J. P., García, J. A., Candresse, T., Gall, O. Le, Revers, F., Cedex, O. 2006. Multiple resistance traits control plum pox virus infection

in *Arabidopsis thaliana*. Molecular Plant-Microbe Interaction. 19 (5): 541-549.

Delaney, T. P., Friedrich, L., Ryals, J. A. 1995. Arabidopsis signa1 transduction mutant defective in chemically and biologically induced disease resistance. Proceedings of the National Academy of Sciences of the United States of America, 92: 6602-6606.

Dempsey, D. A., Klessig, D. F. 2017. How does the multifaceted plant hormone salicylic acid combat disease in plants and are similar mechanisms utilized in humans? Biomed Central Biology, 15: 23.

Derrick, P. M., Barker, H. 1997. Short and long distance spread of potato leafroll luteovirus: effects of host genes and transgenes conferring resistance to virus accumulation in potato. Journal of General Virology , 78: 243-251.

Ding, X., Shintaku, M. H., Carter, S. A., Nelson, R. S. 1996. Invasion of minor veins of tobacco leaves inoculated with tobacco mosaic virus mutants defective in phloem-dependent movement. Proceedings of the National Academy of Sciences of the United States of America. 93 (20): 11155-11160.

Dizadji, A., Koohi-Habibi, M., Izadpanah, K., Dietrich, C., Mossahebi, G. H., Winter, S. 2008. Characterization of lettuce virus X, a new potexvirus infecting lettuce in Iran. Archives of Virology, 153: 1867-1875.

Donchenko, E., Trifonova, E., Nikitin, N., Atabekov, J., Karpova, O. 2018. Alternanthera mosaic potexvirus: several features, properties, and application. Advances in Virology, Article ID 1973705: 1-11.

Ellinger D., Voigt, C. A. 2014. Callose biosynthesis in arabidopsis with a focus on pathogen response: what we have learned within the last decade. Annals of Botany, 114: 1349-1358.

Evallo, E., Taguiam, J. D., Balendres, M. A. 2021. A brief review of plant diseases caused by cactus virus X. Crop Protection, 143: 105566.

Faoro F., Gozzo, F. 2015. Is modulating virus virulence by induced systemic resistance realistic? Plant Science, 234: 1-13.

Folimonova, S. Y., Tilsner, J., 2018. Hitchhikers, highway tolls and roadworks: the interactions of plant viruses with the phloem. Current Opinion in Plant Biology, 43: 82-88.

Forster, R. L. S., Milne, K. S. 1978. Daphne virus X: A Potexvirus from daphne. New Zealand Journal of Agricultural Research, 21(1): 137-142.

Frowd, J. A., Tremaine, J. H. 1977. Physical, chemical, and serological properties of cymbidium mosaic virus. Phytopathology, 67: 43-49.

Fujisawa, I. 1986. Asparagus virus. III: A new member of potexvirus from asparagus. Japanese Journal of Phytopathology, 52(2): 193-200.

García-Arenal, F., McDonald, B. A. 2003. An analysis of the durability of resistance to plant viruses. Phytopathology, 93: 941-952.

Gergerich, R. C., Dolja, V. V. 2006. Introduction to plant viruses, the invisible foe. Plant Health Instructor, online publication.

Glazebrook, J. 2005. Contrasting mechanisms of defense against biotrophic and necrotrophic pathogens. Annual Review of Phytopathology, 43(1): 205-227.

Goodrick, B.J., Kuhn, C.W., Hussey, R.S., 1991. Restricted systemic movement of cowpea chlorotic mottle virus in soybean with nonnecrotic resistance. Phytopathology, 81: 1426-1431.

Gomez, P., Sempere, R. N., Elena, S. F., Aranda, M. A. 2009. Mixed infections of pepino mosaic virus strains modulate the evolutionary dynamics of this emergent virus. Journal of Virology, 83: 12378-12387.

Gosalvez-Bernal, B., Genoves, A., Antonio Navarro, J., Pallas, V., Sanchez-Pina, M. A. 2008. Distribution and pathway for phloem-dependent movement of melon necrotic spot virus in melon plants. Molecular Plant Pathology, 9(4): 447-461.

Guerini, M. N., Murphy, J. F. 1999. Resistance of *Capsicum annuum* 'Avelar' to pepper mottle potyvirus and alleviation of this resistance by co-infection with cucumber mosaic cucumovirus are associated with virus movement. Journal of General Virology, 80: 2785-2792.

Hancinsky, R., Mihalik, D. Mrkvova, M., Candresse, T., Glasa, M. 2020. Plant viruses infecting *Solanaceae* family members in the cultivated and wild environments: a review. Plants, 9(5): 667.

Hanssen, I., Lapidot, M., Thomma, B. 2010. Emerging viral diseases of tomato crops. Molecular Plant-Microbe Interaction, 23: 539-548.

Hashimoto, M., Ozeki, J., Komatsu, K., Senshu, H., Kagiwada, S., Mori, T., Yamaji, Y., Namba, S. 2008. Complete nucleotide sequence of asparagus virus 3. Archives of Virology, 153(1): 219-221.

Ho, L. 1988. Metabolism and compartmentation of imported sugars in sink organs in relation tosinkstrength. Annual Review of Plant Physiology and Plant Molecular Biology, 39: 355-378.

Holmes, F. O. 1930. Local and systemic increase of tobacco mosaic virus. American Journal of Botany, 17(8): 789-805.

Hipper, C., Brault, V., Ziegler-Graff, V., Revers, F. 2013. Viral and cellular factors involved in phloem transport of plant viruses. Frontiers in Plant Science, 4: 1-24.

Hu, J. S., Ferreira, S., Wang, M., Xu, M. Q. 1993. Detection of cymbidium mosaic virus, odontoglossum ringspot virus, tomato spotted wilt virus, and potyviruses infecting orchids in Hawaii. Plant Disease, 77: 464-468.

Huang, P., Dong, Z., Guo, P., Zhang, X. C., Qiu, Y., Li, B., Wang, Y., Guo, H. J. 2020. Salicylic acid suppresses apical hook formation via NPR1-mediated repression of EIN3 and EIL1 in Arabidopsis. Plant Cell, 32: 612-629.

Hull, R. 2014. Plant Virology fifth edition. Elsevier-Academic Press. London. United Kingdom.

Iglesias, V. A., Meins, F., Jr. 2000. Movement of plant viruses is delayed in a β-1,3-glucanase-

deficient mutant showing a reduced plasmodesmatal size exclusion limit and enhanced callose deposition. Plant Journal, 21(2): 157-166.

Ishiga, T., Iida, Y., Sakata, N., Ugajin, T., Hirata, T., Taniguchi, S. 2020. Acibenzolar-*S*-methyl activates stomatal based defense against *Pseudomonas cannabina* pv. *alisalensis* in cabbage. Journal of General Plant Pathology, 86: 48-54.

Ishiga, T., Sakata, N., Ugajin, T., Ishiga, Y., 2021. Acibenzolar-*S*-methyl and probenazole activate stomatal based defense at different times to control bacterial blight of cabbage. Journal of General Plant Pathology. 87(1): 30-34.

Islam, W., Naveed, H., Zaynab, M., Huang, Z., Chen, H. Y. H. 2019. Plant defense against virus diseases; growth hormones in highlights. Plant Signaling & Behavior, 14(6): 1-10.

Jelkmann, W., Martin, R. R., Lesemann, D. E., Vetten, H. J., Skelton, F., 1990. A new potexvirus associated with strawberry mild yellow edge disease. Journal of General Virology, 71: 1251-1258.

Jones, R. A. C, Koenig, R. , and Lesemann, D. E. 1980. Pepino mosaic virus, a new potexvirus from pepino (*Solanum muricatum*). Annals of Applied Biology, 94:61-68.

Jones, R. A. C. 2021. Global plant virus disease pandemics and epidemics. Plants, 10(2), 1-41.

Kappagantu, M, Collum, T. D., Dardick, C., Culver, J. N. 2020. Viral hacks of the plant vasculature: the role of phloem alterations in systemic virus infection. Annual Review of Virology, 7: 351-370.

Kang, B. C., Yeam, I., Jahn, M. M., 2005. Genetics of plant virus resistance. Annual Review of Phytopathology, 43(1): 581-621.

Kawamoto, T., Kawamoto, K., 2014. Preparation of thin frozen sections from nonfixed and undecalcified hard tissues using Kawamoto's film method (2012). Methods in Molecular Biology, 1130: 149-164.

Kenney, J. R., Grandmont, M. E., Mauck, K.E., 2020. Priming melon defenses with acibenzolar-*S*-methyl attenuates infections by phylogenetically distinct viruses and diminishes vector preferences for infected hosts. Viruses, 12: 25.

Kehr, J., Buhtz, A. 2008. Long distance transport and movement of RNA through the phloem. Journal of Experimental Botany, 59: 85-92.

Klap, C., Luria, N., Smith, E., Bakelman, E., Belausov, E., Laskar, O., Lachman, O., Gal-On, A. Dombrovsky, A. 2020. The potential risk of plant-virus disease initiation by infected tomatoes. Plants, 9: 623.

Kock, M. J. D. de, Lemmers, M. E. C., Pham, K. T. K., Lommen, S. T. E. 2003. Onderzoek naar details van bodemgebonden verspreiding van TVX bij tulp. Praktijkonderzoek Plant & Omgeving, Business Unit Bloembollen, Boomkwekerij en Fruit – 23.

Komatsu, K., Yamaji, Y., Ozeki, J., Hashimoto, M., Kagiwada, S., Takahashi, S., Namba, S. 2008. Nucleotide sequence analysis of seven Japanese isolates of plantago asiatica mosaic virus (PlAMV): a unique potexvirus with significantly high genomic and biological variability within the species. Archives of Virology, 153(1):193-8.

Komatsu K, Yamashita K, Sugawara K, Verbeek M, Fujita N, Hanada K, Uehara-Ichiki T, Fuji S. 2017. Complete genome sequence of two highly divergent Japanese isolates of plantago asiatica mosaic virus. Archives of Virology, 162: 581-584.

Komatsu, K., Sasaki, N., Yoshida, T., Suzuki, K., Masujima, Y., Hashimoto, M., Watanabe, S., Tochio, N., Kigawa, T., Yamaji, Y., Oshima, K., Namba, S., Nelson, R. S., Arie, T. 2021. Identification of a proline-kinked amphipathic α-helix downstream from the methyltransferase domain of a potexvirus replicase and its role in virus replication and perinuclear complex formation. Journal of Virology, 95(20): 1-24.

Kostin, V. D., Volkov, Yu. G. 1976. Some properties of the virus affecting *Plantago asiatica* L.

Virusnye Bolezni Rastenij Dalnego Vostoka, 25: 205-210.

Koziel, E.; Otulak-Koziel, K.; Bujarski, J.J. 2021. Plant cell wall as a key player during resistant and susceptible plant virus interactions. Mini Review. Frontiers in Microbiology, 12: 495.

Knapp, E., Flores, R., Scheiblin, D., Modla, S., Czymmek, K., Yusibov, V. 2012. A cryohistological protocol for preparation of large plant tissue sections for screening intracellular fluorescent protein expression. Biotechniques, 52(1): 31-37.

Kwak H. R., Kim M., Kim J., Choi H. S., Seo J.K., Ko, S. J., Kim, J. S. 2018. First report of plantago asiatica mosaic virus in *Rehmannia glutinosa* in Korea. Plant Disease, 102: 1046.

Lee, J. Y., Lu, H. 2011. Plasmodesmata: the battleground against intruders. Trends in Plant Science, 16: 201-210.

Leisner, S. M., Howell, S. H. 1993. Long-distance movement of viruses in plants. Trends in Microbiology, 1(8): 314-317.

Leisner, S. M., Turgeon, R., Howell, S. H. 1993. Effects of host plant development and genetic determinants on the long-distance movement of cauliflower mosaic virus in Arabidopsis. Plant Cell, 5(2): 191-202.

Levy, A., Epel, B. L. 2009. Cytology of the (1,3)-β-glucan (callose) in plasmodesmata and sieve plate pores. In Bacic, A., Fincher, G. B., Stone, B. A. (Eds). Chemistry, Biochemistry, and Biology of (1,3)-β-Glucans and Related Polysaccharides. Academic Press, Elsevier, Burlington, Massachusetts, USA, 439-463.

Lim, S., Igori, D., Zhao, F., Do, Y. S., Cho I. S., Choi G. S., Moon J. S. 2016. Molecular detection and characterization of a divergent isolate of plantago asiatica mosaic virus in *Plantago asiatica*. Virus Disease, 27: 307-310.

Llorens, E., Agusti-Brisach, C., Gonzalez-Hernandez, A.I., Troncho, P., Vicedo,B., Yuste, T., Orero, Ledo, C., Garcia-Agustin, P., Lapena, L. 2017. Bioassimilable sulphur provides effective control

of *Oidium neolycopersici* in tomato, enhancing the plant immune system. Pest Management Science, 73: 1017-1023.

Loebenstein, G. 2001. *Potato X Virus* (PVX; Genus *Potexvirus*). Virus and Virus-like Diseases of Potatoes and Production of Seed-Potatoes, 1931: 87-94.

Lough T. J., Netzler N. E., Emerson S. J., Sutherland P., Carr F., Beck D. L., Lucas W. J., Forster R. L. 2000. Cell-to-cell movement of potexviruses: evidence for a ribonucleic protein complex involving the coat protein and first triple gene block protein. Molecular Plant-Microbe Interaction 13: 962-974.

Lucas, W.J., Ding, B., van der Schoot, C. 1993. Plasmodesmata and the supracellular nature of plants. New Phytologist, 125: 435-476.

Lucas W. J., Gilbertson R. L.1996. How do viruses traffic on the 'vascular highway'? Trends in Plant Science, 1(8): 250-251.

Lucas, W. J., Groover, A., Lichtenberger, R., Furuta, K., Yadav, S. R., Helariutta, Y., He, X. Q., Fukuda, H., Kang, J., Brady, S. M., Patrick, J. W., Sperry, J., Yoshida, A., López-Millán, A. F., Grusak, M. A., Kachroo, P. 2013. The plant vascular system: evolution, development and functions. Journal of Integrative Plant Biology, 55(4): 294-388.

Matsuo, Y., Novianti, F., Takehara, M., Fukuhara, T., Arie, T., Komatsu, K. 2019. Acibenzolar-*S*-methyl restricts Infection of *Nicotiana benthamiana* by plantago asiatica mosaic virus at two distinct stages. Molecular Plant-Microbe Interaction, 32(11): 1475-1486.

Maury, Y., Duby, C., Khetarpal, R.K. 1998. Seed certification for viruses, in: Hadidi, A., Khetarpal, R.K., Koganezawa H. (Eds.). Plant Virus Disease Control (Chap. 18). APS Press, Oregon, USA, 237-248.

Mazzon, M., Marsh, M. 2019. Targeting viral entry as a strategy for broad-spectrum antivirals. F1000Research, 8: 1628.

McLean, B. G., Hempel, F. D., Zambryski, P. C. 1997. Plant intercellular communication via plasmodesmata. Plant Cell, 9: 1043-1054.

Mekuria, T., Bamunusinghe, D., Payton, M., Verchot-Lubicz, J. 2008. Phloem unloading of potato virus X movement proteins is regulated by virus and host factors. Molecular Plant-Microbe Interaction, 21(8): 1106-1117.

Minato, N., Komatsu, K., Okano, Y., Maejima, K. 2014. Efficient foreign gene expression in planta using a plantago asiatica mosaic virus-based vector achieved by the strong RNA-silencing suppressor activity of TGBp1. Archives of Virology, 159: 885-896.

Mochizuki, T., Nobuhara, S., Nishimura, M., Ryang, B. S., Naoe, M., Matsumoto, T., Kosaka, Y., Ohki, S. T. 2016. The entry of cucumber mosaic virus into cucumber xylem is facilitated by co-infection with zucchini yellow mosaic virus. Archives of Virology, 161(10): 2683-2692.

Mrema, E. J., Rubino, F. M., Brambilla, G., Moretto, A., Tsatsakis, A. M., Colosio, C. 2013. Persistent organochlorinated pesticides and mechanisms of their toxicity. Toxicology, 307:74-88.

Murphy, A. M., Gilliland, A., Wong, C., West, J., Davinder, D. P., Carr, J. P. 2001. Signal transduction in resistance to plant viruses. European Journal of Plant Pathology, 107(1): 121-128.

Murphy, A.M., Zhou, T., Carr, J.P. 2020. An update on salicylic acid biosynthesis, its induction and potential exploitation by plant viruses. Current Opinion in Virology, 42: 8-17.

Navarro, J. A., Sanchez-Navarro, J. A., Pallas, V. 2019. Key checkpoints in the movement of plant viruses through the host. Advances in Virus Research, 104: 1-64.

Naylor, M., Murphy, A. M., Berry, J. O., Carr, J. P., 1998. Salicylic acid can induce resistance to plant virus movement. Molecular Plant-Microbe Interaction. 11(9), 860-868.

Nedukha, O. M. 2015. Callose: localization, function, and synthesis in plant cells. Cytology and

Genetic, 49: 49-57.

Nelson, R. S., Li, G., Hodgoson, R. A. J., Beachy, R. N., Shintaku, M. H. 1993. Impeded phloem-dependent accumulation of the masked strain of tobacco mosaic virus. Molecular Plant-Microbe Interaction. 6: 45-54.

Nelson, R. S., van Bel, A. J. E. 1998. The mystery of virus trafficking into , through and out of vascular tissue, in Behnke, H. D. (Eds.). Progress in Botany. Springer, Berlin, Germany, 429-475.

Nijo T., Okano Y., Kondo M., Okuhara H., Sekimura H., Fujimoto Y., Hosoe N., Maejima K., Yamaji Y., Namba S. 2018. Complete genome sequence of a lily virus X isolate from Japan. Genome Announcements, 6:e01462-17.

Noa-Carrazana, J. C., González-de-León, D., Ruiz-Castro, B. S., Piñero, D., Silva-Rosales, L. 2006. Distribution of papaya ringspot virus and papaya mosaic virus in papaya plants (*Carica papaya*) in Mexico. Plant Disease, 90:1004-1011.

Noutoshi, Y., Okazaki, M., Kida, T., Nishina, Y., Morishita, Y., Ogawa, T., Suzuki, H., Shibata, D., Jikumaru, Y., Hanada, A., Kamiya, Y., Shirasu, K. 2012. Novel plant immune-priming compounds identified via high-throughput chemical screening target salicylic acid glucosyltransferases in arabidopsis. Plant Cell, 24: 3795-3804.

Oostendorp, M., Kunz, W., Dietrich, B., Staub, T. 2001. Induced disease resistance in plants by chemicals. European Journal of Plant Pathology, 107(1): 19-28.

Ozeki, J., Takahashi, S., Komatsu, K., Kagiwada, S., Yamashita, K., Mori, T., Hirata, H., Yamaji, Y., Ugaki, M., Namba, S. 2006. A single amino acid in the RNA-dependent RNA polymerase of plantago asiatica mosaic virus contributes to systemic necrosis. Archives of Virology, 151: 2067-2075.

Ozeki, J., Hashimoto, M., Komatsu, K., Maejima, K., Himeno, M., Senshu, H., Kawanishi, T.,

Kagiwada, S., Yamaji, Y., Namba, S. 2009. The N-terminal region of the plantago asiatica mosaic virus coat protein is required for cell-to-cell movement but is dispensable for virion assembly. Molecular Plant-Microbe Interaction, 22: 677-685.

Padmanabhan, M. S., Shiferaw, H., Culver, J. N. 2006. The tobacco mosaic virus replicase protein disrupts the localization and function of interacting AUX/IAA proteins. Molecular Plant-Microbe Interaction, 19(8): 864-873.

Park, M. R., Seo, J. K., Kim, K. H. 2013. Viral and nonviral elements in potexvirus replication and movement and in antiviral Responses. In Maramorosch, K., Murphy, F. A. (Eds). Advances in Virus Research (Volume 87). Academic Press, California, USA, 75-112.

Park M. R., Jeong R. D., Kim K. H. 2014. Understanding the intracellular trafficking and intercellular transport of potexviruses in their host plants. Frontiers in Plant Science, 5: 60.

Pieterse, C. M., Van Wees, S., C., Van Pelt, J.,A., Knoester, M., Laan, R., Gerrits, H., Weisbeek, P. J., van Loon, L. C. 1998. A novel signaling pathway controlling induced systemic resistance in Arabidopsis. Plant Cell, 10(9):1571-1580.

Pieterse C. M., Van der Does, D., Zamioudis, C., Leon-Reyes, A., Van Wees S. C. M. 2012. Hormonal modulation of plant immunity. Annual Review of Cell and Developmental Biology, 28: 489 –521.

Qi, Y., Tsuda, K., Glazebrook, J., Katagiri, F. 2011. Physical association of pattern-triggered immunity (PTI) and effector-triggered immunity (ETI) immune receptors in Arabidopsis. Molecular Plant Pathology, 12(7): 702-708.

Ramajamaki, M. L., Valkonen, J. P. T. 2002. Viral genome-linked protein (VPg) controls accumulation and phloem-loading of a potyvirus in inoculated potato leaves. Molecular Plant-Microbe Interaction. 15, 138–149.

Rao, G. P., Reddy, M. G. 2020. Chapter 38. Overview of yield losses due to plant viruses. In Awasthi,

L. P. (Eds). Applied Plant Virology. Academic Press, 531-562.

R Core Team, 2019. R: A language and environment for statistical computing. R Foundation for Statistical Computing, Vienna, Austria.

Revers, F., Guiraud, T., Houvenaghel, M., Mauduit, T., Gall, O. Le. 2003. Multiple resistance phenotypes to lettuce mosaic virus among *Arabidopsis thaliana* accessions. Molecular Plant-Microbe Interaction, 16(7), 608–616.

Roberts, A.G., Santa Cruz, S., Roberts, I. M., Prior, D. A. M., Turgeon, R., Oparka, K. J. 1997. Phloem unloading in sink leaves of *Nicotiana benthamiana*: comparison of a fluorescent solute with a fluorescent virus. Plant Cell, 9: 1381–1396.

Rubio, L., Galipienso, L., Ferriol, I. 2020. Detection of plant viruses and disease management: relevance of genetic diversity and evolution. Frontiers in Plant Science, 11(July), 1–23.

Sager, R. E., Lee, J. Y. 2014. Plasmodesmata in integrated cell signalling: insights from development and environmental signals and stresses. Journal of Experimental Botany, 65(22), 6337–6358.

Sager, R. E., Lee, J. Y. 2018. Plasmodesmata at a glance. Journal of Cell Science, 131: jcs209346.

Samuel, G. 1934. The movement of tobacco mosaic virus within the plant. Annals of Applied Biology. 21, 90-111.

Santa Cruz, S. 1999. Perspective: phloem transport of viruses and macromolecules - what goes in must come out. Trends in Microbiology, 7 (6): 237–241.

Schneider, I. B., Worley, J. F. 1959. Rapid entry of infectious particles of southern bean mosaic virus into living cells following transport of the particles in the water stream. Virology, 8:243.

Schoch, C. L., Ciufo, S., Domrachev, M., Hotton, C., Kannan, S., Khovanskaya, R., Leipe, D., Mcveigh, R., O'Neill, K., Robbertse, B., et al. 2020. NCBI taxonomy: a comprehensive update on curation, resources and tools. Database.

Scholthof, H. B. 2005. Plant virus transport: motions of functional equivalence. Trends in Plant

Science. 10: 376–382

Seifers, D. L., Harvey, T. L., Haber, S., She, Y. M., Chernushevich, I., Ens, W., and Standing, K.G. 1999. Natural infection of sorghum by foxtail mosaic virus in Kansas. Plant Dis. 83:905-912.

Seron K., Haenni, A.L., 1996. Vascular movement of plant viruses. Mol. Plant. Microbe. Interact. 9 (6), 435-442.

Silva, M.S., Wellink, J. , Goldbach,R.W.,van Lent,J.W. 2002 Phloem loading and unloading of Cowpea mosaic virus in *Vigna unguiculata*, Journal of General Virology. 83:1493–1504.

Sit, T. L., White, K. A., Holy, S., Padmanabhan, U., Eweida, M., Hiebert, I., Mackie, G. A. & Abouhaidar, M. G. (1990). Complete nucleotide sequence of clover yellow mosaic virus RNA. Journal of General Virology 71, 1913-1920.

Slewinski, T. L., Zhang, C., Turgeon, R., 2013. Structural and functional heterogeneity in phloem loading and transport. Frontiers in Plant Science. 4, 1-11.

Sochacki, D., Komorowska, B. (2012). First report of Tulip virus X on tulip in Poland. Plant Dis., 96, 4, 594-594.

Sosnowski MR, Fletcher JD, Daly AM, Rodoni BC, Viljanen-Rollinson, S.L.H (2009) Techniques for the treatment, removal and disposal of host material during programmes for plant pathogen eradication. Plant Pathology 58(4):621-635

Solovyev, A. G., Novikov, V. K., Merits, A., Savenkov, E.I., Zelenina, D. A., Tyulkina, L. G. & Morozov, S. Yu. (1994). Genome characterization and taxonomy of Plantago asiatica mosaic potexvirus. Journal of General Virology 75, 259-267.

Sudarshana, M. R., Wang, H. L., Lucas, W. J., and Gilbertson, R. L. (1998).Dynamics of bean dwarf mosaic geminivirus cell-to-cell and long- distance movement in Phaseolus vulgaris revealed, using the green fluorescent protein. Molecular Plant-Microbe Interaction, 11: 277-291.

Susaimuthu, J., Agindotan, B. O., Miller, L. A., Perry, K. L. 2007. Potato aucuba mosaic virus in

potato in New York state. Plant Disease, 91:1202-11202.

Takeshita, M., Okuda, M., Okuda, S., Hyodo, A., Hamano, K., Furuya, N., Tsuchiya, K. 2013. Induction of antiviral responses by acibenzolar-*S*-methyl against cucurbit chlorotic yellows virus in melon. Phytopathology, 103(9): 960-965.

Tanaka, M., Verbeek, M., Takehara, M., Pham, K., Lemmers, M., Slootweg, C., Arie, T., Komatsu, K. 2019. Differences in infectivity and pathogenicity of two Plantago asiatica mosaic virus isolates in lilies. European Journal of Plant Pathology, 153(3): 813-823.

Thompson, J. R., García-Arenal, F. 1998. The bundle sheath-phloem interface of Cucumis sativus is a boundary to systemic infection by tomato aspermy virus. Molecular Plant-Microbe Interaction, 11:109-114.

Tilsner, J., Amari, K., Torrance, L. 2011. Plasmodesmata viewed as specialised membrane adhesion sites. Protoplasma, 248: 39-60.

Tilsner, J., Linnik, O., Louveaux, M., Roberts, I. M., Chapman, S.N., Oparka, K. J. 2013. Replication and trafficking of a plant virus are coupled at the entrances of plasmodesmata. Journal of Cell Biology, 201: 981-995.

Tournier B, Tabler M, Kalantidis K. 2006. Phloem flow strongly influences the systemic spread of silencing in GFP *Nicotiana benthamiana* plants. The Plant Journal, 47: 383-394.

Trip, P., Gorham, P. R. 1967. Autoradiography study of the pathway of translocation. Canadian Journal of Botany. 45,1567-1573.

Tripathi, D., Jiang, Y. L., Kumar, D. 2010. SABP2, a methyl salicylate esterase is required for the systemic acquired resistance induced by acibenzolar-S-methyl in plants. FEBS Letters, 584 (15): 3458-3463.

Turgeon, R. 1989. The sink-source transition in leaves. Annual Review of Plant Physiology and Plant Molecular Biology, 40:119-138.

Turgeon, R., Wolf, S. 2009. Phloem transport: cellular pathways and molecular trafficking. Annual Review of Plant Biology, 60: 207-221.

Uehara-Ichiki, T., Nakazono-Nagaoka, E., Yamaguchi, M., Ohashi, M., Kodaira, E., Kojima, M., Igarashi, M., Hanada, K., Hishida, A., Fujikawa, T. 2018. Next-generation sequencing and bioassay of viruses in *Rehmannia glutinosa*. Japan Journal of Phytopathology, 84: 151-157.

Ueki, S., Citovsky, V. 2005. Identification of an interactor of cadmium ion-induced glycine-rich protein involved in regulation of callose levels in plant vasculature. Proceedings of the National Academy of Sciences of the United States of America, 102(34): 12089-12094.

Ueki, S., Citovsky, V. 2007. Spread throughout the plant: systemic transport of viruses. In E. Waigmann, E., Heinlein M. (Eds.). Viral Transport in Plants. Springer, Berlin, Germany, 85-118.

Ueki, S., Citovsky, V. 2014. Plasmodesmata-associated proteins. Plant Signaling & Behavior, 9(2): e27899.

Vallad, G. E., Goodman, R. M. 2004. Systemic acquired resistance and induced systemic resistance in conventional agriculture. Crop Science, 44: 1920-1934.

Van der Vlugt, R. A. A., Berendsen, M. 2002. Development of a general potexvirus detection method. European Journal of Plant Pathology, 108(4): 367-371.

Verchot-Lubicz, J., Torrance, L., Solovyev, A.G., Morozov, S.Y., Jackson, A.O., Gilmer, D.(2010) Varied movement strategies employed by triplegene block-encoding viruses. Molecular Plant-Microbe Interaction, 23: 1231-1247.

Verchot-Lubicz, J. 2016. How does the stressed out ER find relief during virus infection? Current Opinion in Virology, 17: 74-79.

Vlot, A. C., Dempsey, D. M. A., Klessig, D. F. 2009. Salicylic acid, a multifaceted hormone to combat disease. Annual Review of Phytopathology, 47: 177-206.

Vuorinen, A. L., Kelloniemi, J., Valkonen, J. P. T. 2011. Why do viruses need phloem for systemic invasion of plants? Plant Science, 181(4): 355-363.

Waigmann, E., Ueki, S., Trutnyeva, K., Citovsky, V. 2004. The ins and outs of nondestructive cell-to-cell and systemic movement of plant viruses. Critical Reviews in Plant Sciences, 23(3): 195-250.

Waigmann E., Heinlein M. 2007. Viral transport in plants. Springer-Verlag. Berlin, Germany.

Wan, J., Cabanillas, D. G., Zheng, H., Laliberté, J. F. 2015. Turnip mosaic virus moves systemically through both phloem and xylem as membrane-associated complexes. Plant Physiology, 167(4): 1374-1388.

Wang, D., Pajerowska-mukhtar, K., Culler, A. H., Dong, X., Carolina, N. 2007. Report salicylic acid inhibits pathogen growth in plants through repression of the auxin signaling pathway. Current Biology, 17(20): 1784-1790.

Wang Y., Li X., Fan B., Zhu C., Chen Z. 2021. Regulation and function of defense-related callose deposition in plants. International Journal of Molecular Sciences 22: 2393.

Ward, E. R., Uknes, S. J., Williams, S. C., Dincher, S. S., Wiederhold, D. L., Alexander D. C., Ahl-Goy P., Metraux J. P., Ryals J. A. 1991. Coordinate gene activity in response to agents that induce systemic acquired resistance. Plant Cell, 3(10): 1085-1094.

Wright, G. C., Bishop, G. W. 1981. Volunteer potatoes as a source of potato leafroll virus and potato virus X. American Potato Journal, 58: 603-609.

Wu, S. W., Kumar, R., Iswanto, A. B. B., & Kim, J. Y. 2018. Callose balancing at plasmodesmata. Journal of Experimental Botany, 69(22): 5325-5339.

Wu, X., Liu, Q., Chai, M., J. Liu, Zhang, L., Cheng, X. 2018. First report of potato aucuba mosaic virus on potato in China. Plant Disease, 102: 2671.

Yoshida, T., Shiraishi, T., Komoda, Y. K., Komatsu, K., Maejima, K., Okano, Y., Fujimoto, Y., Yusa,

A., Yamaji, Y., Namba, S. 2019. The plant noncanonical antiviral resistance protein jax1 inhibits potexviral replication by targeting the viral RNA-dependent RNA polymerase. Journal of Virology, 93(3): e01506-18.

Yusa, A., Iwabuchi, N., Koinuma, H., Keima, T., Neriya, Y., Hashimoto, M., Maejima, K., Yamaji, Y., Namba, S. 2016. Complete genome sequences of two hydrangea ringspot virus isolates from Japan. Genome Announcement, 4(2):e00022-16.

Zanini, A. A., Di Feo, L., Luna, D. F., Paccioretti, P., Collavino, A., Rodriguez, M. S. 2021. Cassava common mosaic virus infection causes alterations in chloroplast ultrastructure, function, and carbohydrate metabolism of cassava plants. Plant Pathology, 70(1), 195–205.

Zavaliev, R., Ueki, S., Epel, B.L., Citovsky, V. 2011. Biology of callose (β-1,3-glucan) turnover at plasmodesmata. Protoplasma, 248: 117-130.

Zavaliev, R. Epel, B.L. 2015. Imaging callose at plasmodesmata using aniline blue: quantitative confocal microscopy. Methods in Molecular Biology, 1217: 105-119.

Zhang, Z., Tong, X., Liu, S., Chai, L., Zhu, F., Zhang, X. 2019. Genetic analysis of a piezo-like protein suppressing systemic movement of plant viruses in *Arabidopsis thaliana*. Scientific Reports, 9 (1): 1–11.